

Itinerant spintronic systems with electrons far from equilibrium

Zur Erlangung des akademischen Grades eines
DOKTORS DER NATURWISSENSCHAFTEN
(Dr. rer. nat.)

von der KIT-Fakultät für Physik des
Karlsruher Instituts für Technologie (KIT)
angenommene

DISSERTATION

von

M.Sc. Ludwig, Tim

Tag der mündlichen Prüfung: 26.07.2019

Referent: Alexander Shnirman
Korreferent: Jörg Schmalian

Abstract

A dynamical mean-field can drive the electron distribution into a far-from-equilibrium state. The electron distribution governs the flow of currents and, thereby, it can influence the dynamics of a mean-field. In turn, a dynamical interplay emerges between mean-fields and electron distributions.

I discuss this interplay for open zero-dimensional systems. It is shown to be particularly interesting in itinerant spintronic systems. In these systems, a dynamical magnetization drives the electron system into a nonequilibrium state. The resulting nonequilibrium distribution affects the flow of charge- and spin-currents and, thereby, it can have a back-action onto the magnetization dynamics.

Contents

1	Introduction	1
I	Introduction to charge transport and strong nonequilibrium effects	7
2	Strong nonequilibrium distributions in voltage biased double tunnel junctions	9
2.1	Voltage biased single tunnel junction	10
2.2	Voltage biased double tunnel junction	12
2.3	The role of internal relaxation	16
2.4	Summary and discussion	18
3	Noise of charge current generated by an FMR-driven itinerant ferromagnet	19
3.1	Description of the system	21
3.2	Phenomenological magnetization dynamics	22
3.3	The precessing magnetization drives the electron system into a nonequilibrium state	23
3.4	Charge current and its noise	25
3.5	A generalization to magnetic tunnel junctions is not straightforward	27
3.6	Summary and discussion	28
II	Dynamical interplay between mean-fields and electron distributions far from equilibrium	29
4	Dynamical interplay between electrical potential and electron distribution	31
4.1	Description of the system	33
4.2	Self-consistency equation for the dynamical electrical potential	35
4.3	Gauge-transformation	37
4.4	Quasiclassical approximation	38
4.5	Derivation of the quasiclassical equation of motion	42
4.6	Fluctuations of the electrical potential	47
4.7	Summary and discussion	49

5	Dynamical interplay between magnetization and electron distributions	51
5.1	Description of the system	52
5.2	Self-consistency equation for the dynamical magnetization	55
5.3	Transition to the magnetization's rotating frame of reference	56
5.4	Quasiclassical approximation	58
5.5	Quasiclassical equation of motion for the magnetization	66
5.6	Summary and discussion	68
III	Magnetic double tunnel junction with a dynamical magnetization	71
6	Magnetic double tunnel junction far from equilibrium	73
6.1	Description of the system	75
6.2	Ferromagnetic regime and transition to rotating frame	77
6.3	Quasiclassical approximation	78
6.4	Landau-Lifshitz-Gilbert-Slonczewski equation	85
6.5	Charge current and its noise	86
6.6	Summary and discussion	89
7	Driven magnetic double tunnel junction	91
7.1	Purely FMR-driving: emergence of additional steady state precessions	94
7.2	Purely voltage bias: sudden switch of stability	98
7.3	Purely thermal bias: hybrid current can enhance the thermoelectric effect	101
7.4	Summary and discussion	104
8	Summary and conclusion	105
IV	Appendices	109
A	Proper treatments of leads and introduction of counting fields	111
A.1	Proper treatment of the leads	111
A.2	Introduction of counting fields	113
B	Wigner transformation and gradient expansion	117
B.1	The Wigner transformation	117
B.2	The Gradient expansion	118

Chapter 1

Introduction

... the reductionist hypothesis does not by any means imply a "constructionist" one:
The ability to reduce everything to simple fundamental laws does not imply
the ability to start from those laws and reconstruct the universe.

quoted from "More Is Different" [Anderson, 1972]

Basic to the field of condensed matter physics is the tension that arises between a microscopic knowledge about particles and their interactions and a desired effective description of a system at a more macroscopic scale. To give two examples: we might know the dynamics of single charges and their interaction via Coulomb-repulsion but desire a description in terms of the charge density; or, we might know the dynamics of single spins and their interactions but desire a description in terms of the magnetization. So, the tension arises between our knowledge on the level of single particles (charges/spins) and our desire for an effective description in terms of their collective behaviour (charge density/magnetization).

One way to get from a microscopic model to a more macroscopic description is the mean-field approach. Instead of keeping track of all the interactions between particles, for each individual particle one considers the interaction averaged over all the other particles of the same type. This average, known as mean-field, describes the system on a collective level. It depends on the distribution of particles among the effective single-particle states. At the same time, however, the single-particle states depend on the mean-field via the remaining interaction. In short, mean-field and single-particle states are interdependent. This interdependency puts a restriction onto possible mean-fields: the mean-field, as average over single-particle states, has to be consistent with the mean-field, that affects those single-particle states. In other words, the mean-field has to be self-consistent.

While it can be quite hard to identify the correct mean-field¹, at equilibrium it is rather straightforward to find the corresponding self-consistency condition. This is done as follows. At first, the interaction is decoupled by introducing a mean-field, which is then assumed to be given but unknown. This results in an effective single-particle Hamiltonian that depends on the mean-field and determines the single-particle states. The particles are distributed among those

¹See for example discussions in [Bruus and Flensberg, 2004, Altland and Simons, 2010].

states according to the equilibrium distribution function; for example a Fermi-distribution for Fermions. Finally, the mean-field is determined by averaging over the single-particle states with respect to the distribution function. This leads to a self-consistency equation: the mean-field depends on the effective single-particle states which, again, depend on the mean-field. In this context, the assumption of equilibrium provides a significant simplification. The equilibrium distribution function (of an open system) depends on the heat- and particle-bath but it does not depend on the system itself.

Far from equilibrium, however, a dynamical mean-field not only governs the single-particle states but also the distribution function. To be more precise, the distribution function depends on the mean-field's history and, therefore, it becomes dynamical itself. This makes the mean-field approach more complicated but also more interesting. In particular, not only the mean-field but also the distribution function has to be self-consistent. Resolving this "double" self-consistency or, correspondingly, the interdependency of mean-field and distribution function, poses the fundamental conceptual problem addressed in this thesis.

Basically, there are two options to proceed: one declares either the mean-field or the distribution function to be of fundamental interest; the other object is then considered as enslaved and it is only of auxiliary character. This leaves some room for choice. However, the strategy might also be dictated by the question one wants to answer or by the observable one wants to determine. When both choices are possible, they lead to complementary approaches (figure 1.1):

- *Kinetic equation.* When the *distribution function* is considered to be *fundamental*, a kinetic equation should be derived to describe the distribution function's dynamics. Then, the mean-field is enslaved to the distribution function, but it still plays an auxiliary role in the kinetic equation. Thus, the kinetic equation is of the Vlasov type rather than the Boltzmann type.
- *Equation of motion.* When the *mean-field* is considered to be *fundamental*, an equation of motion should be derived to describe the mean-field's dynamics. While the distribution function will be enslaved to the mean-field, it still plays an auxiliary role in the derivation of the equation of motion.

In this thesis I concentrate on the *equation of motion* approach with a particular focus on the interplay between the dynamical mean-field and the dynamical (auxiliary) distribution function. Besides being of broad conceptual interest, this interplay can be particularly relevant in spintronic systems, where a dynamical magnetization drives the electron system away from equilibrium. The resulting nonequilibrium electron distribution can have a strong back-action onto the magnetization dynamics. This is explicitly demonstrated for a driven magnetic double tunnel junction, where the adjustments of the distribution function can change the magnetization dynamics qualitatively.

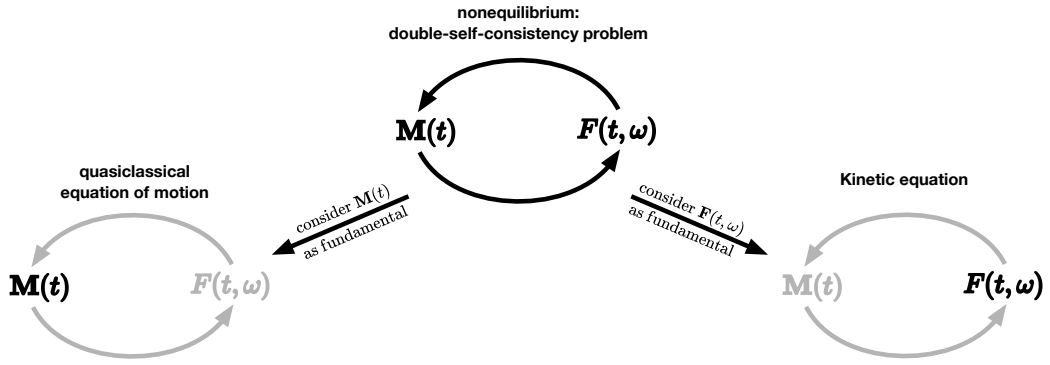


Figure 1.1: Far from equilibrium a double-self-consistency problem arises: both, the dynamical mean-field $M(t)$ and the dynamical distribution function $F(t, \omega)$, have to be self-consistent. The double-self-consistency problem can be resolved into a "standard" self-consistency problem by declaring either the mean-field or the distribution function to be fundamental while treating the other object as an auxiliary quantity. If one treats the distribution function as fundamental, one would need to derive a kinetic equation for $F(t, \omega)$, where $M(t)$ plays only an auxiliary role. The view taken in this thesis is the opposite one: The mean-field $M(t)$ is considered to be the fundamental object; its dynamics is determined by an equation of motion which, however, is influenced by the distribution function $F(t, \omega)$.

Outline

This thesis is organized into three main parts: roughly speaking, from simple over complex to applications. The first part serves as an introduction into the topics of strong nonequilibrium effects and charge transport with a particular focus on noise. In the second part, I focus on the dynamical interplay between mean-fields and electron distributions far from equilibrium. In the third part, this interplay is discussed for the magnetization dynamics in a driven magnetic double tunnel junction.

While all chapters can be read independently, as a minimal subset I suggest to read chapter 3, which poses the basic problem, and chapter 7, which presents the general solution and discusses its significance; for details see below.

Part I: Introduction to charge transport and strong nonequilibrium effects

The first part of this thesis serves as an introduction to charge transport and strong nonequilibrium effects.

In chapter 2, I compare a voltage biased single tunnel junction to a voltage biased double tunnel junction. A special focus is put on the role of the electron distribution function in charge transport. In particular, this allows me to give a definition of *strong* nonequilibrium. In addition, the comparison between single and double tunnel junctions allows for a nice introduction to noise.

In chapter 3, I consider a double tunnel junction where an itinerant ferromagnet (middle region) is tunnel-coupled to two normal metal leads. The magnetization is driven into a steady state precession by a ferromagnetic resonance (FMR) setup. The precessing magnetization, in turn, drives the electron system into a nonequilibrium state. A strong nonequilibrium distribution emerges. It is governed by the geometrical Berry-phase (associated with the precession of the

magnetization) and it governs the noise of charge current. In turn, the charge current noise can be measured to gain information about the magnetization dynamics.

Part II: Dynamical interplay between mean-fields and electron distributions far from equilibrium

Motivated by the discussion in chapter 3, I consider the interplay between mean-fields and far-from-equilibrium electron distributions in part II. It presents the technical advancements achieved in [Ludwig et al., 2017, Ludwig et al., 2019b] and forms the technical backbone of this thesis. However, without losing the main message, readers who are not interested in technical details might skip part II.

In chapter 4, I consider a voltage biased double tunnel junction where a quantum dot (middle region) is tunnel-coupled to two normal metal leads. The electrons in the dot interact via Coulomb-repulsion. This gives rise to an electrical potential which is the mean-field or, more formally, the Hubbard-Stratonovich field corresponding to the Coulomb-repulsion. The goal is to determine the quasiclassical equation of motion for the electrical potential. Generically, the quasiclassical equation of motion is derived—in the path-integral version of Keldysh formalism—by variation of the action with respect to quantum components. As specific result, I obtain the RC -relaxation law. A particular focus is put on the interplay between electrical potential and electron distribution function. It leads to a correction of the RC -relaxation law which is also known as quantum capacity. Its origin can be traced back to the Pauli exclusion principle which is repulsive, just as Coulomb-repulsion. Thus, the quantum capacity affects the dynamics quantitatively but not qualitatively.

In chapter 5, I consider an itinerant ferromagnet which is embedded between two normal metal leads and driven with a ferromagnetic-resonance-type setup. A specific focus is put on a careful derivation of the magnetization's quasiclassical dynamics where the interplay between magnetization dynamics and electron distribution is taken into account. Thereby, chapter 5 provides the technical background for the discussion in chapter 3: it confirms that—for nonmagnetic leads—the magnetization's angular motion is not influenced by the adjustments in the electron distribution. For the dynamics of the magnetization length, however, the adjustments in the distribution function turn out to be essential. Analog to chapter 4 the adjustments of the electron distribution function give rise to a quantum capacity and, again, its origin can be traced back to the Pauli exclusion principle. However, in strong contrast to Coulomb-repulsion (chapter 4), the exchange interaction is attractive and, thus, competes with the repulsive Pauli exclusion principle. In turn, it is essential for the length dynamics to include adjustments of the distribution function.

Part III: Application to a driven magnetic double tunnel junction

In part III, I consider the interplay between a dynamical magnetization and a far-from-equilibrium electron distribution for a driven magnetic double tunnel junction. As justified in part II,

I focus on the magnetization's angular motion and disregard the dynamics of the magnetization length as well as the electrical potential.

In chapter 6, I derive the quasiclassical equation of motion for the magnetization's angular dynamics. As a result, the Landau-Lifshitz-Gilbert-Slonczewski equation is obtained. The Landau-Lifshitz-Gilbert equation describes the dissipative dynamics of a magnetization in an external magnetic field. Due to the presence of a magnetic lead, this equation is supplemented by the Slonczewski spin-transfer-torque (STT) term which describes how spin-polarized currents affect the magnetization dynamics. Interestingly, even in absence of external bias the STT-term remains. This is possible, as the interplay between magnetization dynamics and electron distribution drives the electron system into a nonequilibrium state. In turn, charge- and spin-currents are driven through the whole system even when neither voltage nor thermal bias is applied. This results in a universal STT-term which depends only on the magnetization dynamics but not on the way of driving.

In chapter 7, I discuss the effects of the universal Slonczewski STT-term for the dynamics of the magnetization. I focus on three types of driving separately: ferromagnetic-resonance-type driving; driving via voltage bias; and driving via thermal bias. In all three cases, very distinctive features of the magnetization's angular motion can be traced back to the universal STT-term or, correspondingly, to the adjustments of the electron distribution to the magnetization dynamics. This demonstrates the relevance of distribution functions for magnetization dynamics in spintronic systems.

Relation to published articles

This thesis is based on three articles which I have published together with my coauthors Igor S. Burmistrov, Yuval Gefen, and my supervisor Alexander Shnirman:

- *"Strong nonequilibrium effects in spin-torque systems"*
[Ludwig et al., 2017]
- *"Thermally driven spin transfer torque system far from equilibrium: Enhancement of thermoelectric current via pumping current"*
[Ludwig et al., 2019b]
- *"Current noise geometrically generated by a driven magnet"*
[Ludwig et al., 2019a]

Because my thesis is based on the insights gained in working on these publications, I will switch from writing "I" to writing "we" in the following to acknowledge the essential contributions of Igor S. Burmistrov, Yuval Gefen, and Alexander Shnirman. While the focus of each of these publications was on a specific physical effect, the focus of this thesis is on the methodical advancements we have achieved in those works.

Part I

Introduction to charge transport and strong nonequilibrium effects

Chapter 2

Strong nonequilibrium distributions in voltage biased double tunnel junctions

This chapter compares a voltage biased single tunnel junction (figure 2.1) with a voltage biased double tunnel junction (figure 2.2) out of a twofold purpose: on the one hand, we demonstrate how the study of charge current and its noise can yield insights into the internal structure of a physical system; on the other hand, we show that the electron distribution plays a key role in charge transport and vice versa. A particular focus is put on the origin of a strong nonequilibrium distribution in the middle region of a driven double tunnel junction.

The knowledge of the average charge current I is not sufficient to distinguish between single and double tunnel junctions. A measurement resulting in Ohm's law $I = g_t V$ allows to infer the total conductance g_t which, however, contains only information about the system as a whole. Thus, the total conductance is not sufficient to distinguish between an opaque single tunnel junction and a double tunnel junction with more transparent junctions. However, single and double tunnel junctions differ in the following way: electrons tunnel through the whole system either in one step or in two steps, which leads to a different noise of charge current. In other words, the noise of charge current S can reveal the internal structure of a system.

In single and double tunnel junctions, charge is transported by tunneling of electrons from one system into another. For a tunneling event to occur, the state *from* which an electron tunnels has to be *filled* (otherwise, there is no electron to tunnel) and the state *into* which the electron tunnels has to be *empty* (otherwise, tunneling would be blocked by Pauli exclusion principle). In other words, tunneling of electrons depends on the distribution of electrons among the available states. Accordingly, the distribution function plays a key role in determining of the charge current and its noise. We emphasize, however, that there is not only a oneway influence of the electron distribution onto the charge transport but also vice versa. The effect of charge transport onto the distribution function is particularly important for the double tunnel junction. There a *strong* nonequilibrium electron distribution can arise, which means that the distribution is *even locally* far from equilibrium; see figure 2.2. A more precise definition of strong nonequilibrium is given in section 2.3, where internal relaxation and the approach to equilibrium are discussed.

The remainder of this thesis is based on the discussion of strong nonequilibrium and charge

transport given in this chapter. The approach taken here is rather intuitive but it is backed up by formal derivations; see appendix A. For more detailed introductions, interested readers are referred to [Blanter and Büttiker, 2000, Nazarov and Blanter, 2009a]. Readers who are familiar with both, charge transport and electron distributions far from equilibrium, might easily skip this chapter or use it as a short reminder by skimming through the figures and numbered equations.

2.1 Voltage biased single tunnel junction

In this section, a voltage-biased single tunnel junction is discussed in order to clarify the role of electron distributions for charge transport. A single tunnel junction is a thin insulating layer which is placed between two metallic leads; see figure 2.1. Classically, an insulating layer blocks the transport of electrons. Quantum mechanically, however, electrons can tunnel through the insulating layer and, thereby, go from one lead into the other. Nevertheless, due to Pauli exclusion principle, an electron can only tunnel through the junction, if an empty state is available in the other lead. Whether certain states are empty or full is described by the distribution function. Thus, knowing the leads' distribution functions is essential to determine the charge current and its noise in the single tunnel junction.

2.1.1 Description of a single tunnel junction

A single tunnel junction consists of an insulating layer which is placed between two leads; see figure 2.1. Leads are large conducting (metallic) systems with effectively noninteracting electrons and a possibility to control the distribution function externally. Here, the leads are described by their respective density of states ρ_l, ρ_r and distribution function $f_l(\omega), f_r(\omega)$, where indices l and r are for left and right. The insulating layer is characterized by $|t|^2$ which describes how transparent the layer is¹.

We assume the leads to be in (local) equilibrium. Then, their distribution functions are given by Fermi-distributions $f_l(\omega) = 1/[e^{(\omega-\mu_l)/T_l} + 1]$ and $f_r(\omega) = 1/[e^{(\omega-\mu_r)/T_r} + 1]$ with electrochemical potentials μ_l, μ_r and temperatures T_l, T_r . For simplicity, the temperatures are assumed to be equal $T_l = T_r =: T$. The electrochemical potentials are assumed to be different in both leads, which corresponds to a voltage $V = \mu_l - \mu_r$ that is applied across the junction. In turn, a charge current will flow.

2.1.2 The average charge current

The average charge current I is defined via the net transported charge Q by $\langle Q \rangle = \int dt I$ and can be guessed by simple arguments. For an electron to tunnel from left to right, it has to go from a filled state in the left lead to an empty state in the right lead. Thus, the left-to-right current $I_{l \rightarrow r}$ depends on the left lead's *density of filled states* $\rho_l f_l(\omega)$ and the right lead's *density of empty states* $\rho_r (1 - f_r(\omega))$. Assuming the tunneling to be energy conserving, the

¹The notation $|t|^2$ is motivated by the tunneling Hamiltonian approach, where the tunnel coupling is characterized by a tunneling matrix t ; see for example [Nazarov and Blanter, 2009a, Altland and Simons, 2010].

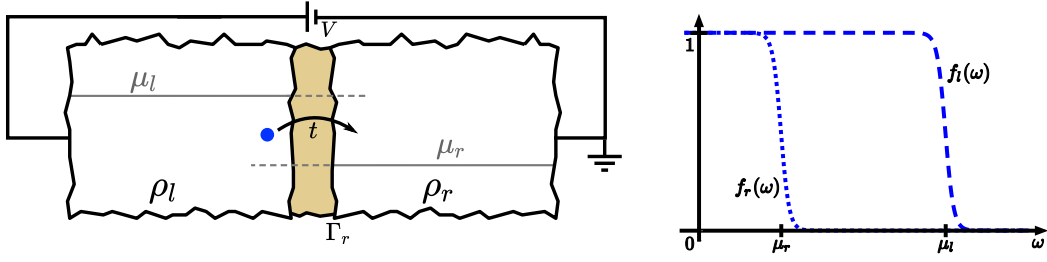


Figure 2.1: (left) Schematic representation of a single tunnel junction: two leads are tunnel-coupled to each other; the leads are characterized by their densities of states ρ_l, ρ_r and the tunnel coupling is characterized by a tunneling matrix t . With the voltage $V = \mu_l - \mu_r$ applied, electrons tunnel from the left lead to the right lead at a rate $\Gamma_r = \pi|t|^2\rho_r$. (right) The leads' equilibrium distribution functions are shown.

left-to-right current is given by $I_{l \rightarrow r} = 2\pi|t|^2 \int d\omega \rho_l f_l(\omega) \rho_r (1 - f_r(\omega))$, which is proportional to $|t|^2$ or, correspondingly, the transparency. Analogously, the right-to-left current is given by $I_{r \rightarrow l} = 2\pi|t|^2 \int d\omega \rho_r f_r(\omega) \rho_l (1 - f_l(\omega))$. The net current is now obtained as $I = I_{l \rightarrow r} - I_{r \rightarrow l}$, where we count charges flowing to the right positively and charges flowing to the left negatively. A short calculation yields the Landauer formula [Landauer, 1957],

$$I = \rho_l \Gamma_r \int d\omega [F_r(\omega) - F_l(\omega)], \quad (2.1)$$

where the densities of states have been assumed to be approximately constant and we defined the rate for left-to-right tunneling $\Gamma_r = \pi|t|^2\rho_r$ and the "new" distribution function $F_{l/r}(\omega) = 1 - 2f_{l/r}(\omega)$. Because $F_{l/r}(\omega)$ and $f_{l/r}(\omega)$ are in one-to-one correspondence, in the following we refer to both as distribution functions.

At low temperatures the Landauer formula (2.1) can be easily interpreted as follows. The integral $\frac{1}{2} \int d\omega [F_r(\omega) - F_l(\omega)] = V$ determines the energy interval in which states are filled in the left lead and empty in the right lead. Multiplied by the density of states ρ_l , this energy interval determines the number of electrons in the left lead that can tunnel into the right lead. This number, in turn, determines the charge current when multiplied by the rate Γ_r . Explicitly,

$$I = gV, \quad (2.2)$$

with the dimensionless conductance $g = 2\rho_l\Gamma_r$. In words, the average charge current is described by Ohm's law, where the conductance is determined by the density of states of the left lead and the rate for tunneling into the right lead.

2.1.3 The noise of charge current

Besides the average charge current I , we are also interested in the noise of charge current S , defined by $\langle\langle Q^2 \rangle\rangle = \langle Q^2 \rangle - \langle Q \rangle^2 =: \int dt S$. It contains additional information about the system. Because of the square in $\langle\langle Q^2 \rangle\rangle$, the left-to-right current $I_{l \rightarrow r}$ and the right-to-left current $I_{r \rightarrow l}$ both contribute positively to the noise—in contrast to the average current $I = I_{l \rightarrow r} - I_{r \rightarrow l}$. Thus,

the simplest possible guess is $S = I_{l \rightarrow r} + I_{r \rightarrow l}$ and, indeed, it turns out to be correct. It follows,

$$S = \rho_l \Gamma_r \int d\omega [1 - F_l(\omega)F_r(\omega)] . \quad (2.3)$$

We emphasize the close relation to the average charge current (2.1); the integrand $[F_l - F_r]$ turned into $[1 - F_l F_r]$. Explicitly, the noise is given by,

$$S = gV \coth(V/2T) . \quad (2.4)$$

At high temperatures ($T \gg V$), we obtain the standard thermal noise $S = 2gT$, which is also known as Johnson-Nyquist noise [Johnson, 1928, Nyquist, 1928]. At low temperatures ($T \ll V$), we obtain $S = g|V|$ which is also known as shot noise [Schottky, 1918].

The relation between signal (average current) and noise (noise of current) contains information about the physical system (single tunnel junction) that goes beyond the information contained in the signal alone [Landauer, 1998]. Quite often, this additional information can be conveniently conveyed in the noise-to-signal ratio $\mathcal{F} = S/I$ also known as Fano factor [Fano, 1947]. The Fano factor is particularly useful in the shot noise limit ($T \ll V$), where we obtain $\mathcal{F} = 1$ for the single tunnel junction. This is often interpreted as tunneling of quasi particles with *unit* charge in *single steps*. This interpretation becomes clearer in comparison to the double tunnel junction discussed in the next section.

2.2 Voltage biased double tunnel junction

In this section, a voltage biased double tunnel junction is discussed. It is shown how a strong nonequilibrium electron distribution develops and which role it plays in charge transport. For that purpose, we consider a quantum dot (zero-dimensional system) which is tunnel-coupled to two leads which are kept at different electrochemical potentials; see figure 2.2. Again, our goal is to determine the charge current and its noise, such that we can compare the double tunnel junction to the single tunnel junction discussed in the previous section.

2.2.1 Description of a double tunnel junction

We consider a quantum dot which is tunnel-coupled to two leads, see figure 2.2. The dot is characterized by its density of states ρ_d and the electrons in the dot are assumed to be effectively noninteracting. The coupling to the leads is characterized by the tunneling rates Γ_l and Γ_r . We assume the leads to be in (local) equilibrium. Then, their distribution functions are given by Fermi-distributions $f_l(\omega) = 1/[e^{(\omega - \mu_l)/T_l} + 1]$ and $f_r(\omega) = 1/[e^{(\omega - \mu_r)/T_r} + 1]$ with electrochemical potentials μ_l, μ_r and temperatures T_l, T_r . For simplicity, the temperatures are assumed to be equal $T_l = T_r =: T$. The electrochemical potentials are assumed to be different which corresponds to a voltage $V = \mu_l - \mu_r$ applied across the double tunnel junction. In turn, a charge current flows.

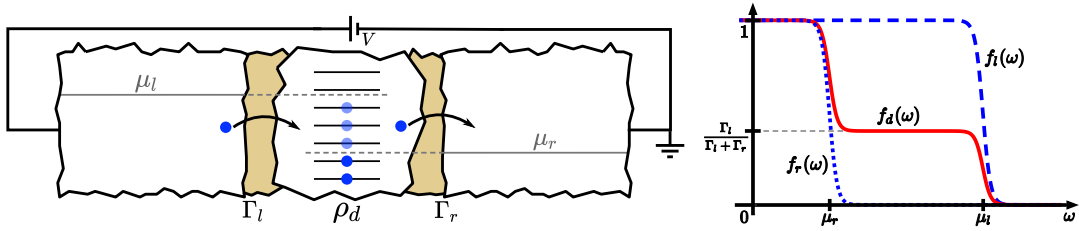


Figure 2.2: (left) This figure schematically shows a double tunnel junction: a quantum dot (zero-dimensional system) is tunnel-coupled to two normal metal leads. The quantum dot is characterized by its density of states ρ_d . The tunnel coupling to the leads is characterized by the tunneling rates Γ_l and Γ_r for left and right lead respectively. A voltage $V = \mu_l - \mu_r$ is applied, which drives the system away from equilibrium. (right) The leads' equilibrium distribution functions $f_l(\omega)$, $f_r(\omega)$ are shown in blue (dotted/dashed) and the dot's nonequilibrium distribution function $f_d(\omega)$ is shown in red (solid). The distribution function of the dot $f_d(\omega) = [\Gamma_l f_l(\omega) + \Gamma_r f_r(\omega)] / (\Gamma_l + \Gamma_r)$ is a superposition of those of the leads.

2.2.2 Average charge current and the strong nonequilibrium distribution

As far as the average charge current is concerned, a double tunnel junction can be viewed as two single tunnel junctions in series. This allows us to apply the single tunnel junction result, equation (2.1), separately to each junction. The current entering the dot through the left and right junctions are given by,

$$I_l = \rho_d \Gamma_l \int d\omega [F_d(\omega) - F_l(\omega)], \quad (2.5)$$

$$I_r = \rho_d \Gamma_r \int d\omega [F_d(\omega) - F_r(\omega)], \quad (2.6)$$

where the dot's density of states ρ_d was assumed to be approximately constant. The current through each junction depends on the distribution function of the dot $F_d(\omega) = 1 - 2f_d(\omega)$ which, however, is still unknown.

The distribution function of the dot is governed by the coupling to the leads which affects the dot in two important ways. First, it allows electrons to tunnel on or off the dot which renders the single-particle states in the dot unstable (finite lifetime); this is described by the tunneling rates Γ_l, Γ_r . Second, the leads provide heat and particle baths for the dot; this is described by the distribution functions of the leads $f_l(\omega), f_r(\omega)$. If a small system is coupled to a single heat and particle bath, it adopts the temperature and electrochemical potential of the bath. In other words, it acquires the bath's distribution function. However, if a small system is coupled to two baths with different distribution functions, it acquires a distribution function which is a "compromise" between those of the baths.

Fortunately, the dot's distribution function can be found with rather straightforward reasoning. For concreteness and simplicity, we assume the electrochemical potential of the left lead to be larger than that of the right lead $\mu_l > \mu_r$ and we assume the temperature to be much smaller than the applied voltage $T \ll V$. Starting from an arbitrary initial distribution function on the dot, we consider three energy intervals separately:

- Energy below the lower electrochemical potential $\omega < \mu_r < \mu_l$: Empty states get filled,

since electrons with the same energy are available in the leads and, thus, can tunnel into the dot. Filled states stay filled, since tunneling out of the dot is blocked by Pauli-principle.

- Energy between the electrochemical potentials $\mu_r < \omega < \mu_l$: In all states electrons are continually tunneling out of the dot into the right lead, where empty states are available. Simultaneously, electrons are continually tunneling into the dot from the left lead, where "fresh" electrons are provided. The filling factor of these states is determined by the balance between incoming electrons (rate: Γ_l) and outgoing electrons (rate: Γ_r).
- Energy above the upper electrochemical potential $\mu_r < \mu_l < \omega$: Filled states get emptied since electrons can tunnel into the leads (no Pauli-blocking). Empty states stay empty, since no electrons with these energies are available in the leads.

Thus, after the decay of transient effects, we obtain the stationary distribution function of the dot as a superposition of the leads' distribution functions,

$$F_d(\omega) = \frac{1}{\Gamma_l + \Gamma_r} [\Gamma_l F_l(\omega) + \Gamma_r F_r(\omega)] ; \quad (2.7)$$

see figure 2.2. This distribution function is often referred to as two-step distribution function; in contrast to the Fermi-distribution which would be one-step. The length of the lower step is determined by the applied voltage $V = \mu_l - \mu_r$. The height of the lower step is determined by the ratio of the tunneling rates $\Gamma_l/(\Gamma_l + \Gamma_r)$.

Knowing the dot's distribution function, we can now determine the currents flowing through each of the junctions. It follows, $I_l = \frac{\rho_d \Gamma_l \Gamma_r}{\Gamma_l + \Gamma_r} \int d\omega [F_r(\omega) - F_l(\omega)]$ for the current entering the dot from the left lead and, analogously, $I_r = \frac{\rho_d \Gamma_l \Gamma_r}{\Gamma_l + \Gamma_r} \int d\omega [F_l(\omega) - F_r(\omega)]$ for the current entering the dot from the right lead. These currents are of equal magnitude but opposite in sign $I_l = -I_r$, as required by charge conservation. Explicitly, the net current $I = I_r = -I_l$ is described by Ohm's law,

$$I = g_t V , \quad (2.8)$$

with the total dimensionless conductance $g_t = \frac{g_l g_r}{g_l + g_r}$, where $g_l = 2\rho_d \Gamma_l$ and $g_r = 2\rho_d \Gamma_r$ are the conductances of the left and right junction separately. This total conductance is the standard result for macroscopic electronics with two resistors in series. However, in strong contrast to the macroscopic case, the electron distribution of the middle region (quantum dot) is far from equilibrium.

It is important to note that, it is not possible to distinguish between single and double tunnel junctions by a measurement of the average current alone. Such a measurement yields the conductance of the whole system, but it cannot be inferred, if this total conductance arises either from a single tunnel junction or from two tunnel junctions in series. To obtain this information about the internal structure of a system, we have to go beyond the average current and consider the noise of charge current.

2.2.3 The noise of charge current

In contrast to the average current, for the noise of charge current the double tunnel junction cannot be viewed as two separate single tunnel junctions in series. Would we try to do so, we would find $S_l = -2\rho_d\Gamma_l \int d\omega [F_d(\omega)F_l(\omega) - 1] = g_l [4T + \frac{2\Gamma_r}{\Gamma_l + \Gamma_r} [V \coth(V/2T) - 2T]]$ for the noise in the left junction and $S_r = -2\rho_d\Gamma_r \int d\omega [F_d(\omega)F_r(\omega) - 1] = g_r [4T + \frac{2\Gamma_l}{\Gamma_l + \Gamma_r} [V \coth(V/2T) - 2T]]$ for the noise in the right junction. These results, however, cannot be correct. The noise would be different in both junctions $S_l \neq S_r$ which would violate charge conservation.

Charge conservation is violated in this seemingly straightforward approach, because the dot's distribution function is treated too naively. Contrary to the leads' distributions, the dot's distribution function is not externally controlled; and, therefore, cannot be assumed to be fixed or even stationary. Instead, the dot's distribution function is governed by the coupling to the leads and it is influenced by the tunneling of each single electron. A *stationary* distribution function leads to a *stationary* number of electrons in the dot. This number, however, has to change with each electron tunneling into or out of the dot. Because on *average* as many electrons tunnel into the dot as out of it, this did not create a problem for the *average* charge current. To determine the noise, however, the dot's distribution has to be considered as a dynamical object which can react to the tunneling of single electrons.

Unfortunately, there is no intuitive way to guess the correct expression for the noise. But, at least, it is straightforward to derive the correct result via counting-fields; see appendix A. For the left junction follows

$$S_l = \rho_d\Gamma_l \int d\omega \left\{ [1 - F_d(\omega)F_l(\omega)] - \frac{\Gamma_l}{\Gamma_l + \Gamma_r} [F_d(\omega)F_d(\omega) - 2F_d(\omega)F_l(\omega) + 1] \right\}. \quad (2.9)$$

The first term is analogous to the single tunnel junction case. The second term accounts for changes in the distribution function due to tunneling of electrons into or out of the dot. For the right junction follows analogously

$$S_r = \rho_d\Gamma_r \int d\omega \left\{ [1 - F_d(\omega)F_r(\omega)] - \frac{\Gamma_r}{\Gamma_l + \Gamma_r} [F_d(\omega)F_d(\omega) - 2F_d(\omega)F_r(\omega) + 1] \right\}. \quad (2.10)$$

And indeed, inserting the dot's nonequilibrium distribution (2.7) leads to $S_l = S_r$, as required by charge conservation. Besides the qualitative importance for restoring charge conservation, the correction due to the dynamic distribution function is also quantitatively important: it is of the same order as the terms obtained for a stationary distribution. Explicitly, the noise of charge current $S = S_l = S_r$ is given by,

$$S = g_t \left[2T + \frac{(\Gamma_l^2 + \Gamma_r^2)}{(\Gamma_l + \Gamma_r)^2} [V \coth(V/2T) - 2T] \right]. \quad (2.11)$$

At high temperatures ($T \gg V$), we obtain the standard thermal noise $S = 2g_t T$, known as Johnson-Nyquist noise [Johnson, 1928, Nyquist, 1928]. At low temperatures ($T \ll V$), we obtain $S = g_t |V| (\Gamma_l^2 + \Gamma_r^2) / (\Gamma_l + \Gamma_r)^2$, known as shot noise [Schottky, 1918].

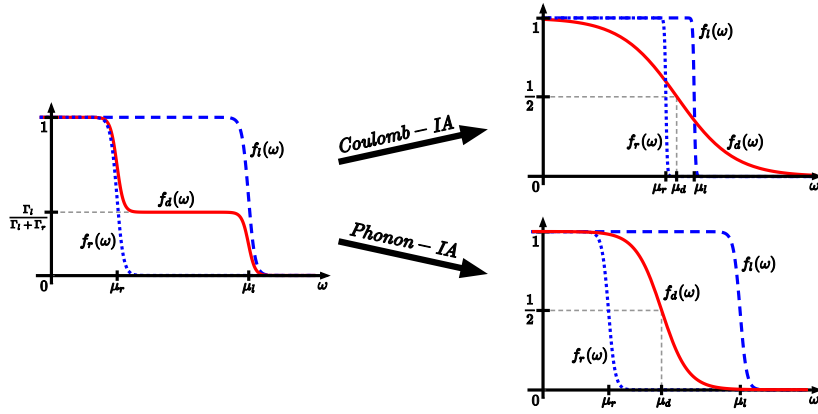


Figure 2.3: We consider relaxation via internal Coulomb interaction and via interaction with a phonon-bath. We show three limiting cases for the dot distribution function. Without internal relaxation, the distribution function of the dot will be a superposition of the lead distribution functions (left); the distribution function is so far from equilibrium (strong nonequilibrium) that electrochemical potential μ_d and temperature T_d are ill defined. In the limit of strong coupling to phonons (lower right), the electron system will adjust to the temperature of the phonon bath $T_d = T_{ph}$; the electrochemical potential will be determined by charge conservation $\mu_d = (\Gamma_l \mu_l + \Gamma_r \mu_r) / (\Gamma_l + \Gamma_r)$. In the limit of strong relaxation via Coulomb interaction (upper right), the electrochemical potential will be determined by charge conservation again $\mu_d = (\Gamma_l \mu_l + \Gamma_r \mu_r) / (\Gamma_l + \Gamma_r)$; however, the electron system cannot expel its energy to an external bath and, thus, heats up due to the driving $T_d = \mathcal{O}(|V|)$.

In the previous section, we claimed that the relation between the signal (average current) and the noise (noise of current) contains information about the physical system (double tunnel junction) that goes beyond the information contained in the signal alone [Landauer, 1998]. This additional information can be conveniently conveyed in the noise-to-signal ratio $\mathcal{F} = S/I$ known as Fano factor [Fano, 1947]. In particular in the shot noise limit ($T \ll V$)—where the Fano factor of the single tunnel junction is $\mathcal{F} = 1$ —the Fano factor of the double tunnel junction becomes $\mathcal{F} = (\Gamma_l^2 + \Gamma_r^2) / (\Gamma_l + \Gamma_r)^2$. In the special case of $\Gamma_l = \Gamma_r$, the Fano factor of the double tunnel junction becomes $\mathcal{F} = 1/2$. This is often interpreted as tunneling of quasi-particles with *unit* charge in *two-steps*, that is, through two tunnel junctions. So, even when the total conductance is the same, single and double tunnel junctions can be distinguished by a measurement of the noise of charge current.

2.3 The role of internal relaxation

In this section, we consider how internal relaxation mechanisms affect the two-step distribution function. We focus on the two limiting cases of *negligible* and *strong* internal relaxation which correspond to a *strong nonequilibrium* and an *equilibrium* distribution function. Because internal relaxation mechanisms are assumed to be negligible in the remainder of this thesis, a qualitative discussion is sufficient here. Readers interested in a more quantitative discussion along similar lines are referred to [Nazarov and Blanter, 2009b].

2.3.1 Approach to equilibrium

The two-step distribution function (2.7) was derived for the quantum dot under the assumption of vanishing internal relaxation. Internal relaxation arises from electron-phonon interaction or electron-electron interaction (Coulomb). Both interactions allow electrons to gain or lose energy and, thereby, to redistribute themselves among the available states in the dot. In turn, the distribution function is changed; see figure 2.3.

In general, interactions are expected to cause a system to relax towards equilibrium; correspondingly, towards an equilibrium distribution. To characterize the strength of internal relaxation, we introduce a generic relaxation rate Γ_{int} . This allows us to define two limiting cases: we speak of *strong nonequilibrium* when internal relaxation is negligible compared to the coupling to the leads $\Gamma_{\text{int}} \ll \Gamma_r, \Gamma_l$; and we speak of *strong internal relaxation* when the internal relaxation rate is much larger than the coupling to the leads $\Gamma_{\text{int}} \gg \Gamma_r, \Gamma_l$. In the strong nonequilibrium case, the distribution function is governed by the coupling to the leads and a two-step distribution function develops in the dot. In contrast, for strong internal relaxation an equilibrium distribution function is expected to develop in the dot $f_d^{\text{eq}}(\omega) = 1/[e^{(\omega - \mu_d)/T_d} + 1]$. However, the precise form of the equilibrium distribution, in particular the temperature, will depend on the type of internal relaxation mechanism. As two generic examples, we consider relaxation via electron-phonon interaction and via Coulomb interaction. We emphasize that the conserved quantities are different for these interactions.

2.3.2 Relaxation via coupling to phonons

By relaxation via electron-phonon interaction, the electrons in the dot can gain energy from the phonon system or they can lose energy to it. However, the number of electrons in the dot is conserved. The phonon system acts as a heat bath (temperature T_{ph}) but not as a particle bath. When the internal relaxation via phonons is strong enough ($\Gamma_{\text{int}} \gg \Gamma_l, \Gamma_r$), an equilibrium distribution function $f_d^{\text{eq}}(\omega) = 1/[e^{(\omega - \mu_d)/T_d} + 1]$ will develop. The temperature of the electrons adjusts to that of the phonon bath $T_d = T_{\text{ph}}$. In contrast, the electrochemical potential μ_d is related to the electron number and, thus, is not governed by the phonon system. Instead, it will be governed by charge conservation and the tunnel coupling to the leads which provide particle baths. Charge conservation demands the current entering from the left to be the same as the current going out to the right $I_l = -I_r$, where I_l and I_r are determined by equations (2.5) and (2.6). This leads to the electrochemical potential $\mu_d = (\Gamma_l \mu_l + \Gamma_r \mu_r)/(\Gamma_l + \Gamma_r)$, which is a superposition of the electrochemical potentials of the leads.

2.3.3 Relaxation via electron-electron interaction

By relaxation via Coulomb interaction, electrons scatter from each other and thereby redistribute their energy among the other electrons in the dot. Thus, the Coulomb interaction conserves the particle number and the total energy of the dot's electron system. In strong contrast to the electron-phonon interaction, there is no other bath than the leads. In turn, elec-

trochemical potential and temperature are governed by the coupling to the leads. Again, the electrochemical potential can be determined from charge conservation $I_l = -I_r$; it follows $\mu_d = (\Gamma_l \mu_l + \Gamma_r \mu_r) / (\Gamma_l + \Gamma_r)$. Analogously, the temperature can be determined from the conservation of the energy current [Nazarov and Blanter, 2009b]. The temperature will be of the order of the driving strength, that is, $T_d = \mathcal{O}(|V|)$; or of the order of the temperature of the leads T , if it is larger than $|V|$.

2.3.4 General remarks on internal relaxation

We emphasize that the electrochemical potential is the same for both, Coulomb interaction and coupling to phonons. This is a consequence of the conservation of particle number in both relaxation mechanisms. The major difference between Coulomb interaction and coupling to phonons is the temperature that develops in the dot. This difference arises, since the electron system's energy is conserved under electron-electron interaction but not under electron-phonon interaction.

Before concluding this section, we note that the noise of charge current is harder to determine in presence of internal relaxation. Would we use equations (2.9) and (2.10) with the equilibrium distributions obtained in the limit of strong internal relaxation, we would find $S_l \neq S_r$ which violates charge conservation. In other words, when internal relaxation is considered, the equations for the noise of charge current, (2.9) and (2.10), have to be modified further.

2.4 Summary and discussion

We have shown that it is possible to distinguish between a *single* tunnel junction and a *double* tunnel junction by their Fano factor or, correspondingly, by measuring the charge current *and* its noise. For that purpose, we derived the charge current and its noise: for the single tunnel junction we obtained equations (2.1) and (2.3); and for each junction of the double tunnel junction we obtained equations (2.5), (2.6) and (2.9), (2.10). We focused on the key role of the distribution functions for charge transport. For the double tunnel junction, particular emphasis was put on the dot's strong nonequilibrium distribution that develops when internal relaxation is absent.

Finally, we should note that, alternatively, it is possible to consider the two tunnel junctions together with the dot as a single scattering region with some total transparency. The total transparency can then be determined without any knowledge about the distribution function of the dot. Actually, this point of view is more common [Blanter and Büttiker, 2000, Nazarov and Blanter, 2009a]. However, it downgrades the role of the dot and, therefore, is less useful for the discussions in the following chapters.

Chapter 3

Noise of charge current generated by an FMR-driven itinerant ferromagnet

The study of noise is interesting from at least two points of view: in technical applications, noise can disturb the functionality of a device; in physical systems, noise can carry information about the system which cannot be obtained from average quantities [Landauer, 1998, Blanter and Büttiker, 2000, Nazarov and Blanter, 2009a]. From both points of view, technical and physical, it is valuable to develop a deeper insight into the generation of noise in any specific system: either to reduce the noise in technical applications, or to gain additional insights into a physical system. As discussed in chapter 2, a standard example for the latter is provided by single and double tunnel junctions which can be distinguished by an analysis of their noise; see also [Blanter and Büttiker, 2000, Nazarov and Blanter, 2009a]. In the field of spintronics, the study of noise can be useful to gain insights into magnetization dynamics [Foros et al., 2009, Arakawa et al., 2015, Kamra and Belzig, 2016b, Kamra and Belzig, 2016a, Cascales et al., 2015, Virtanen and Heikkilä, 2017, Aliev and Cascales, 2018].

In this chapter, we consider a small itinerant ferromagnet that is tunnel coupled to two normal metal leads and exposed to an external magnetic field, which can be used to drive the magnetization; see figure 3.1. We study the charge current and its noise, which is generated by the driven ferromagnet. We consider a situation without external bias, that is, neither voltage nor thermal bias is applied. In this unbiased situation, the average charge current vanishes by symmetry, because there is no preferred direction for charge flow. However, the noise of charge current remains and, at low temperatures, it is governed by the dynamics of the magnetization.

The ferromagnet is assumed to be small enough, such that we can use the macrospin approximation [Berkov and Miltat, 2008]. In the macrospin approximation, the magnetization is described as a single time-dependent vector $\mathbf{M} = M(\sin \theta \cos \phi, \sin \theta \sin \phi, \cos \theta)$. The magnetization length M is assumed to define the largest relevant scale in the magnet and, for simplicity, it is assumed to be constant. The angular dynamics is described phenomenologically by the Landau-Lifshitz-Gilbert (LLG) equation $\dot{\mathbf{m}} = \mathbf{m} \times \mathbf{B} - \alpha \mathbf{m} \times \dot{\mathbf{m}}$, where $\mathbf{m} = \mathbf{M}/M$ is the direction of the magnetization; see for example [Tserkovnyak et al., 2005]. The first term in the LLG equation describes the precession of the magnetization around the external magnetic field

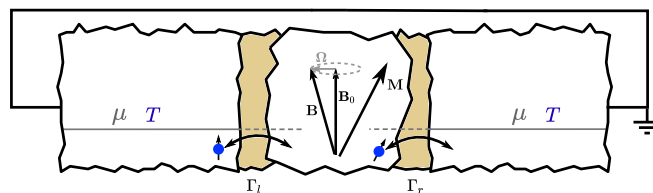


Figure 3.1: Schematic view of the system: a small ferromagnet (zero-dimensional) is tunnel-coupled to two normal metal leads. The small ferromagnet is characterized by its spin-dependent density of states ρ_σ . The tunnel coupling to the leads is characterized by the tunneling rates Γ_l and Γ_r for tunneling into the left and right lead respectively. We consider an unbiased situation, that is, neither voltage nor thermal bias is applied. Thus, electrochemical potentials and temperatures are equal in both leads $\mu := \mu_l = \mu_r$ and $T := T_l = T_r$. The magnetization dynamics drives the electron system in the small ferromagnet away from equilibrium. In turn, the small ferromagnet acquires a nonequilibrium electron distribution, despite the absence of bias.

B. The second term, known as Gilbert damping, describes the relaxation of the magnetization. Considering a small ferromagnet, we assume internal relaxation mechanisms to be negligible compared to the coupling to the leads. The Gilbert damping is then dominated by the coupling to the leads [Tserkovnyak et al., 2002], such that internal Gilbert damping can be disregarded.

The Gilbert damping tends to relax the magnetization towards its energetic minimum, which is in parallel to the external magnetic field. We consider a magnetic field with a large but constant component B_0 in one direction and, perpendicular to it, a small driving component Ω oscillating with frequency ω_d ; that is, $\mathbf{B} = (\Omega \cos \omega_d t, \Omega \sin \omega_d t, B_0)$. The oscillating part drives the magnetization away from its energetic minimum. In competition with Gilbert damping, a steady state precession develops. That is, the magnetization precesses at a constant polar angle θ with a constant frequency $\dot{\phi}$. Despite the absence of external bias, this steady state precession drives the magnet's electron system into a strong nonequilibrium state. In other words, a strong nonequilibrium distribution develops in the small ferromagnet. This nonequilibrium distribution governs the noise of charge current.

In principle, the magnet's distribution function should be determined from a kinetic equation. In practice, however, this is a hard task because of the time-dependent magnetization, which renders the effective single-particle Hamiltonian time-dependent as well. Many problems arising from this time dependence can be circumvented by changing into the rotating frame of the magnetization. In the rotating frame, the effective single-particle Hamiltonian becomes approximately time-independent, which significantly simplifies the determination of the distribution function. With internal relaxation being negligible, the rotating-frame distribution function is governed by the dynamics of the magnetization combined with the coupling to the leads. As a result, we obtain a nonequilibrium distribution function in the rotating frame, figure 3.2, which determines the noise of charge current that is generated by the precessing magnetization.

This chapter is based mainly on our publication [Ludwig et al., 2019a]. It serves as a simple introduction to the ideas discussed in this thesis and in [Ludwig et al., 2017, Ludwig et al., 2019b, Ludwig et al., 2019a] correspondingly. In particular, we discuss the influence of a dynamical magnetization (mean-field) onto the distribution function. Here—contrary to later chapters—the distribution function has no back-action onto the magnetization's angular dynam-

ics, because the leads are nonmagnetic. This allows us to determine the magnetization dynamics phenomenologically and to consider only afterwards its effects onto the distribution function. The discussion in this chapter is kept as simple as possible. Readers not satisfied by the qualitative arguments given here, will likely find answers to their open questions in later chapters; in particular chapter 5 and chapter 6.

3.1 Description of the system

Motivated by the universal Hamiltonian for metallic quantum dots [Kurland et al., 2000], the small itinerant ferromagnet is described by a simple model Hamiltonian $H_s = \sum_{\alpha\sigma} \varepsilon_\alpha c_{\alpha\sigma}^\dagger c_{\alpha\sigma} - J\hat{\mathbf{S}}^2$, where $c_{\alpha\sigma}^\dagger, c_{\alpha\sigma}$ are creation and annihilation operators for electrons in orbital states α with spin σ and corresponding orbital energy ε_α . The total spin operator is defined by $\hat{\mathbf{S}} = \frac{1}{2} \sum_{\alpha\sigma\sigma'} c_{\alpha\sigma}^\dagger \boldsymbol{\sigma}_{\sigma\sigma'} c_{\alpha\sigma}$, where $\boldsymbol{\sigma}$ is the vector of Pauli matrices. The exchange interaction $-J\hat{\mathbf{S}}^2$ tends to align spins for positive values of the exchange constant J . We assume the exchange constant to be large enough, such that the system is deep in the Stoner phase. In other words, the system can save energy by spontaneously polarizing electron spins and, in turn, a magnetization builds up on the system. To describe this situation, we use the mean-field approach¹ and approximate $-J\hat{\mathbf{S}}^2 \approx -\mathbf{M}\hat{\mathbf{S}} + \frac{M^2}{4J}$, where the magnetization $\mathbf{M} = 2J\langle\hat{\mathbf{S}}\rangle$ is the mean-field corresponding to the total spin. For simplicity, we assume the magnetization length $M = |\mathbf{M}|$ to be approximately constant, which can be justified deep in the Stoner regime, when the fluctuations of the length are small compared to the length itself. Then, the Hamiltonian of the small ferromagnet can be written as $H_s = \sum_{\alpha\sigma\sigma'} [h_s]_{\alpha\sigma\sigma'} c_{\alpha\sigma}^\dagger c_{\alpha\sigma'}$ with the effective single-particle Hamiltonian,

$$h_s = \varepsilon_\alpha - \mathbf{M}\boldsymbol{\sigma}/2, \quad (3.1)$$

where the constant term $+\frac{M^2}{4J}$ is absorbed into ε_α . The dynamics of the magnetization will be described phenomenologically below.

The leads are assumed to be normal metals. The tunnel coupling between leads and ferromagnet is characterized by the tunneling rates Γ_l, Γ_r , where l, r is for left and right. The leads provide heat and particle baths for the ferromagnet. This is characterized by the distribution functions of the leads; we assume equilibrium distributions $f_l(\omega) = 1/[\exp[(\omega - \mu_l)/T_l] + 1]$ and $f_r(\omega) = 1/[\exp[(\omega - \mu_r)/T_r] + 1]$. We consider an unbiased situation; that is, in both leads we assume equal electrochemical potentials $\mu_l = \mu_r =: \mu$ and equal temperatures $T_l = T_r =: T$.

We emphasize that, in strong contrast to the leads, the magnet's distribution function is not externally controlled and, thus, cannot be fixed by assumption. Instead, the magnet's distribution function is governed by the distribution functions of the leads jointly with the dynamics of the magnetization [Ludwig et al., 2017, Ludwig et al., 2019b, Ludwig et al., 2019a].

¹The basic operator relation for the mean-field approximation is $\hat{A}\hat{B} = [\Delta\hat{A} + \langle\hat{A}\rangle][\Delta\hat{B} + \langle\hat{B}\rangle] \approx \Delta\hat{A}\langle\hat{B}\rangle + \langle\hat{A}\rangle\Delta\hat{B} + \langle\hat{A}\rangle\langle\hat{B}\rangle = \hat{A}\langle\hat{B}\rangle + \langle\hat{A}\rangle\hat{B} - \langle\hat{A}\rangle\langle\hat{B}\rangle$, where the deviations from the expectation values $\Delta\hat{A} = (\hat{A} - \langle\hat{A}\rangle)$ and $\Delta\hat{B} = (\hat{B} - \langle\hat{B}\rangle)$ are assumed to be small in some sense and, thus, are only kept up to first order.

3.2 Phenomenological magnetization dynamics

The angular dynamics of the magnetization is phenomenologically described by the Landau-Lifshitz-Gilbert equation [Tserkovnyak et al., 2005],

$$\dot{\mathbf{m}} = \mathbf{m} \times \mathbf{B} - \alpha \mathbf{m} \times \dot{\mathbf{m}}, \quad (3.2)$$

where $\mathbf{m} = \mathbf{M}/M$ is the direction of the magnetization. The first term, $\mathbf{m} \times \mathbf{B}$, describes the precession of the magnetization around the external magnetic field. The external magnetic field is chosen to have a large constant component B_0 in one direction and, perpendicular to it, a small oscillating part with strength Ω and frequency ω_d ; explicitly $\mathbf{B} = (\Omega \cos \omega_d t, \Omega \sin \omega_d t, B_0)$. This describes a ferromagnetic resonance setup, where the oscillating part can be used to drive the magnetization. The second term of the Landau-Lifshitz-Gilbert equation $-\alpha \mathbf{m} \times \dot{\mathbf{m}}$, known as Gilbert damping, describes the damping of the magnetization due to its angular motion. Because Gilbert damping is assumed to be dominated by the coupling to the leads, the Gilbert damping coefficient is given by $\alpha = (\rho_\uparrow + \rho_\downarrow)(\Gamma_l + \Gamma_r)/(2S)$, with the magnet's spin-dependent density of states ρ_σ and spin-length $S = M/(2J)$. For an explicit discussion of the magnetization dynamics, it is convenient to change to the coordinate form of the Landau-Lifshitz-Gilbert equation,

$$\sin \theta \dot{\phi} = -\sin \theta B_0 + \cos \theta \cos(\phi - \omega_d t) \Omega - \alpha \dot{\theta}, \quad (3.3)$$

$$\sin \theta \dot{\theta} = \alpha \sin^2 \theta \dot{\phi} + \sin \theta \sin(\phi - \omega_d t) \Omega, \quad (3.4)$$

where the angles θ and ϕ characterize the magnetization direction $\mathbf{m} = (\sin \theta \cos \phi, \sin \theta \sin \phi, \cos \theta)$.

In absence of driving, $\Omega = 0$, the equations (3.3) and (3.4) reduce to $\dot{\phi} = -B_0 - \alpha \dot{\theta}/\sin \theta$ and $\dot{\theta} = \alpha \sin \theta \dot{\phi}$. Using the smallness of the Gilbert damping coefficient for large spin $\alpha \propto 1/S$, the precession frequency is approximated as $\dot{\phi} \approx -B_0$. In turn, $\dot{\theta} = -\alpha \sin \theta B_0 < 0$ and the magnetization relaxes towards the north pole ($\theta = 0$), where \mathbf{M} is aligned with \mathbf{B} .

In presence of driving, $\Omega \neq 0$, the magnetization dynamics is determined by a competition between Gilbert damping and driving field. While Gilbert damping tends to relax the magnetization towards its energetically most favourable state (aligned with the external magnetic field), the driving field excites the magnetization away from the energetic minimum. In this case, it is convenient to recast the equations of motion (3.3) and (3.4) to,

$$\dot{\varphi} = (B_0 + \omega_d) - \Omega \cot \theta \cos \varphi + \alpha \dot{\theta}/\sin \theta, \quad (3.5)$$

$$\dot{\theta} = -\Omega \sin \varphi + \alpha \omega_d \sin \theta - \alpha \sin \theta \dot{\varphi}, \quad (3.6)$$

where $\varphi = \omega_d t - \phi$ describes how much the magnetization lags behind the driving field. Introducing φ eliminates the explicit time dependence from the equations of motion. This makes it straightforward to analyze the magnetization's long-time behaviour; that is, the behaviour after the decay of transient effects. The coordinates φ and θ will relax to stationary values φ_0 and θ_0 . In the long-time limit the magnetization will, thus, precess with the frequency of the driving field $\dot{\phi}_0 = \omega_d$ and at a constant polar angle $\theta = \theta_0$. The precise stationary solutions are determined

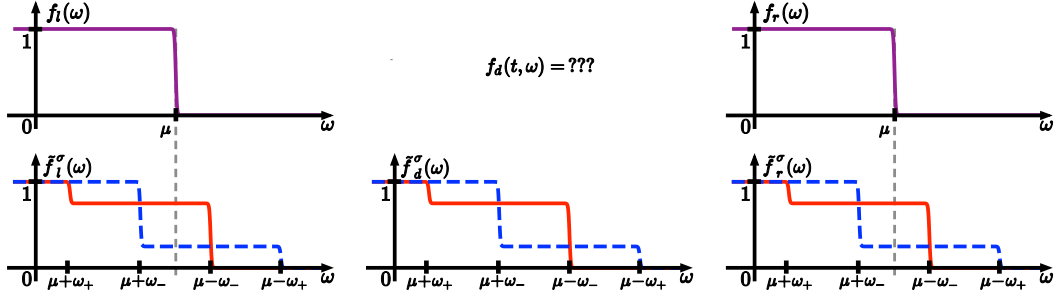


Figure 3.2: (Upper row) Illustration of the main problem: in the laboratory frame the distribution functions of the leads are known, but the distribution function of the small ferromagnet is hard to determine due to the time dependence of the magnetization. (Lower row) Illustration of the basic idea for solution. We change to the magnetization's rotating frame of reference by a time-dependent rotation in spin-space. The rotation is chosen such that the Hamiltonian becomes approximately time-independent. The leads' rotating-frame distribution functions acquire a nontrivial structure in energy- and spin-space (red solid = spin-up; blue dashed = spin-down). As the Hamiltonian is time-independent, the distribution function of the small ferromagnet becomes a superposition of the rotating-frame distribution functions of the leads. The figure is derived from a figure in [Ludwig et al., 2019a].

by $B_0 + \omega_d = \Omega \cot \theta_0 \cos \varphi_0$ and $\alpha \omega_d \sin \theta_0 = \Omega \sin \varphi_0$. Explicitly, $\sin^2 \theta_0 = \{[(B_0 + \omega_d)^2 + (\alpha \omega_d)^2 + \Omega^2]/2 - \sqrt{[(B_0 + \omega_d)^2 + (\alpha \omega_d)^2 + \Omega^2]^2/4 - \Omega^2(\alpha \omega_d)^2}\}/(\alpha \omega_d)^2$ which is shown in figure 3.3. Two stationary solutions for θ_0 arise due to the symmetry of $\sin \theta_0$ around $\theta_0 = \pi/2$: one at the northern hemisphere ($\theta_0 < \pi/2$) and one at the southern hemisphere ($\theta_0 > \pi/2$). Their stability can be analyzed by expanding the equations of motion around the stationary solutions (use $\theta = \theta_0 + \delta\theta$, $\varphi = \varphi_0 + \delta\varphi$ and expand in $\delta\theta$, $\delta\varphi$). For weak driving ($\Omega < \alpha B_0$), the stationary solutions closer to the north pole ($\theta = 0$) are stable while the other stationary solution is unstable.

In the following, we focus solely on steady state precessions of the magnetization, that is, $\theta = \theta_0$ and $\dot{\phi} = \dot{\phi}_0 = \omega_d$. For notational simplicity, we drop the index 0. The goal is to understand how the magnetization dynamics influences the electron distribution in the small ferromagnet and, thereby, the charge transport through it.

3.3 The precessing magnetization drives the electron system into a nonequilibrium state

The precessing magnetization affects the electrons in the small ferromagnet via the effective single-particle Hamiltonian (3.1). Despite the absence of voltage or thermal bias, the precessing magnetization creates a nonequilibrium situation for the electron system. In particular, the electron distribution function is driven away from equilibrium.

In principle, the electron distribution function should be determined from a (quantum) kinetic equation, which could be derived in Keldysh formalism; compare chapter 5. In practice, however, the kinetic equation will be hard to solve due to the magnetization's time dependence which transfers to the effective single-particle Hamiltonian. Instead of trying to solve the time-dependent kinetic equation, we make a transition into the rotating frame of the magnetization, which allows us to circumvent many of the complications arising from the magnetization's time

dependence.

We change to the rotating frame of reference of by performing a rotation R in spin-space, such that

$$R^\dagger \mathbf{M} \boldsymbol{\sigma} R = M \boldsymbol{\sigma}_z. \quad (3.7)$$

This rotation diagonalises the magnetic part of the Hamiltonian, equation (3.1), and makes it time independent. However, the magnetization's time dependence is transferred to the rotation operator R and, therefore, this transformation comes at a cost. A new term $Q = -iR^\dagger \dot{R}$, known as Berry-connection, is generated by the time-derivative in the Schrödinger equation. The rotating-frame single-particle Hamiltonian becomes,

$$\tilde{h}_s = \varepsilon_\alpha - M \frac{\boldsymbol{\sigma}_z}{2} + Q. \quad (3.8)$$

It is very important to note that, besides the Hamiltonian, the distribution functions have to be rotated. The rotating-frame distributions of the leads are given by²

$$\tilde{f}_{l/r}(t, t') = R^\dagger(t) f_{l/r}(t - t') R(t'), \quad (3.9)$$

where $f_{l/r}(t - t')$ are the inverse Fourier-transforms $\omega \rightarrow (t - t')$ of the leads' laboratory-frame distribution functions $f_{l/r}(\omega)$.

Motivated by [Shnirman et al., 2015], we choose an explicit Euler-angle representation for the rotation $R = e^{-i\frac{\phi}{2}\sigma_z} e^{-i\frac{\theta}{2}\sigma_y} e^{i\frac{\chi}{2}\sigma_z}$, where χ is a gauge-freedom. For the Berry-connection follows $Q = Q_\parallel + Q_\perp$, with the spin-diagonal contribution $Q_\parallel = [\dot{\phi}(1 - \cos\theta) - \dot{\chi}] \frac{\boldsymbol{\sigma}_z}{2}$ and the spin-off-diagonal contribution $Q_\perp = e^{i\chi\sigma_z} \dot{\phi} \sin\theta \frac{\boldsymbol{\sigma}_x}{2} e^{i\phi\sigma_z}$. The spin-diagonal contribution Q_\parallel carries information about the Berry-phase. In other words, Q_\parallel gives an additional splitting of energies between spin-up and spin-down states, which is governed by the magnetization dynamics. However, analogously to [Shnirman et al., 2015], Q_\parallel is eliminated from the Hamiltonian \tilde{h}_s by fixing the gauge-freedom to $\chi = \dot{\phi}(1 - \cos\theta)$. The spin-off-diagonal contribution Q_\perp carries information about (Landau-Zener) transitions between spin-up and spin-down states. These transitions are suppressed by the large length of magnetization M . In turn, we disregard them. The rotating-frame Hamiltonian is reduced to

$$\tilde{h}_s \approx \varepsilon_\alpha - M \frac{\boldsymbol{\sigma}_z}{2}, \quad (3.10)$$

which is diagonal in spin-space and constant in time. Similarly, the large magnetization allows us to disregard spin-off-diagonal parts of the rotating-frame distribution functions. For the remaining spin-diagonal parts $\tilde{f}_{l/r}^\sigma(\omega) := [\tilde{f}_{l/r}]_{\sigma\sigma}(\omega)$ of the leads' rotating-frame distribution

²A distribution function is a two time-quantity. It necessarily depends on frequency, as it contains information at which energy levels are filled. But a distribution function may also depend on time. Thus, $f(\tilde{t}, \omega)$ is a proper form, where \tilde{t} is interpreted as a Wigner-mean-time-coordinate and, in turn, ω is the frequency corresponding to time-differences. Thus, for the leads' distribution functions follows $f_{l/r}(\omega) \rightarrow f_{l/r}(t - t')$. The spin-space rotations R^\dagger, R are one-time objects. So, equation (3.9) is a natural guess for the rotating-frame distribution function. This guess is confirmed by formal derivations in chapters 5 and 6.

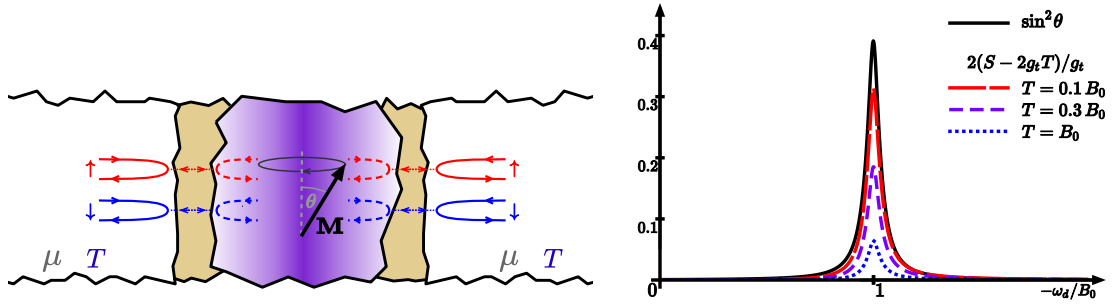


Figure 3.3: (left) The small ferromagnet acts as a spin-fountain [Tserkovnyak et al., 2002, Brataas et al., 2002, Tserkovnyak et al., 2005], that is, it expels spin-up electrons and attracts spin-down electrons. In each junction separately, the spin-resolved charge currents balance each other such that the average charge current vanishes. However, the fluctuations of the spin-resolved charge currents can differ from each other, giving rise to noise of charge current. The left subfigure is reprinted (with aesthetic modifications) from [Ludwig et al., 2019a]. (right) We show the stationary solution for the polar angle θ as $\sin^2 \theta$ in dependence on the driving frequency ω_d . The peak at $\omega_d = -B_0$ is typical for ferromagnetic resonance. We also show the noise of charge current for different temperatures. For better comparability, we subtracted the thermal part $S = 2g_t T$ and divided by the total conductance g_t ; and we multiplied by 2. At low temperatures (red long-dashed), the noise of charge current clearly resembles the FMR-peak. But even at higher temperatures (purple dashed, blue dotted), the FMR-structure is still visible. The right subfigure is reprinted (with slight modifications) from [Ludwig et al., 2019a]; the naming of the x -axis is changed, and (because of a differently defined S) factors of 2 are changed for the noise.

functions follows

$$\tilde{f}_{l/r}^\sigma(\omega) = \cos^2 \frac{\theta}{2} f_{l/r}(\omega + \sigma \omega_-) + \sin^2 \frac{\theta}{2} f_{l/r}(\omega + \bar{\sigma} \omega_+), \quad (3.11)$$

where $\bar{\sigma}$ denotes the spin-polarization opposite to σ . The specific choice of gauge χ did not eliminate the Berry-phase altogether, but rather transferred it from the Hamiltonian to the distribution functions, where it is contained in $\omega_\pm = \dot{\phi}(1 \pm \cos \theta)/2$.

Changing to the rotating frame makes both, the spin-diagonal part of the leads' distribution functions and the magnet's Hamiltonian, time-independent. In turn, the magnet's distribution function is given by a superposition of the leads' distribution functions. For the spin-diagonal part of the distribution function of the small ferromagnet it follows in general

$$\tilde{f}_s^\sigma(\omega) = [\Gamma_l \tilde{f}_l^\sigma(\omega) + \Gamma_r \tilde{f}_r^\sigma(\omega)] / \Gamma_\Sigma, \quad (3.12)$$

where we defined $\Gamma_\Sigma = \Gamma_l + \Gamma_r$; compare chapter 2. In absence of bias, the distribution functions of the leads are equal $\tilde{f}_l^\sigma(\omega) = \tilde{f}_r^\sigma(\omega)$. In turn, the distribution functions are equal in all three systems $\tilde{f}_s^\sigma(\omega) = \tilde{f}_l^\sigma(\omega) = \tilde{f}_r^\sigma(\omega)$; this is illustrated in figure 3.2.

3.4 Charge current and its noise

Knowing the small ferromagnet's distribution function, we are in position to determine the charge current and its noise. For a double tunnel junction, the average charge current can be determined from the Landauer-formula (2.5) and the noise of charge current can be determined from the associated noise-formula (2.9). One should be a little careful, though, as the magnet's

distribution function is only known in the rotating frame. Thus, we need to find the rotating-frame equivalent of the Landauer-formula (2.5) and the associated noise formula (2.9). Fortunately, a simple physical argument leads to the correct result: the charge current and its noise are observables which have to be independent of the frame of reference and, in turn, the structures of the formulas for charge current and its noise remain intact in the rotating frame; only the distribution functions have to be replaced by their rotating-frame versions. For the charge current follows,

$$I_l = \sum_{\sigma} \rho_{\sigma} \Gamma_l \int d\omega [\tilde{F}_l^{\sigma}(\omega) - \tilde{F}_s^{\sigma}(\omega)], \quad (3.13)$$

and for the noise follows,

$$S_l = \sum_{\sigma} \rho_{\sigma} \Gamma_l \int d\omega \left\{ [1 - \tilde{F}_s^{\sigma}(\omega) \tilde{F}_l^{\sigma}(\omega)] - \frac{\Gamma_l}{\Gamma_{\Sigma}} [\tilde{F}_s^{\sigma}(\omega) \tilde{F}_s^{\sigma}(\omega) - 2\tilde{F}_s^{\sigma}(\omega) \tilde{F}_l^{\sigma}(\omega) + 1] \right\}, \quad (3.14)$$

where $\tilde{F}_{s/l}^{\sigma}(\omega) = 1 - 2\tilde{f}_{s/l}^{\sigma}(\omega)$ and we assumed the density of states ρ_{σ} and the tunneling rates Γ_l, Γ_r to be independent of energy. Spin-off-diagonal contributions are disregarded, as they are suppressed by the large magnetization-length M . For the right junction, the results are analog with the replacements $\Gamma_l \rightarrow \Gamma_r$ and $\tilde{F}_l^{\sigma}(\omega) \rightarrow \tilde{F}_r^{\sigma}(\omega) := 1 - 2\tilde{f}_r^{\sigma}(\omega)$. As can be checked explicitly, the charge current and its noise are equal in both junctions, that is, $I := I_l = -I_r$ and $S := S_l = S_r$, which is required by charge conservation (at zero-frequency). In absence of bias, the average charge current vanishes,

$$I = 0 \quad (3.15)$$

The noise, however, remains

$$S = 2g_t T + g_t \sin^2 \theta \left(\dot{\phi} \coth \frac{\dot{\phi}}{2T} - 2T \right) / 2, \quad (3.16)$$

with the total conductance $g_t = \sum_{\sigma} 2\rho_{\sigma} \frac{\Gamma_l \Gamma_r}{\Gamma_l + \Gamma_r}$. At high temperature ($T \gg |\dot{\phi}|$), we obtain the usual thermal noise $S \approx 2g_t T$. At low temperatures ($T \ll \sin^2 \theta |\dot{\phi}|$), however, the noise remains $S = g_t \sin^2 \theta |\dot{\phi}|$ despite the absence of average charge current. This noise is proportional to the precession (frequency) of the magnetization $|\dot{\phi}|$, which drives the electron system. In the sense of being proportional to driving, the low temperature noise is of the shot noise type. However, in contrast to many other instances of shot noise, the Fano factor (noise-to-signal ratio) is infinite $\mathcal{F} = S/I = \infty$ even in the limit of zero temperature. This can be understood as follows. The precessing magnetization drives spin-up electrons out of the magnet and attracts spin-down electrons into it [Tserkovnyak et al., 2002, Brataas et al., 2002]. As far as the charge current is concerned, the average spin-up and spin-down currents cancel each other—separately for each junction—which leads to a vanishing charge current. However, these spin-resolved charge currents fluctuate separately in each junction and for each spin-polarization. These fluctuations give rise to the shot noise of the charge current; see figure 3.3.

Because the noise is governed by the precessing magnetization, it contains information about the magnetization dynamics. In particular for FMR-experiments at low temperatures, the noise

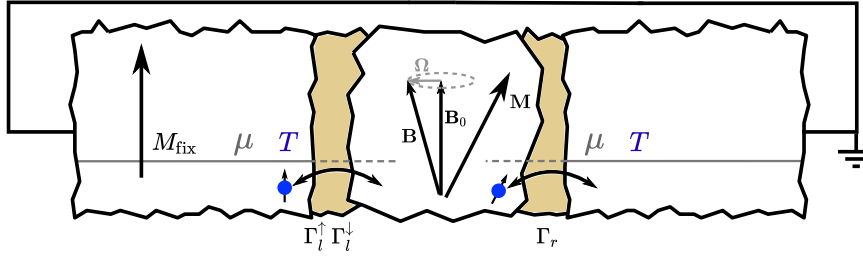


Figure 3.4: This figure schematically shows a magnetic (double) tunnel junction: a small ferromagnet (zero-dimensional) is tunnel-coupled to two leads, where one lead is a ferromagnet itself. The tunnel coupling to the leads is characterized by the tunneling rates Γ_l^\uparrow and Γ_l^\downarrow , where the tunneling rate to the magnetic lead becomes spin-dependent due to the lead's spin-dependent density of states. Even without external bias, the dynamics of the magnetization not only drives the electron distribution away from equilibrium but also pumps charge current and spin current through the system.

of charge current clearly resembles the peak structure of the ferromagnetic resonance; see figure 3.3. From this point of view, it would be very interesting to generalize the approach to magnetic tunnel junctions. In other words, we would like to consider a similar system but with one lead being magnetic. Unfortunately, this generalization is far from straightforward.

3.5 A generalization to magnetic tunnel junctions is not straightforward

The generalization to a magnetic tunnel junction, figure 3.4, is not straightforward because the magnetization dynamics and the distribution function become interdependent. This interdependence is based on the interplay of three effects:

- A dynamic magnetization in steady state precession acts as a spin-fountain and emit spin-currents into the adjacent leads [Tserkovnyak et al., 2002, Brataas et al., 2002, Tserkovnyak et al., 2005]; with one lead being magnetic, this will be accompanied by a charge current [Tserkovnyak et al., 2008].
- The magnetic tunnel junction acts as a spin-filter and, thereby, a charge current flowing through the whole system is accompanied by a spin-current [Moosera et al., 2007].
- A flowing spin-current influences the magnetization dynamics of the small ferromagnet via the spin-transfer-torque [Slonczewski, 1996, Berger, 1996].

In short: the precession of the magnetization induces a spin-current which affects the precession of the magnetization. Thus, we cannot repeat the previous approach. Instead, the magnetization-dynamics has to be determined in a self-consistent way; see chapters 5 and 6.

3.6 Summary and discussion

We have determined the noise of charge current that is generated by a ferromagnet with a magnetization in a steady state precession. The precessing magnetization drives the electron system into a nonequilibrium state. The associated nonequilibrium distribution gives rise to the noise of charge current. Interestingly, this noise remains finite at low temperature, despite the absence of an average charge current. The noise, being governed by the precessing magnetization, contains useful information about its dynamics. This was explicitly demonstrated for the ferromagnetic resonance setup at low temperatures.

Finally, we discussed why the generalization to a magnetic tunnel junction is not straightforward: a phenomenological description of the magnetization dynamics would fail because of its interplay with the nonequilibrium electron distribution. Thus, a self-consistent description of the magnetization dynamics is necessary. Such a self-consistent description is discussed in chapters 5 and 6; the resulting equation of motion is extensively discussed in chapter 7.

Part II

Dynamical interplay between mean-fields and electron distributions far from equilibrium

Chapter 4

Dynamical interplay between electrical potential and electron distribution

For the description of charge transport, the electron distribution plays a key role. In equilibrium, the distribution function is characterized by an electrochemical potential and a temperature. Far from equilibrium, however, the distribution function becomes more complicated. Specifically in interacting systems, an interplay sets in between distribution function and interaction. The goal of this chapter is to discuss and understand this interplay for a driven system with Coulomb interaction.

For that purpose, we consider a quantum dot with Coulomb interaction which is tunnel-coupled to two normal metal leads; see figure 4.1. In other words, we consider a double tunnel junction with a small (0-dimensional) region between the two junctions in which the electrons are interacting via Coulomb repulsion. The leads are assumed to be in local equilibrium with electrochemical potentials μ_l, μ_r and temperatures T_l, T_r , where l, r is for left lead and right lead respectively. The system can be driven out of equilibrium by application of a voltage bias $V = \mu_l - \mu_r$; for simplicity, we assume the temperatures to be equal in both leads $T_l = T_r = T$. The Coulomb interaction gives rise to an electrical potential, which can be viewed as the mean-field corresponding to the Coulomb interaction. From this point of view, the electrical potential is determined by the dot's capacity C combined with the number of electrons on the dot (minus background charges).

The electrical potential fluctuates when electrons tunnel into or out of the dot, which is possible at finite temperature or when a voltage is applied. In any case, the electrical potential fluctuates around a stationary optimal value, provided that the external conditions (voltage and temperature) are fixed. When deviating from this optimal value, the electrical potential relaxes back to it. This relaxation process is associated with a flow of charge current through the tunnel junctions (resistors). From a classical perspective, such a relaxation process is described by the RC -relaxation law; that is, $\delta\dot{V}_d = -\frac{1}{RC}\delta V_d$, where δV_d is the deviation from the optimal electrical potential, R is the resistance of the tunnel junctions (parallel), and C is the electrical capacity of the dot. From a quantum perspective, however, the RC -relaxation law is incomplete. While the capacity C accounts for the Coulomb repulsion, it misses out on the repulsion due to

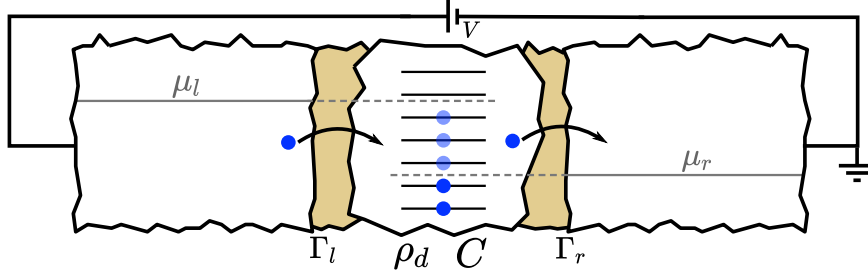


Figure 4.1: Schematic view of the system: a quantum dot (zero-dimensional system) is tunnel-coupled to two normal metal leads. The dot is characterized by its single-particle density of states ρ_d and by its electrical capacity C . The coupling to the leads is characterized by the tunneling rates Γ_l and Γ_r for tunneling into the left and right lead respectively. A voltage can be applied across the system when the leads' electrochemical potentials μ_l, μ_r are different. For simplicity, the temperatures are assumed to be equal in both leads.

Pauli principle. According to Pauli principle, two electrons cannot simultaneously occupy the same state. Thus, an additional electron entering the dot has to fill an unoccupied state which, then becomes occupied. In other words, the distribution function changes with the tunneling of electrons. The effective chemical potential has to increase by the level spacing, correspondingly, by the inverse density of states $1/\rho_d$. In result, when an electron tunnels into or out of the dot, then the net change in electrochemical potential has two contributions: first, the electrical potential is increased by $\frac{1}{C}$ due to Coulomb repulsion; second, the effective chemical potential is increased by $1/\rho_d$ due to Pauli principle. In short, the electrochemical potential is increased by $\frac{1}{C} + \frac{1}{\rho_d}$; see figure 4.4. As the difference in electrochemical potentials determines the flow of charge current, the RC -relaxation law is changed to $\delta\dot{V}_d = -\frac{1}{RC^*} \delta V_d$, where the capacity is changed to $\frac{1}{C^*} = \frac{1}{C} + \frac{1}{\rho_d}$. In this context, the density of states ρ_d is also known as quantum capacity [Büttiker et al., 1993] and, as demonstrated below, it is intimately related to the change in distribution function. Formally, the quantum capacity emerges from the dynamical interplay between electrical potential and electron distribution.

This chapter is based on the method which we developed in references [Ludwig et al., 2017, Ludwig et al., 2019b]. The method developed there can be considered as a strong nonequilibrium version of the Ambegaokar-Eckern-Schön approach [Ambegaokar et al., 1982, Eckern et al., 1984] and its $SU(2)$ -generalization developed in [Shnirman et al., 2015]. Here, we closely follow [Ludwig et al., 2019b], which contains the discussion of this chapter as a subproblem. In contrast to references [Ludwig et al., 2017, Ludwig et al., 2019b], in this chapter we focus only on Coulomb-repulsion and shift the more involved discussion of exchange interaction into the next two chapters. The upside of this separate discussion is a more accessible presentation of the method, whereas the downside is that we apply "heavy machinery" (Keldysh formalism) to derive a small correction (quantum capacity) which has been explained above in a single paragraph. However, the detailed derivation of the quantum capacity pays off in the next chapter about exchange interaction, where an inclusion of the quantum capacity is absolutely essential for a consistent description of the dynamical magnetization length.

4.1 Description of the system

We consider a quantum dot (0-dimensional system) which is tunnel-coupled to two normal metal leads; see figure 4.1. The electrons in the dot are assumed to interact via Coulomb interaction. The system can be driven away from equilibrium by application of a voltage or thermal bias across the dot; but, for simplicity, the temperatures are assumed to be equal in both leads.

4.1.1 Hamiltonian, tunneling rates, and distribution functions

Motivated by the universal Hamiltonian for metallic quantum dots [Kurland et al., 2000], the quantum dot is modelled by the Hamiltonian

$$H_d = \sum_{\alpha} \varepsilon_{\alpha} c_{\alpha}^{\dagger} c_{\alpha} + E_c (\hat{N} - N_0)^2, \quad (4.1)$$

where $c_{\alpha}^{\dagger}, c_{\alpha}$ are creation and annihilation operators for electrons in single-particle states α with corresponding energy ε_{α} . The charging interaction $E_c (\hat{N} - N_0)^2$ accounts for the Coulomb-repulsion, where the charging energy $E_c = \frac{1}{2C}$ is determined by the electrical capacity C , $\hat{N} = \sum_{\alpha} c_{\alpha}^{\dagger} c_{\alpha}$ is the operator for the total electron number, and N_0 accounts for the positive background charge.

The leads are assumed to be effectively noninteracting systems and the tunneling between leads and dot is assumed to be spin-conserving. Here, the leads are described via their effects onto the dot; a more detailed description of the leads is given in appendix A. The dot is affected by the tunnel coupling to the leads in two important ways. *As a first effect*, the tunnel coupling allows electrons to tunnel into and out of the dot and, thereby, gives rise to a finite lifetime for electron-states in the dot. This effect is described by rates Γ_l, Γ_r for tunneling into the left and right lead respectively. We assume the tunneling rates Γ_l, Γ_r to be independent of the states in the dot which is justified for many channels in each lead that are weakly and randomly coupled to the states in the dot [Ludwig et al., 2017]; see also appendix A. *As a second effect*, the leads provide heat and particle baths for the dot. This is described by the distribution functions of the leads $f_l(\omega), f_r(\omega)$. The distribution functions of the leads are directly controlled, such that we can assume them to be fixed to equilibrium: $f_l(\omega) = 1/[e^{[\omega - \mu_l]/T_l} + 1]$ for the left lead and $f_r(\omega) = 1/[e^{[\omega - \mu_r]/T_r} + 1]$ for the right lead. For simplicity, we assume the leads to have the same temperature $T_l = T_r := T$. The electrochemical potentials μ_l, μ_r are allowed to be different, such that a situation with voltage bias $V = \mu_l - \mu_r$ can be described.

We emphasize that, in contrast to the leads, the distribution function of the quantum dot cannot be controlled directly. Thus, we cannot assume its distribution function to be fixed to any specific distribution. Instead, the dot's distribution function has to be determined jointly from the coupling to the leads, their distribution functions, and the interactions of the electrons in the dot.

4.1.2 The effective action for the electrical potential

When a voltage is applied across the double tunnel junction, the system is driven into a nonequilibrium state. To describe this situation, we employ the Keldysh formalism in its path-integral version [Kamenev and Levchenko, 2009, Kamenev, 2011, Altland and Simons, 2010]. The Keldysh generating function is $\mathcal{Z} = \int D[\bar{\Psi}, \Psi] e^{i\mathcal{S}}$, with the action formally given by $\mathcal{S} = i \oint_K dt [\bar{\Psi} i\partial_t \Psi - H(\bar{\Psi}, \Psi)]$. Here, $\bar{\Psi}, \Psi$ denote all fermionic fields and $H(\bar{\Psi}, \Psi)$ is the full Hamiltonian which should include the leads and the tunnel coupling. As the electrons in the leads are assumed to be noninteracting, they can be integrated out immediately; see appendix A. For the resulting action of the dot follows

$$\mathcal{S} = \oint_K dt [\bar{\Psi} (i\partial_t - \hat{\Sigma}) \Psi - H_d(\bar{\Psi}, \Psi)] , \quad (4.2)$$

where from now on $\bar{\Psi}, \Psi$ denote the fermionic fields of the dot only. Furthermore, we defined the self-energy operator $\hat{\Sigma}$ by $\hat{\Sigma}\Psi(t) = \oint dt' \Sigma(t-t')\Psi(t')$. This operator includes the information about the coupling to the leads in the self-energy $\Sigma = \Sigma_l + \Sigma_r$, where Σ_l and Σ_r arise respectively from the coupling to the left and right lead. The tunneling rates are contained in the self-energy's retarded and advanced part $\Sigma^{R/A}(\omega) = \mp i(\Gamma_l + \Gamma_r)$. The leads' distribution functions are contained in the self-energy's Keldysh part $\Sigma^K(\omega) = -2i(\Gamma_l F_l(\omega) + \Gamma_r F_r(\omega))$, where $F_{l/r}(\omega) = 1 - 2f_{l/r}(\omega)$. We refer to $F_{l/r}(\omega)$ also as distribution function, since it is in one-to-one correspondence with $f_{l/r}(\omega)$.

The charging interaction renders the action (4.2) quite nontrivial. To proceed, this interaction is decoupled by a Hubbard-Stratonovich transformation based on the identity

$$e^{-iE_C \oint_K dt (N-N_0)^2} = \int DV_d e^{i \oint_K dt \left[\frac{V_d^2}{4E_C} - V_d(N-N_0) \right]} . \quad (4.3)$$

The Keldysh partition function becomes $\mathcal{Z} = \int D[\bar{\Psi}, \Psi] \int DV_d e^{i\mathcal{S}}$, where the new action is given by

$$\mathcal{S} = \oint_K dt \bar{\Psi} \left[i\partial_t - \underbrace{(\epsilon_\alpha + V_d)}_{h_d} - \hat{\Sigma} \right] \Psi + \underbrace{\oint_K dt \left(\frac{V_d^2}{4E_C} + V_d N_0 \right)}_{\mathcal{S}_{\text{HS}}} . \quad (4.4)$$

The Hubbard-Stratonovich (HS) action \mathcal{S}_{HS} describes the "free" Hubbard-Stratonovich field V_d . The HS-field V_d couples to the underlying electron system via h_d , which is the effective single-particle Hamiltonian for electrons in the dot. Because the HS-field V_d couples to the charge operator ($\hat{N} - N_0$) exactly like an electrical potential, we refer to V_d as the dot's electrical potential.

We emphasize that the distribution function of the dot does not explicitly appear in the action (4.4), even though this action contains all necessary information about the dot's distribution. Knowing the distribution function is important, as it crucially influences the dynamics of the electrical potential V_d . However, this influence is not only in one-way. Instead, the dot's electron distribution and the dynamics of its electrical potential are strongly interdependent. This

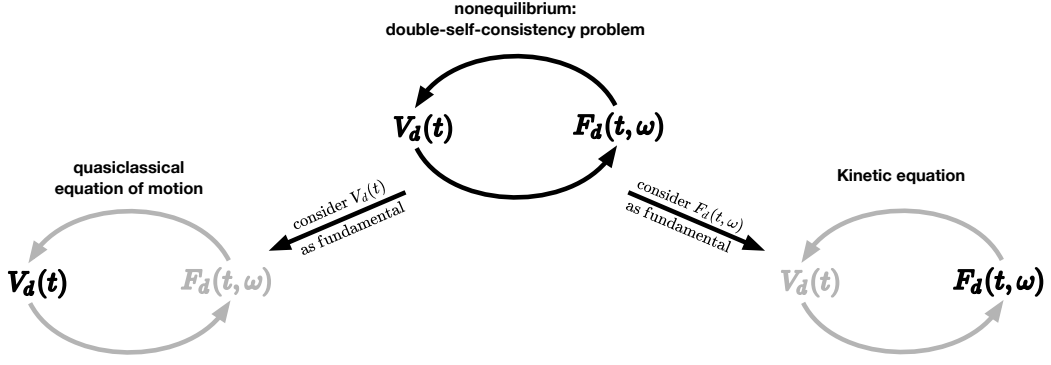


Figure 4.2: Far from equilibrium a double-self-consistency problem arises: both, the dynamical mean-field $V_d(t)$ and the dynamical distribution function $F_d(t, \omega)$, have to be self-consistent. The double-self-consistency problem can be resolved into a "standard" self-consistency problem by declaring either the mean-field or the distribution function to be fundamental while treating the other object as an auxiliary quantity. If one treats the distribution function as fundamental, one would need to derive a kinetic equation for $F_d(t, \omega)$, where $V_d(t)$ plays only an auxiliary role. The view taken in this thesis is the opposite one: The mean-field is considered to be the fundamental object; its dynamics is determined by an equation of motion which, however, is influenced by the distribution function.

interdependence is demonstrated in the following, where we derive the quasiclassical equation of motion for V_d while putting a special focus on the role of the electron distribution function.

4.2 Self-consistency equation for the dynamical electrical potential

Being mainly interested in the dynamics of the electrical potential, we integrate out the fermionic fields. This integration is straightforward, as the HS-transformation made the action (4.4) quadratic in fermionic fields. The resulting determinant is re-exponentiated to obtain $\mathcal{Z} = \int DV_d e^{i\mathcal{S}}$ with the new action

$$\mathcal{S} = -i \text{tr} \ln \left[\underbrace{i\partial_t - h_d - \Sigma}_{G^{-1}} \right] + \mathcal{S}_{\text{HS}} , \quad (4.5)$$

where G^{-1} defines the effective single-particle Green's function G . The dominating contributions to the Keldysh partition function are determined by the saddle-points of the action \mathcal{S} . In other words, the most relevant trajectories of V_d are determined by the corresponding saddle-point equation. At first glance, it might appear strange to consider the dominating contributions to the Keldysh partition function, as $\mathcal{Z} = 1$ by construction of the Keldysh formalism. However, the trajectories dominating \mathcal{Z} will also be dominant in most observables which only modify the pre-exponential factor.

Among all types of saddle-points, the quasiclassical saddle-point is particularly important. Formally, it is defined by the variation of the action (4.5) with respect to the quantum component. Thus, the quasiclassical saddle-point equation is given by $\left. \frac{\delta \mathcal{S}}{\delta V_d^q(t)} \right|_{q=0} = 0$, where $\dots|_{q=0}$ means to set quantum components to zero. A direct variation leads to

$$CV_d^c(t) = -\frac{i}{2} \text{tr} [G_c(t, t)] - N_0 , \quad (4.6)$$

where the classical Green's function G_c has to be determined from its inverse defined by $G_c^{-1} = G^{-1}|_{q=0}$. The expression $-\frac{i}{2} \text{tr}[G_c(t, t)]$ determines the number of electrons on the dot. Basically, equation (4.6) determines the dot's electrical potential $V_d^c(t)$ in terms of its electrical capacity C and the number of charges on the dot $-\frac{i}{2} \text{tr}[G_c(t, t)] - N_0$. Because the classical Green's function G_c depends on the electrical potential V_d^c , equation (4.6) is a self-consistency equation for the electrical potential V_d^c . To be more precise, the classical Green's function is a functional of the electrical potential $G_c[V_d^c]$ and depends on the past values of V_d^c . Thus, equation (4.6) determines the present value of V_d^c by the past values of V_d^c . In other words, this equation is the quasiclassical equation of motion for the dot's electrical potential.

Unfortunately, it is not easy to obtain an explicit form of the quasiclassical equation of motion (4.6). The difficulties arise due to the interdependence of the electrical potential V_d^c and the distribution function of electrons in the dot $F_d(\bar{t}, \omega)$, which is contained in the Keldysh part of the Green's function G_c . In other words, the electrical potential V_d^c depends on the distribution function $F_d(\bar{t}, \omega)$ which, however, depends on the (history of) the electrical potential V_d^c ; see figure 4.2. Several strategies exist to deal with such an interdependence. At first, one should decide if the distribution function or the electrical potential (HS-field) is considered to be the fundamental object. One could determine the full fermionic Green's function directly from the action (4.4). This would lead to a kinetic equation, where the distribution function F_d is the fundamental object and the electrical potential V_d takes only an auxiliary role. However, by integrating out the fermionic fields, we have already decided for the alternative of treating the electrical potential as fundamental. The distribution function F_d is then only an auxiliary object which is enslaved to the dynamics of V_d^c . As a result, we obtained the self-consistency equation (4.6).

Independent of the first decision about the fundamental object, one has to decide between a recursive and a self-consistent approach. In a recursive approach, we would start from a guessed trajectory of the electrical potential and use it to determine the distribution function. The distribution function would then be used to determine a new trajectory of the electrical potential. This process would then be repeated again and again for the resulting trajectory. If one is lucky, this approach converges to the correct result. A recursive approach is often preferable in numerical calculations; see for example [Mahfouzi, 2014]. In this thesis, however, we want to proceed analytically. For that purpose, a self-consistent approach is much more suitable. Instead of starting from a given trajectory, we do not assume any specific trajectory, we determine the classical Green's function $G_c[V_d^c]$ under rather general assumptions. In turn, we find an explicit form of the equation of motion (4.6). Finally, we have to check, if the assumptions are consistent with the dynamics described by the explicit equation of motion. In short: we have to check our assumptions for self-consistency.

For the problem at hand, it is possible to proceed in a direct way. However, it is instructive to pursue a different approach of the AES-type [Ambegaokar et al., 1982, Eckern et al., 1984], which turns out to be much more powerful for exchange interaction as considered in chapters 5 and 6.

4.3 Gauge-transformation

The classical Green's function is hard to determine because of the electrical potential, which makes the effective single-particle Hamiltonian time-dependent. Following the Ambegaokar-Eckern-Schön-idea [Ambegaokar et al., 1982, Eckern et al., 1984], we perform a gauge-transformation to make h_d time-independent. For that purpose, we go back to the action (4.4) and perform a $U(1)$ -gauge-transformation (in short: rotation) for the fermionic fields $\Psi \rightarrow U\Psi$ and $\bar{\Psi} \rightarrow \bar{\Psi}U^*$ with

$$U = e^{-i\psi} , \quad (4.7)$$

where ψ is a gauge field and should not be confused with the fermionic fields $\bar{\Psi}, \Psi$. The gauge field ψ can be an arbitrary differentiable function of time; only the boundary conditions on the Keldysh contour should be respected. We exploit this freedom of ψ below. Integrating out fermions again, leads to

$$\mathcal{S} = -i \text{tr} \ln \left[\underbrace{U^* (i\partial_t - h_d - \Sigma) U}_{\tilde{G}^{-1}} \right] + \mathcal{S}_{\text{HS}} , \quad (4.8)$$

where \tilde{G}^{-1} defines the gauge-transformed Green's function \tilde{G} . More explicitly, the transformed inverse Green's function is given by

$$\tilde{G}^{-1} = i\partial_t - \underbrace{(\varepsilon_\alpha + V_d - \psi)}_{\tilde{h}_d} - \underbrace{U^* \Sigma U}_{\tilde{\Sigma}} . \quad (4.9)$$

The gauge-transformation affects the self-energy $\tilde{\Sigma}$ and the Hamiltonian \tilde{h}_d . The self-energy is nonlocal in time and, thus, is affected by a time-dependent gauge transformation. The Hamiltonian acquires a new term $\psi = iU^* \dot{U}$, since the time-derivative acts on the gauge-transformation. It is this new term in the Hamiltonian, which allows us to simplify the problem by a specific choice of gauge.

4.3.1 Choosing a specific gauge

Because the major difficulty in the determination of the Green's function arises from the electrical potential's time dependence, we use the gauge-freedom ψ to eliminate the time-dependent part of V_d from the gauge-transformed Hamiltonian \tilde{h}_d . For that purpose, we assume the electrical potential to fluctuate around a constant value. Accordingly, we split $V_d = V_{d0} + \delta V_d$ into a part V_{d0} which is constant on the Keldysh contour and another part δV_d which is purely dynamical on the Keldysh contour. Now, the most straightforward choice of gauge seems to be $\psi = \delta V_d$, as it would completely eliminate the dynamical part of the electrical potential. It would follow $\psi_+(-T_K) - \psi_-(-T_K) = \oint_K dt \psi = \oint_K dt \delta V_d = \int dt \delta V_d^q = \delta V_d^q(\omega = 0) = 2T_K \delta V_{d0}^q$, where the Keldysh contour is from $-T_K$ to $+T_K$ and back again. Unfortunately, this would violate the boundary condition on the Keldysh countour $\psi_+(-T_K) - \psi_-(-T_K) = 2\pi n$ with $n \in \mathbb{Z}$. While such a violation of the boundary condition is possible in principle, it is technically quite demand-

ing and rather inconvenient in practice. For convenience we respect the boundary condition and make a slightly different choice,

$$\psi_{\pm} = \delta V_d^{\pm} \mp \frac{\delta V_{d0}^q}{2}, \quad (4.10)$$

which eliminates all of δV_d except for the quantum zero mode δV_{d0}^q . In turn, the action becomes

$$\mathcal{S} = -i \text{tr} \ln \left[\underbrace{i\partial_t - \xi_{\alpha} - \delta V_{d0}^q/2 - U^* \Sigma U}_{\tilde{G}^{-1}} \right] + \mathcal{S}_{\text{HS}}, \quad (4.11)$$

where the constant part of the electrical potential is included in the single-particle energy $\xi_{\alpha} = \varepsilon_{\alpha} + V_{d0}$. While the dynamical part of the electrical potential is eliminated from the Hamiltonian, it is shifted to the rotated self-energy $U^* \Sigma U$. This is as far as we can get without approximation.

4.3.2 Tunneling- versus quasiclassical-approximation

In the original Ambegaokar-Eckern-Schön-approach a central idea was to expand the action in the rotated self-energy, which is related to tunneling [Ambegaokar et al., 1982, Eckern et al., 1984]. To justify this expansion, tunneling has to be small in some sense. However, this is not possible for a double tunnel junction, since tunneling is the only mechanism which can change the amount of electrons in the middle region (dot) between the two tunnel junctions. Thus, tunneling cannot be a small effect, because there simply is no other effect compared to which it could be small.

Since tunneling is the only process by which the number of electrons in the dot can be changed, it is essential for the dot's electron distribution. This does not mean that an expansion in tunneling is never possible. In situations where the distribution function of each subsystem is known a priori and can be controlled externally, an expansion in tunneling can be possible. For example in single tunnel junctions—as originally considered by Ambegaokar-Eckern-Schön [Ambegaokar et al., 1982, Eckern et al., 1984]—such an expansion works. Here, however, an expansion in tunneling is no option. Would we expand in tunneling, the information about the dot's distribution function would be lost. Thus, we have to deviate from the original Ambegaokar-Eckern-Schön idea from here on.

As we are interested in the quasiclassical equation of motion for the electrical potential V_d (correspondingly ψ) we plan to vary the action with respect to quantum components. Thereby, we automatically keep only the terms of first order in quantum components; higher orders contribute to noise. So, we can make a quasiclassical approximation by expanding the action in quantum components.

4.4 Quasiclassical approximation

As the quasiclassical approximation corresponds to an expansion in quantum components, it is convenient to separate terms of different order in quantum components. In particular, we separate the zeroth order from the rest. For that purpose, we switch to the Keldysh rotated picture

$(+, -) \rightarrow (c, q)$, with the standard combinations for classical components $U_c = \frac{1}{2}(U_+ + U_-)$ and quantum components $U_q = U_+ - U_-$. In addition, we introduce a purely classical rotation $U_k = U_c|_{q=0}$, where $\dots|_{q=0}$ means to set all quantum components to zero. With this, the action can be re-organized to

$$\mathcal{S} = -i \text{tr} \ln \left[\underbrace{i\partial_t - \xi_\alpha - U_k^* \Sigma U_k}_{\tilde{G}_c^{-1}} - \delta V_{d0}^q / 2 - \delta \Sigma \right] + \mathcal{S}_{\text{HS}} , \quad (4.12)$$

where the rotated self-energy $U^* \Sigma U = U_k^* \Sigma U_k + \delta \Sigma$ was split into a purely classical part $U_k^* \Sigma U_k = U^* \Sigma U|_{q=0}$ and the rest $\delta \Sigma = U^* \Sigma U - U_k^* \Sigma U_k$. By construction $\delta \Sigma$ is at least of first order in quantum components. Thus, the inverse classical Green's function \tilde{G}_c^{-1} contains all terms of zeroth order in quantum components; note that $\tilde{G}_c^{-1} = \tilde{G}^{-1}|_{q=0}$. Now, the quasiclassical approximation, correspondingly the expansion in quantum components, is formally straightforward.

4.4.1 Expansion in quantum components

Now, an expansion in quantum components corresponds to expansions in the quantum zero mode δV_{d0}^q and in the deviation $\delta \Sigma$ from the purely classical rotated self-energy. For the first order in δV_{d0}^q follows the zero mode action

$$\mathcal{S}_{\text{ZM}} = \frac{i}{2} \text{tr} [\tilde{G}_c \delta V_{d0}^q] . \quad (4.13)$$

Explicitly taking the trace over time-space leads to

$$\mathcal{S}_{\text{ZM}} = \delta V_{d0}^q \int dt \frac{i}{2} \text{tr} [\tilde{G}_c(t, t)] , \quad (4.14)$$

where the trace over orbital- and Keldysh-space remains and is considered below. The zero-mode action will be important for the determination of the classical zero mode V_{d0} around which the electrical potential fluctuates. The first order expansion in $\delta \Sigma$ yields an AES-like¹ action

$$\mathcal{S}_{\text{AES}} = i \text{tr} [\tilde{G}_c \delta \Sigma] . \quad (4.15)$$

To first order in quantum components follows

$$\mathcal{S}_{\text{AES}} = - \int dt \int dt' \text{Im} [U_q(t) \alpha(t, t') U_c^*(t')] , \quad (4.16)$$

where the trace was explicitly taken over time- and Keldysh-space. Furthermore, we used that the anti-Keldysh component of the classical Green's function vanishes. The kernel function is defined by

$$\alpha(t, t') = \text{tr} [\tilde{G}_c^R(t, t') \Sigma^K(t' - t) + \tilde{G}_c^K(t, t') \Sigma^A(t' - t)] . \quad (4.17)$$

¹In the original AES-approach, one would have the full rotated self-energy $U^* \Sigma U$ instead of the deviation $\delta \Sigma$. Then, however, the purely classical part of the self-energy would be missing in the classical Green's function.

The AES-like action is intimately linked to tunneling of electrons, as it is governed by $\delta\Sigma$ which contains the information about the tunnel coupling to the leads. We emphasize, however, that it also depends on the dynamical part of the electrical potential δV_d via the gauge field ψ . The Hubbard-Stratonovich action is straightforwardly determined to

$$\mathcal{S}_{\text{HS}} = C \int dt \tilde{\psi}_c \psi_q + (CV_{d0} + N_0) \delta V_d^q(\omega = 0), \quad (4.18)$$

where an integration by parts was performed to shift the time-derivative from ψ_q to ψ_c .

We emphasize that we have not yet obtained an explicit form of the ZM-action and the AES-like action, whereas the HS-action was easy to obtain in its explicit form. This reflects the fact that the HS-action describes the "free" Hubbard-Stratonovich field, whereas the ZM-action and the AES-like action describe the interplay of the Hubbard-Stratonovich field with the underlying electron system. This interplay is governed by the classical Green's function, which describes the electron system in the time-dependent electrical potential (HS-field). Thus, \tilde{G}_c has to be determined before we can obtain an explicit form of the ZM-action and the AES-like action.

4.4.2 Determination of the classical Green's function

The classical Green's function \tilde{G}_c describes the dot's electron system and has to be determined from its inverse

$$\tilde{G}_c^{-1} = i\partial_t - \xi_\alpha - U_k^* \Sigma U_k, \quad (4.19)$$

as originally defined in equation (4.12). The stationary part of the electrical potential V_{d0} shifts the single-particle energies $\xi_\alpha = \varepsilon_\alpha + V_{d0}$. The dynamical part of the electrical potential ψ_c governs the rotated self-energy $U_k^* \Sigma U_k$, which is the most complicated term in \tilde{G}_c^{-1} .

The rotated self-energy $U_k^* \Sigma U_k$ carries twofold information: the unrotated self-energy Σ carries information about the coupling to the leads; in addition, the rotations U_k, U_k^* carry information about the dynamical part of the electrical potential. The rotations do not affect the retarded and advanced parts of the self-energy $\Sigma^{R/A}(t-t') = \mp i(\Gamma_l + \Gamma_r) \delta(t-t')$, since these parts are local in time. In turn, for $U_k^*(t) \Sigma^{R/A}(t-t') U_k(t')$ we find the Wigner-transform

$$[U_k^* \Sigma^{R/A} U_k](\bar{t}, \omega) = \mp i(\Gamma_l + \Gamma_r), \quad (4.20)$$

where the result is independent of both, the frequency ω corresponding to the time-difference $t-t'$ and the center-of-mass time-coordinate $\bar{t} = \frac{t+t'}{2}$. In contrast to the retarded and advanced part of the self-energy, the Keldysh part $\Sigma^K(t-t') = -2i[\Gamma_l F_l(t-t') + \Gamma_r F_r(t-t')]$ is nonlocal in time due to the leads' distribution functions $F_l(t-t')$ and $F_r(t-t')$. Therefore, the Keldysh part is affected by the $U(1)$ -rotations and becomes

$$[U_k^* \Sigma^K U_k](t, t') = -2i[\Gamma_l \tilde{F}_l(t, t') + \Gamma_r \tilde{F}_r(t, t')]. \quad (4.21)$$

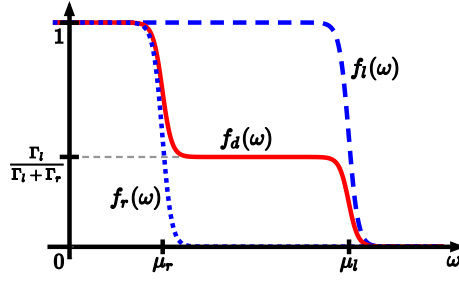


Figure 4.3: The figure shows the equilibrium (Fermi-)distribution functions of the leads (blue dashed/dotted) and the *stationary* distribution function of the dot (red solid). The dot's stationary distribution function is a superposition of the lead distribution functions and, thus, it is a strong nonequilibrium distribution, unless the leads are in equilibrium with each other.

The $U(1)$ -rotations are absorbed into the definition of the rotated distribution functions,

$$\tilde{F}_{l/r}(t, t') = U_k^*(t) F_{l/r}(t - t') U_k(t'), \quad (4.22)$$

which combine information about the dynamics of the dot's electrical potential and the leads' electron distribution functions.

In order to determine the classical Green's function \tilde{G}_c , it is convenient to proceed in a perturbative way and expand around the stationary situation with $\dot{\psi}_c = 0$. For that purpose, we rewrite the rotated self-energy $U_k^* \Sigma U_k = \Sigma + (U_k^* \Sigma U_k - \Sigma)$, where Σ is the stationary part and $(U_k^* \Sigma U_k - \Sigma)$ describes the deviation from the stationary part. Then, the inverse classical Green's function becomes,

$$\tilde{G}_c^{-1} = \underbrace{i\partial_t - \xi_\alpha - \Sigma}_{\tilde{G}_s^{-1}} - (U_k^* \Sigma U_k - \Sigma), \quad (4.23)$$

where \tilde{G}_s^{-1} defines the stationary Green's function \tilde{G}_s . The stationary Green's function is straightforward to determine, as it does not contain any dynamical field. For the retarded and advanced parts follows

$$\tilde{G}_s^{R/A}(\omega) = \frac{1}{\omega - \xi_\alpha \pm i\Gamma_\Sigma}, \quad (4.24)$$

with the total tunneling rate $\Gamma_\Sigma = \Gamma_l + \Gamma_r$. For the Keldysh part follows

$$\tilde{G}_s^K(\omega) = \frac{-2i\Gamma_\Sigma}{(\omega - \xi_\alpha)^2 + \Gamma_\Sigma^2} \tilde{F}_s(\omega), \quad (4.25)$$

where the stationary distribution function $\tilde{F}_s(\omega) = [\Gamma_l F_l(\omega) + \Gamma_r F_r(\omega)] / \Gamma_\Sigma$ is just a superposition of the leads' unrotated distribution functions $F_l(\omega)$ and $F_r(\omega)$, since there is no rotation in the stationary situation. The dot's stationary distribution function shows strong nonequilibrium features as can be seen in figure 4.3.

Would we restrict the analysis to the stationary situation, then we would lose the interesting interplay between the dynamical electrical potential (HS-field) and strong nonequilibrium distribution function. So, to take this interplay into account, we have to go beyond the stationary

Green's function and include higher orders in $(U_k^* \Sigma U_k - \Sigma)$. That is, the full classical Green's function should be considered

$$\tilde{G}_c = \tilde{G}_s + \underbrace{\tilde{G}_s (U_k^* \Sigma U_k - \Sigma) \tilde{G}_s + \dots}_{\tilde{G}_d}, \quad (4.26)$$

where the dynamical Green's function \tilde{G}_d contains the corrections due to the dynamics of the electrical potential. In the following, we focus on the stationary contribution \tilde{G}_s at first and only afterwards discuss the dynamical contribution \tilde{G}_d .

4.5 Derivation of the quasiclassical equation of motion

Now, knowing the classical Green's function, we can determine an explicit form of the zero-mode action (4.14) and the AES-like action (4.16). In combination with the Hubbard-Stratonovich action (4.18) the action is given by $\mathcal{S} = \mathcal{S}_{\text{HS}} + \mathcal{S}_{\text{AES}} + \mathcal{S}_{\text{HS}}$ to first order in quantum components. From the action, we have to determine two equations: the zero-mode equation to determine V_{d0} around which the electrical potential fluctuates; and the quasiclassical equation of motion which governs the dynamical part δV_d^c of the electrical potential.

4.5.1 The zero-mode equation

To obtain the zero-mode equation for V_{d0} , the action is varied with respect to the quantum zero-mode δV_{d0}^q . In other words, the zero-mode equation is $\left. \frac{\delta \mathcal{S}}{\delta V_{d0}^q} \right|_{q=0} = 0$. More explicitly,

$$C V_{d0} = \langle N \rangle - N_0, \quad (4.27)$$

where $\langle N \rangle = \frac{1}{2T_K} \int_{-T_K}^{T_K} dt N(t)$ is the time-average of the number of electrons on the dot $N(t) = -i \text{tr}[\tilde{G}_c(t, t)]$. This zero-mode equation is straightforward to interpret: the average electrical potential V_{d0} is determined by the electrical capacity C and the average number of charges on the dot $\langle N \rangle - N_0$.

An approximation for the average number $\langle N \rangle$ can be obtained as follows. Since the number of electrons $N(t)$ fluctuates around a stationary value, the average number $\langle N \rangle \approx -i \text{tr}[\tilde{G}_s(t, t)] = -\frac{i}{2\pi} \int d\omega \text{tr}[\tilde{G}_s(\omega)] = \int d\omega \rho_d(\omega) \tilde{f}_s(\omega)$ can be approximated with the stationary Green's function; where we defined the broadened density of states $\rho_d(\omega) = \sum_{\alpha} \frac{1}{\pi} \frac{\Gamma_{\Sigma}}{(\omega - \xi_{\alpha})^2 + \Gamma_{\Sigma}^2}$ and the stationary distribution function is $\tilde{f}_s(\omega) = [1 - \tilde{F}_s(\omega)]/2$. Furthermore, we note that one must be careful when taking the trace over Keldysh space at equal times [Kamenev and Levchenko, 2009, Kamenev, 2011].

4.5.2 Relaxation of the electrical potential for a stationary distribution function

When the electrical potential deviates by δV_d^c from its optimal/average value V_{d0} , there are too many or too few electrons on the dot. Then, the dot expels electrons into the leads or absorbs

electrons from the leads, until the electrical potential reaches its optimal/average value V_{d0} again. In other words, the dynamical part of the electrical potential tends to relax to zero $\delta V_d^c \rightarrow 0$. The relaxation dynamics is described by the AES-like action \mathcal{S}_{AES} . At first, we focus on the contributions from the stationary Green's function \tilde{G}_s or, correspondingly, the stationary distribution function \tilde{F}_s . Only in the next subsection, we go beyond this stationarity approximation and discuss the dynamical interplay between electrical potential and strong nonequilibrium distribution function.

The AES-like action (4.16) contains the full dynamical information in the kernel function (4.17). Focusing on stationary contributions, we replace the classical Green's function by the stationary Green's function $\tilde{G}_c \rightarrow \tilde{G}_s$. The stationary kernel function is defined by $\alpha_s^R(t-t') = \text{tr}[\tilde{G}_s^R(t-t')\Sigma^K(t'-t) + \tilde{G}_s^K(t-t')\Sigma^A(t'-t)]$. More explicitly,

$$\alpha_s(\omega) = \rho_d \int d\omega' \left\{ \Gamma_l [\tilde{F}_s(\omega') - F_l(\omega' - \omega)] + \Gamma_r [\tilde{F}_s(\omega') - F_r(\omega' - \omega)] \right\}, \quad (4.28)$$

where we disregarded the imaginary part and—for the stationary Green's function; equations (4.24) and (4.25)—we assumed the density of states to be approximately constant $\rho_d(\omega') \approx \rho_d$. The kernel function contains two contributions: one arising from the coupling to the left lead ($\propto \Gamma_l$) and one arising from the coupling to the right lead ($\propto \Gamma_r$). We emphasize, however, that the dot's stationary distribution function $\tilde{F}_s(\omega) = [\Gamma_l F_l(\omega) + \Gamma_r F_r(\omega)]/\Gamma_\Sigma$ depends on the distribution functions and tunneling rates of both leads. Thereby, a strong formal relation is created between these contributions. However, after performing the frequency integration follows

$$\alpha_s(\omega) = (g_l + g_r) \omega, \quad (4.29)$$

where $g_l = 2\rho_d\Gamma_l$ and $g_r = 2\rho_d\Gamma_r$ are the dimensionless conductances of left and right junction separately. A transformation back into time-space yields $\alpha_s(t-t') = i(g_l + g_r) \delta'(t-t')$. For the AES-like action follows

$$\mathcal{S}_{\text{AES},s} = -(g_l + g_r) \int dt \dot{\psi}_c \psi_q, \quad (4.30)$$

where we approximated $U_c = e^{-i\psi_c} \cos \frac{\psi_q}{2} \approx e^{-i\psi_c}$ and $U_q = -2ie^{-i\psi_c} \sin \frac{\psi_q}{2} \approx -i\psi_q e^{-i\psi_c}$.

Now, the quasiclassical equation of motion is found by a variation with respect to ψ_q ; formally $\frac{\delta \mathcal{S}}{\delta \psi_q(t)}|_{q=0} = 0$. Explicitly, we obtain $C\dot{\psi}_c = -(g_l + g_r)\psi_c$, where the left side originates from the HS-action (4.18) and the dissipative right side originates from the AES-like action (4.30). The zero-mode action (4.14) does not contribute to the dynamics. The resulting equation of motion is brought into a more familiar form by replacing $\dot{\psi}_c = \delta V_d^c$, which leads to

$$\delta \dot{V}_d^c = -\frac{g_l + g_r}{C} \delta V_d^c. \quad (4.31)$$

This is the classical *RC*-relaxation law for the dot's electrical potential. The relaxation is governed by the electrical capacity C and the resistance $R = \frac{1}{g_l + g_r}$ which is for both junctions in parallel. The physics behind this equation is simple. When too many electrons are on the dot, then the electrical capacity C determines the deviation of the electrical potential δV_d from its

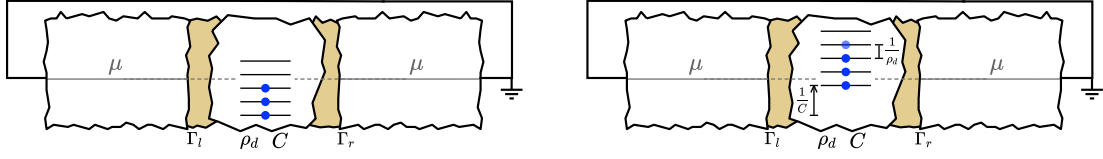


Figure 4.4: This figure illustrates the origin of quantum capacity. For simplicity, we consider an unbiased situation $\mu_l = \mu_r = \mu$ at low temperature $T < \frac{1}{C}, \frac{1}{\rho_d}$. When an electron tunnels onto the dot (for example due to a thermal fluctuation), then all single-particle levels are shifted to higher energies due to Coulomb-repulsion, correspondingly, due to an increase in *electrical* potential by the inverse electrical capacity $\frac{1}{C}$. Due to Pauli exclusion principle, the additional electron has to occupy a state which was previously empty. Thereby, the *chemical* potential is increased by the level-spacing $\frac{1}{\rho_d}$. In this context, the density of states ρ_d is also known as quantum capacity. In total, the *electrochemical* potential is increased by $\frac{1}{C} + \frac{1}{\rho_d}$. As the difference in electrochemical potentials governs the flow of charge current, the RC -relaxation law becomes $\delta\tilde{V}_d = -g_\Sigma(\frac{1}{C} + \frac{1}{\rho_d})\delta V_d$.

optimal value V_{d0} . The deviation relaxes to zero by tunneling of electrons out of the dot. That is, a current flows through the tunnel junctions (conductances g_l, g_r) which have to be considered as being "in parallel" in the sense of electronics (the current flows out of the dot; in contrast to through the dot). To summarize: driven by Coulomb-repulsion ($\frac{1}{C}\delta V_d^c$) electrons are expelled into the leads through the tunnel junctions ($g_l + g_r$).

While this result seems very reasonable, the argument is slightly incomplete: If more electrons are on the dot, then not only more charges are on the dot (electrical potential is increased) but also more particles are on the dot (chemical potential is increased); see figure 4.4. In other words, additional electrons have to occupy higher lying single-particle states because of Pauli exclusion principle. As the higher lying states are occupied until the system relaxes again, the dynamical changes in the distribution function are essential to describe effects related to a dynamical chemical potential.

4.5.3 Dynamical interplay between electrical potential and distribution function

In this final subsection, we discuss the interplay between the dynamical electrical potential and a dynamical distribution function. The information about the dynamical contribution to the distribution function is contained in the dynamical Green's function $\tilde{G}_d = \tilde{G}_s(U_k^*\Sigma U_k - \Sigma)\tilde{G}_s + \dots$, where ... includes higher orders in $(U_k^*\Sigma U_k - \Sigma)$ as originally defined in equation (4.26). Interestingly, the retarded and advanced parts of $(U_k^*\Sigma U_k - \Sigma)$ vanish, due to the time-locality of $\Sigma^{R/A}$. This has two consequences: the second and higher order terms in $(U_k^*\Sigma U_k - \Sigma)$ disappear from \tilde{G}_d , since these terms contain at least one retarded or advanced part²; furthermore, only the Keldysh part remains in the first order. To summarize, the retarded and advanced contributions vanish

$$\tilde{G}_d^{R/A} = 0, \quad (4.32)$$

²That the expansion terminates at some point suggest that we found an exact solution (apart from nonperturbative contributions). And indeed, from equation (4.19) on, we could have proceeded in an exact manner. Due to the time-locality of the self-energy's retarded and advanced parts $\Sigma^{R/A}$, it is straightforward to determine the retarded and advanced parts of the classical Green's function $\tilde{G}_c^{R/A} = \tilde{G}_s^{R/A}$. In turn, the classical Keldysh Green's function is found as $\tilde{G}_c^K = \tilde{G}_c^R U_k^* \Sigma^K U_k \tilde{G}_c^A$, which agrees with the expansion $\tilde{G}_c^K = \tilde{G}_s^K + \tilde{G}_d^K$.

and the Keldysh part is given by

$$\tilde{G}_d^K = \tilde{G}_s^R (U_k^* \Sigma^K U_k - \Sigma^K) \tilde{G}_s^A. \quad (4.33)$$

Thus, the dynamical electrical potential (contained in U_k^*, U_k) modifies only the Keldysh part \tilde{G}_d^K . In less technical words, the dynamical electrical potential only affects the distribution function but not the Hamiltonian. This is at the core of the dynamical interplay between electrical potential and distribution function. More precisely, it is "half" of this interplay: influence of the dynamical electrical potential onto the distribution function. To find the other "half" of this interplay, we have to consider how the dynamical distribution function affects the equation of motion for the electrical potential.

Since tunneling of electrons is governed by distribution functions, the AES-like action is modified by the dynamical distribution function of the dot. To determine this modification, we consider the dynamical kernel function $\alpha_d(t, t') = \text{tr}[\tilde{G}_d^K(t, t') \Sigma^A(t' - t)]$, which is obtained from $\alpha_c(t, t')$ by the replacement $\tilde{G}_c \rightarrow \tilde{G}_d$. Then, by construction we have $\alpha_c(t, t') = \alpha_s(t, t') + \alpha_d(t, t')$. Using the explicit form of the dynamical Keldysh Green's function $\tilde{G}_d^K(t, t')$, the dynamical kernel function becomes

$$\alpha_d(t, t''') = \int dt' \int dt'' (U_k^*(t') U_k(t'') - 1) \beta(t, t', t'', t'''), \quad (4.34)$$

with $\beta(t, t', t'', t''') = \text{tr}[G_s^R(t - t') \Sigma^K(t' - t'') G_s^A(t'' - t''') \Sigma^A(t''' - t)]$. In contrast to the stationary contribution $\alpha_s(t - t')$, the dynamical contribution $\alpha_d(t, t''')$ is a real two time-quantity, because of its dependence on the dynamical electrical potential via $U_k^*(t') U_k(t'')$. In frequency space $(t - t') \rightarrow \omega_1$, $(t' - t'') \rightarrow \omega_2$, and $(t'' - t''') \rightarrow \omega_3$ follows

$$\beta(\omega_1, \omega_2, \omega_3) = i4\Gamma_\Sigma^2 \rho_d \frac{\omega_2}{\omega_1 - \omega_3 + i2\Gamma_\Sigma} + \beta(\omega_1, \omega_2 = 0, \omega_3), \quad (4.35)$$

where the first term is calculated as $\beta(\omega_1, \omega_2, \omega_3) - \beta(\omega_1, \omega_2 = 0, \omega_3)$. The remaining contribution $\beta(\omega_1, \omega_2 = 0, \omega_3)$ diverges with natural cutoff of the bandwidth. However, by definition $\beta(\omega_1, \omega_2 = 0, \omega_3)$ is independent of ω_2 . In turn, it is proportional to $\delta(t' - t'')$ in time-space, such that it vanishes in combination with $(U_k^*(t') U_k(t'') - 1)$. Therefore, $\beta^R(\omega_1, \omega_2 = 0, \omega_3)$ does not contribute to $\alpha_d(t, t''')$. A transformation back into time-space yields

$$\alpha_d(t, t''') = i2\Gamma_\Sigma g_\Sigma \delta(t - t''') \int_{-\infty}^t dt' e^{-2\Gamma(t-t')} U_c^*(t') \dot{U}_c(t'), \quad (4.36)$$

with $g_\Sigma = 2\Gamma_\Sigma \rho_d = g_l + g_r$. It is, now, straightforward to determine the dynamical contribution to the AES-like action,

$$\mathcal{S}_{\text{AES},d} = 2\Gamma_\Sigma g_\Sigma \int dt \psi_q(t) \int_{-\infty}^t dt' e^{-2\Gamma_\Sigma(t-t')} \dot{\psi}_c(t'), \quad (4.37)$$

where $U_c^*(t') \dot{U}_c(t') = -i\dot{\psi}_c(t')$ was used. The distinctive feature of this dynamical contribution is its retarded nature: at time t the past values of $\dot{\psi}_c(t')$ are relevant on a time-scale of the inverse

tunneling rate $\frac{1}{2\Gamma_\Sigma}$. We discuss this retardation feature more deeply in the equation of motion.

The equation of motion in two forms

The equation of motion can be derived as before, that is, we add up the relevant contributions of the action $\mathcal{S} = \mathcal{S}_{\text{AES},s} + \mathcal{S}_{\text{AES},d} + \mathcal{S}_{\text{HS}}$ and take the variation with respect to $\psi_q(t)$: formally, $\left. \frac{\delta \mathcal{S}}{\delta \psi_q(t)} \right|_{q=0} = 0$. Explicitly follows

$$C \delta \dot{V}_d(t) = -g_\Sigma \delta V_d(t) + 2\Gamma_\Sigma g_\Sigma \int_{-\infty}^t dt' e^{-2\Gamma_\Sigma(t-t')} \delta V_d(t'). \quad (4.38)$$

where we used $\psi_c = \delta V_d^c$ and dropped the superscript c for classical components. The term on the left side arises from the HS-action. The terms on the right side arise from the AES-like action: the first term arises from the stationary part; the second term arises from the dynamical part. Before interpreting this integro-differential equation of motion, we recast it into a purely differential form³,

$$\delta \dot{V}_d = -g_\Sigma \left(\frac{1}{C} + \frac{1}{\rho_d} \right) \delta V_d. \quad (4.39)$$

Both forms of the equation of motion, differential and integro-differential, give useful insights into the dynamics of the electrical potential and its interplay with the distribution function.

Retardation effect: time-scale of the adjustments in the distribution function

To interpret the resulting equation of motion, we recall an important point which we have already emphasized several times: the dynamical Green's function \tilde{G}_d describes adjustments of the dot's electron distribution to the dynamics of its electrical potential. In turn, the retardation effect in the integro-differential equation of motion can be interpreted as follows: the dynamics of the electrical potential influences the distribution function; an altered distribution function changes the flow of charge current; a different flow of charge current has a back-action onto the dynamics of the electrical potential. By this mechanism, the dynamical electrical potential depends on its own past via its interplay with the distribution function. The distribution function adjusts to a new electrical potential by the tunneling of electrons, which takes place on the time-scale of the inverse tunneling rate. In other words, the distribution function adjusts on the time-scale of the inverse tunneling rate $\tau_{\text{dist.}} = 1/\Gamma_\Sigma$ and, thus, the retardation effect memorizes the electrical potential's past dynamics on this time-scale.

Quantum capacity: a small correction due to Pauli-principle

The differential form of the equation of motion (4.39) is analog to the RC-relaxation law (4.31), but with a renormalized capacity $\frac{1}{C^*} = \left(\frac{1}{C} + \frac{1}{\rho_d} \right)$. The correction $\frac{1}{\rho_d}$ is due to the Pauli exclusion principle. In this context, the density of states ρ_d is also known as quantum capacity [Büttiker

³This can be achieved by a Fourier-transformation for example. Alternatively, one can note that the right hand side is equal to $\partial_t \left[-g_\Sigma \int_{-\infty}^t dt' e^{-2\Gamma_\Sigma(t-t')} \delta V_d^c(t') \right]$, then integrate the equation once and use the result to eliminate the retarded integral from the right side of the integro-differential form of the equation of motion.

et al., 1993]. To understand the origin of the quantum capacity, we consider an unbiased situation at low temperature. The tunneling of an electron onto the dot has two effects related to the electrochemical potential: first, due to Coulomb-repulsion an additional electron increases the dot's *electrical* potential and, thereby, shifts the energy of all single-particle levels by $\frac{1}{C}$; second, due to Pauli exclusion principle an additional electron has to occupy a higher lying single-particle level (not filled by another electron) and, thereby, increases the *chemical* potential by the level-spacing $\frac{1}{\rho_d}$. Combining both effects: with each additional electron that tunnels onto the dot, the *electrochemical* potential is increased by $\frac{1}{C^*} = \left(\frac{1}{C} + \frac{1}{\rho_d}\right)$; see figure 4.4. This increase in electrochemical potential defines how many single-particle states are shifted above the electrochemical potentials of the leads and, thereby, it governs the relaxation process.

In physical systems that are large compared to the atomic scale, the quantum capacity only contributes a small correction to the relaxation dynamics. The electrical capacity typically scales with the surface of the system $C \sim L^2$. In contrast, the quantum capacity, correspondingly, the density of states typically scales with the volume of the system $\rho_d \sim L^3$. Thus, for large systems follows $\frac{1}{\rho_d} \ll \frac{1}{C}$ and the quantum capacity is negligible for the relaxation.

It is also useful to consider the negligibility of the quantum capacity from a formal point of view. For that purpose, the equation of motion (4.39) is recasted into $\delta\dot{V}_d = -2\Gamma_\Sigma \left(\frac{\rho_d}{C} + 1\right) \delta V_d$. We see that the relaxation rate of δV_d is always larger than $2\Gamma_\Sigma$ and becomes much larger for $\frac{1}{\rho_d} \ll \frac{1}{C}$. Thus, for large systems the electrical potential relaxes to its stationary value much faster than the distribution function is able to adjust ($\tau_{\text{dist.}} = 1/\Gamma_\Sigma$). In turn, the effects related to the distribution function's dynamics should be expected to be small. So, from this formal point of view the quantum capacity should be expected to yield only a small correction. This is indeed what we have found. We emphasize that this argument is based on the fact that Coulomb-repulsion (capacity) and Pauli exclusion principle (quantum capacity) are both repulsive and, thus, combine to a faster relaxation. The situation is completely different for an attractive interaction which competes with Pauli principle. Such a case is discussed for exchange interaction in the next chapter.

4.6 Fluctuations of the electrical potential

The RC -relaxation law describes the dissipative dynamics of the electrical potential. Dissipation is closely linked to fluctuations. At equilibrium, this link is described rather universally by fluctuation-dissipation-theorems; see for example [Negele and Orland, 1998, Van Kampen, 2007, Altland and Simons, 2010]. Out of equilibrium, however, fluctuations must be carefully derived from the action. For that purpose, we have to include the second order in quantum components which give rise to fluctuation terms in the equation of motion [Schmid, 1982, Eckern et al., 1990]. The RC -relaxation law (4.31) becomes a stochastic equation of motion

$$C \delta\dot{V}_d = -g_\Sigma \delta V_d + \xi, \quad (4.40)$$

which is also known as a Langevin equation. The stochasticity of the Langevin term ξ is governed by the second order in quantum components of the AES-like action (4.15) and we obtain $\langle \xi \rangle = 0$ and $\langle \xi \xi \rangle(\omega) = g_\Sigma [(\Gamma_l^2 + \Gamma_r^2) 2\omega \coth[\omega/2T] + \Gamma_l \Gamma_r 2(\omega - V) \coth[(\omega - V)/2T] + \Gamma_l \Gamma_r 2(\omega + V) \coth[(\omega + V)/2T]] / \Gamma_\Sigma^2$. With help of Fourier-transformation, it is straightforward to solve the Langevin equation (4.40) for $\delta V_d(\omega)$ and, in turn, to determine the correlation function,

$$C^2 \langle \delta V_d \delta V_d \rangle(\omega) = \frac{\langle \xi \xi \rangle(\omega)}{\omega^2 + \left(\frac{g_\Sigma}{C}\right)^2}. \quad (4.41)$$

This result describes the fluctuation of charges on the dot $C\delta V_d$ in terms of the RC -relaxation rate $\frac{g_\Sigma}{C}$ and the correlator of the Langevin term $\langle \xi \xi \rangle(\omega)$. In equilibrium ($V = 0$) and at low frequency ($\omega \ll T$), the Langevin term is governed by the coupling to the leads (conductance g_Σ) and the baths' temperature T ; more precisely, $\langle \xi \xi \rangle(0) = 4g_\Sigma T$ which is the typical result for thermal noise. In contrast, when a voltage is applied, the system is driven away from equilibrium. At low temperature and low frequency ($T, \omega \ll V$), the Langevin term is then governed by the voltage $\langle \xi \xi \rangle(0) = 4(\Gamma_l \Gamma_r / \Gamma_\Sigma^2) g_\Sigma V$ which is the typical result for shot noise in the double tunnel junction.

More interesting than the concrete result, in the present context, is the effect of the quantum capacity. As the quantum capacity changes the dissipative dynamics, it should change the fluctuations as well. Naively, one might expect from the renormalized RC -relaxation law (4.39) that the quantum capacity renormalizes the capacity everywhere. However, our preliminary results indicate that this is not the case. To include the noise related to quantum capacity, we have to go beyond the AES-like action and include terms of second order in $\delta\Sigma$ which also contain terms of second order in quantum components. Then, using the method of [Schmid, 1982, Eckern et al., 1990] again, we obtain the Langevin equation

$$C\delta\dot{V}_d(t) = -g_\Sigma \delta V_d(t) + 2\Gamma_\Sigma g_\Sigma \int_{-\infty}^t dt' e^{-2\Gamma_\Sigma(t-t')} \delta V_d(t') + \bar{\xi}(t), \quad (4.42)$$

where $\bar{\xi}$ is the new noise term which includes effects of the quantum capacity. Besides the presence of the retardation effect in the equation of motion, the quantum capacity leads to a renormalized noise. Explicitly, $\langle \bar{\xi} \rangle = 0$ and $\langle \bar{\xi} \bar{\xi} \rangle(\omega) = \frac{\omega^2}{\omega^2 + (2\Gamma_\Sigma)^2} \langle \xi \xi \rangle(\omega)$. Interestingly, the renormalized noise vanishes $\langle \bar{\xi} \bar{\xi} \rangle(\omega) \rightarrow 0$ for low frequencies $\omega \ll 2\Gamma_\Sigma$. This can be interpreted as follows. The information about the past is stored in the distribution function. The distribution function relaxes back to the stationary case on the time-scale of tunneling. Thus, information about the past is lost on the time-scale of the inverse tunneling rate $1/\Gamma_\Sigma$. Note, however, that the same is true for the electrical potential. Thus, the renormalization factor $\frac{\omega^2}{\omega^2 + (2\Gamma_\Sigma)^2}$ cancels out and we obtain,

$$C^2 \langle \delta V_d \delta V_d \rangle(\omega) = \frac{\langle \xi \xi \rangle(\omega)}{\omega^2 + \left(\frac{g_\Sigma}{C^*}\right)^2}. \quad (4.43)$$

So, in contrast to the naive expectation, the renormalized capacity $C^* = \left(\frac{1}{C} + \frac{1}{\rho_d}\right)^{-1}$ governs only the RC -relaxation-rate $\frac{g_\Sigma}{C^*}$, whereas the number of charges on the dot $C\delta V_d$ is still governed

by the electrical capacity C . This is reasonable, as the quantum capacity is related to changes in chemical potential, but not to changes in electrical potential.

4.7 Summary and discussion

In this chapter, we considered a double tunnel junction with an interacting middle region (dot) and derived the quasiclassical equation of motion for the dot's electrical potential. As a result, we obtained the RC -relaxation law (4.39). A particular focus was put on the interplay between the dot's dynamical electrical potential and its distribution function. This interplay gave rise to the quantum capacity ρ_d which renormalized the capacity to $\frac{1}{C^*} = \frac{1}{C} + \frac{1}{\rho_d}$. The electrical capacity C is closely related to the Coulomb-repulsion and the quantum capacity (density of states) ρ_d is closely related to the Pauli exclusion principle. Because Coulomb-repulsion and Pauli exclusion principle are both repulsive, the quantum capacity does not change the dynamics of the electrical potential in a qualitative way. The situation would be completely different for an attractive interaction, which competes with Pauli principle; for a discussion, see chapter 5.

Knowing the dynamics of the electrical potential and the corresponding distribution function, we could determine the current and noise for the charge transport through the dot. Formally, we would introduce counting fields; see appendix A. For long measurement times, however, we would approximate the electrical potential by the stationary value V_{d0} to which it relaxes. Practically, this brings us back to the discussion of chapter 2. Would we want to include fluctuations of the electrical potential, we had to go beyond the first order of quantum components. Disregarding the quantum capacity, we reproduced standard results for the fluctuations of the electrical potential. Namely, we obtained thermal fluctuations in equilibrium and fluctuations of the shot-noise type for strong driving ($V \gg T$). However, to obtain precise results, the quantum capacity should be taken into account. In the context of fluctuations, the quantum capacity takes a subtle role: it renormalizes the RC -relaxation rate $\frac{g\Sigma}{C^*}$ but it does not renormalize the capacity in the relation between electrical potential and the number of additional electrons on the dot $C\delta V_d$. Due to this subtle role, it would be interesting to study the effect of quantum capacity for the tunneling density of states [Meir and Wingreen, 1992], for the zero-bias anomaly [Altland and Egger, 2009], for the $P(E)$ -theory [Ingold and Nazarov, 1992], and for out-of-equilibrium Korshunov-instantons [Titov and Gutman, 2016]. These topics are not addressed in this thesis but remain interesting problems for further study.

On the technical side, we have extended the AES-approach [Ambegaokar et al., 1982, Eckern et al., 1984] to situations where the distribution function of a system (dot) is not externally controlled. We performed a gauge transformation analog to references [Ambegaokar et al., 1982, Eckern et al., 1984]. However, we had to deviate from [Ambegaokar et al., 1982, Eckern et al., 1984], since an expansion in tunneling is not possible for the double tunnel junction. Tunneling cannot be a small effect, as it is the only effect which can change the number of particles in to dot. Consequently, by an expansion in tunneling we would lose the information about the distribution function of the middle region. It is possible to partially restore the lost information with great intuition; see for example [Altland and Egger, 2009, Altland and Simons, 2010]. How-

ever, the interplay between dynamical electrical potential and the distribution function would be lost. Instead of expanding in tunneling, we perform a quasiclassical approximation. That is, we expand in quantum components. Thereby, the information about the dot's distribution function is kept intact and we can study its effects onto the quasiclassical dynamics of the electrical potential.

Chapter 5

Dynamical interplay between magnetization and electron distributions

In itinerant ferromagnets, the magnetization consists of spins of the conduction-band electrons. At the same time, the magnetization acts as an internal magnetic field for these electron spins. When exposed to an external magnetic field, the magnetization precesses around this field and relaxes towards it, if energy and angular momentum can be dissipated. In any case, the dynamics of the magnetization renders the effective single-particle Hamiltonian time-dependent and, thereby, it drives electrons away from equilibrium.

This chapter presents a discussion of the magnetization dynamics of an itinerant ferromagnetic quantum dot which is tunnel-coupled to two leads and exposed to an external magnetic field; see figure 5.1. Using the macrospin approximation, we describe the magnetization by a single vector $\mathbf{M} = M(\sin \theta \cos \phi, \sin \theta \sin \phi, \cos \theta)$. The leads are assumed to be normal metals. For simplicity, we consider an unbiased situation; that is, temperatures and electrochemical potentials are equal in both leads. The external magnetic field $\mathbf{B} = (\Omega \cos \omega_d t, \Omega \sin \omega_d t, B_0)$ is assumed to have a large but constant component B_0 in one direction and, perpendicular to it, an oscillating part with strength Ω and frequency ω_d . This describes a ferromagnetic resonance (FMR) setup, where the oscillating part can be used to drive the magnetization.

Our goal is to derive a quasiclassical equation of motion for the magnetization. As result, we obtain the Landau-Lifshitz-Gilbert equation (5.54) for the angular motion and a separate equation (5.55) for the length dynamics. Because the leads are nonmagnetic, the angular dynamics decouples from the length dynamics. Our main focus in the derivation is on the interplay between magnetization dynamics and electron distribution. The magnetization dynamics drives the electron system into a strong nonequilibrium state which is reflected in nonequilibrium distribution functions. The magnetization's angular motion is not influenced by the electron distribution. In contrast, magnetization's length dynamics is significantly influenced by its interplay with the electron distribution. The interplay between length dynamics and distribution function gives rise

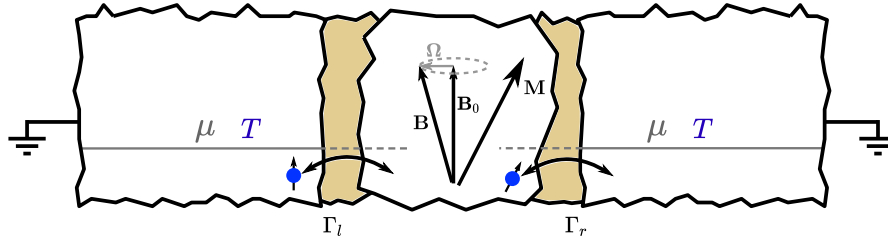


Figure 5.1: The figure schematically shows the system discussed in this chapter. A ferromagnetic quantum dot is exposed to an external magnetic field \mathbf{B} and tunnel-coupled to two normal metal leads. As we consider an unbiased setup, the leads are in equilibrium with each other, that is, temperatures $T_l = T_r =: T$ and electrochemical potentials $\mu_l = \mu_r =: \mu$ are equal in both leads. The tunneling between the dot and the leads is described by tunneling rates Γ_l and Γ_r for the left and right lead respectively. The tunnel coupling allows the ferromagnetic dot to dissipate energy and angular momentum into the leads. This allows the magnetization to relax towards its energetically most favourable state which is parallel to the external magnetic field. The oscillating part of the external magnetic field (strength Ω , frequency ω_d), however, can be used to drive the magnetization away from its energetic minimum into a steady state precession.

to the quantum capacity (similar to chapter 4), which turns out to be an essential for a consistent description of the dynamical magnetization length.

Technically, this chapter is based on the method developed in references [Ludwig et al., 2017, Ludwig et al., 2019b]. Though, the physical setup is that of [Ludwig et al., 2019a], correspondingly, that of chapter 3. Instead of repeating a discussion of charge current and its noise, we focus on the dynamics of the magnetization. In this way, we provide a formal background for three central assumptions of chapter 3: (i) length can be assumed constant for the description of the angular motion; (ii) the angular motion can be described independent of the distribution functions (for nonmagnetic leads); (iii) spin-off-diagonal contributions can be disregarded for a large magnetization length. Another purpose of this chapter is to demonstrate how angular and length dynamics of the magnetization can be treated in parallel.

For simplicity, we disregard the interaction in the Coulomb channel. This is possible, when the corresponding electrical potential relaxes on time-scales that are short compared to the time-scales of the magnetization's dynamics. This is usually the case for large magnetization length. However, it is straightforward to include Coulomb repulsion along the lines of chapter 4; at least when the conductance of the tunnel junctions is large enough [Ludwig et al., 2017, Ludwig et al., 2019b].

5.1 Description of the system

We consider an itinerant ferromagnetic quantum dot which is exposed to an external magnetic field and tunnel-coupled to two normal metal leads; see figure 5.1. We assume that neither voltage nor thermal bias is applied across the system. However, we allow the external magnetic field to be time-dependent and, thereby, the ferromagnet can be driven out of equilibrium.

5.1.1 Hamiltonian, tunneling rates, and distribution functions

Motivated by the universal Hamiltonian [Kurland et al., 2000], we model the ferromagnetic quantum dot by

$$H_d = \sum_{\alpha\sigma} \varepsilon_\alpha c_{\alpha\sigma}^\dagger c_{\alpha\sigma} - J\mathbf{S}^2 - \mathbf{B}\mathbf{S}, \quad (5.1)$$

where $c_{\alpha\sigma}^\dagger, c_{\alpha\sigma}$ are creation and annihilation operators for electrons in single-particle states α with spin σ and the corresponding single-particle energy ε_α . The total spin operator is defined by $\mathbf{S} = \frac{1}{2} \sum_{\alpha\sigma\sigma'} c_{\alpha\sigma}^\dagger \boldsymbol{\sigma}_{\sigma\sigma'} c_{\alpha\sigma'}$. We assume a positive exchange constant J , such that the exchange interaction $-J\mathbf{S}^2$ tends to align the spins of electrons in the dot. We assume the exchange constant J to be large enough, such that the dot is deep in the Stoner regime¹. The coupling to the external magnetic field is included via the Zeeman-energy of the total spin $-\mathbf{B}\mathbf{S}$. To describe a ferromagnetic resonance (FMR) setup, we assume the external magnetic field to have a large but constant component B_0 and, perpendicular to it, a smaller oscillating part Ω which can be used to drive the magnetization. That is, $\mathbf{B} = (\Omega \cos \omega_d t, \Omega \sin \omega_d t, B_0)$, where ω_d is the driving frequency.

The leads are assumed to be effectively noninteracting systems and the tunnel coupling between dot and leads is assumed to be spin-conserving. Here, the leads are included into the description via their effect onto the dot; but a more detailed description of leads and tunnel coupling is given in appendix A. The tunnel coupling to the leads affects the dot in two important ways. *As a first effect*, the tunnel coupling allows electrons to tunnel into and out of the dot, which is described by tunneling rates Γ_l, Γ_r for tunneling into left and right lead respectively. The tunneling rates Γ_l, Γ_r are assumed to be independent of the dot's single-particle states, which is justified when many channels of each lead are weakly and randomly coupled to the states in the dot [Ludwig et al., 2017]; see also appendix A. *As a second effect*, the leads provide heat and particle baths for the dot, which is described by the distribution functions $f_l(\omega), f_r(\omega)$. The leads' distribution functions are assumed to be controlled in an experiment, such that we can assume them to be fixed to equilibrium. At equilibrium the (Fermi-)distribution functions are fully determined by the electrochemical potentials μ_l, μ_r and the temperatures T_l, T_r ; explicitly for the left lead $f_l(\omega) = 1/[e^{(\omega-\mu_l)/T_l} + 1]$ and for the right lead $f_r(\omega) = 1/[e^{(\omega-\mu_r)/T_r} + 1]$. As we consider an unbiased situation, the electrochemical potentials and the temperatures are equal in both leads, that is, $\mu_l = \mu_r = \mu$ and $T_l = T_r = T$.

We emphasize that, in contrast to the leads, the distribution function of the ferromagnetic dot cannot be controlled directly. Thus, we cannot assume its distribution function to be fixed to any specific distribution. Instead, the distribution function of the ferromagnetic dot has to be determined jointly from the distribution functions of the leads and the dynamics of the magnetization.

¹Basically this means that the Stoner-criterion $J\rho_d > 1$ is clearly satisfied, where ρ_d is the dot's single-particle density of states.

5.1.2 The effective action

Despite the absence of external bias, the dynamics of the magnetization drives the electron system into a nonequilibrium state. Thus, we use the Keldysh formalism to describe the system [Kamenev and Levchenko, 2009, Kamenev, 2011, Altland and Simons, 2010]. The Keldysh generating function is $\mathcal{Z} = \int D[\bar{\Psi}, \Psi] e^{i\mathcal{S}}$ with the action

$$\mathcal{S} = \oint_K dt [\bar{\Psi}(i\partial_t - \hat{\Sigma})\Psi - H_d(\bar{\Psi}, \Psi)] , \quad (5.2)$$

where $\bar{\Psi}, \Psi$ denote all fermionic fields of the dot. For compact notation, we have introduced the self-energy operator $[\hat{\Sigma}\Psi](t) = \oint_K dt' \Sigma(t-t')\Psi(t')$, where the self-energy $\Sigma = \Sigma_l + \Sigma_r$ contains all the necessary information about the coupling to the leads; Σ_l and Σ_r arise from the coupling to left and right lead respectively. The information about tunneling rates is contained in the retarded and advanced parts $\Sigma^{R/A}(\omega) = \mp i(\Gamma_l + \Gamma_r)$. The information about the leads' distribution functions is contained in the Keldysh part $\Sigma^K = -2i[\Gamma_l F_l(\omega) + \Gamma_r F_r(\omega)]$, where $F_{l/r}(\omega) = 1 - 2f_{l/r}(\omega)$. Since $F_{l/r}(\omega)$ and $f_{l/r}(\omega)$ are in one to one correspondence, we refer to both as distribution functions. We assumed the density of states in both leads to be approximately constant, such that the tunneling rates are constant in energy.

The exchange interaction in the Hamiltonian renders the action (5.2) quite nontrivial, as it is a contribution quartic in fermionic fields. To proceed, we decouple this interaction by a Hubbard-Stratonovich (HS) transformation

$$e^{iJ \oint_K dt \mathbf{S}^2} = \int D\mathbf{B}_{exc} e^{-i \oint_K dt \left(\frac{\mathbf{B}_{exc}^2}{4J} - \mathbf{B}_{exc} \mathbf{S} \right)} , \quad (5.3)$$

where the HS-field \mathbf{B}_{exc} is the exchange field. This field can be viewed as the mean-field an electron spin experiences due to the exchange-interaction with the other electron spins. The Keldysh partition function becomes $\mathcal{Z} = \int D[\bar{\Psi}, \Psi] \int D\mathbf{M} e^{i\mathcal{S}}$ with the new action

$$\mathcal{S} = \oint_K dt \bar{\Psi} \left[i\partial_t - \underbrace{\left(\varepsilon_\alpha - \frac{\mathbf{M} \cdot \boldsymbol{\sigma}}{2} \right)}_{h_d} - \hat{\Sigma} \right] \Psi - \underbrace{\oint_K dt \frac{(\mathbf{M} - \mathbf{B})^2}{4J}}_{\mathcal{S}_{HS}} , \quad (5.4)$$

where $\mathbf{M} = \mathbf{B}_{exc} + \mathbf{B}$ is the magnetization. Actually, it would be more precise to refer to \mathbf{B}_{exc} as magnetization, but in typical ferromagnets the internal field \mathbf{B}_{exc} is much larger than the external field \mathbf{B} . Thus, $\mathbf{M} \approx \mathbf{B}_{exc}$, which justifies to refer also to \mathbf{M} as magnetization. The HS-action \mathcal{S}_{HS} describes the "free" action of the HS-field \mathbf{M} . The coupling between \mathbf{M} and the underlying electron system is described by the the effective single-particle Hamiltonian h_d .

We emphasize that the dot's distribution function does not appear explicitly in the action (5.4). This is in contrast to the leads, as their distribution function is explicitly contained in the self-energy. The dot's distribution function, however, has to be determined from the action. It is governed by the coupling to the leads and the dynamics of the magnetization.

5.2 Self-consistency equation for the dynamical magnetization

In many cases, the most relevant contributions to the Keldysh partition function \mathcal{Z} are determined by the saddle-points of the action. Even though $\mathcal{Z} = 1$ by construction, the saddle-points of the action govern many observables, provided that these are accounted for by only pre-exponential factors. A type of saddle-points of special importance are quasiclassical saddle-points which are found by variation of the action with respect to quantum components.

In order to determine the quasiclassical saddle-point equation for the magnetization \mathbf{M} , we integrate out the fermionic fields. After re-exponentiating the resulting determinant follows

$$\mathcal{S} = -i \text{tr} \ln \left[\underbrace{i\partial_t - h_d - \Sigma}_{G^{-1}} \right] + \mathcal{S}_{\text{HS}} , \quad (5.5)$$

where G^{-1} we defines the effective single-particle Green's function G . To be precise, G should be called auxiliary Green's function. For the full Green's function the HS-field should be averaged out. In this sense, all single-particle objects discussed in the following are of auxiliary character.

A direct variation of the action with respect to the quantum components of the magnetization \mathbf{M}_q leads to the quasiclassical saddle-point equation $\frac{\delta \mathcal{S}}{\delta \mathbf{M}_q} \Big|_{q=0} = 0$, where $\dots|_{q=0}$ means to set all quantum components to zero. Explicitly, we obtain

$$\frac{1}{2J} \mathbf{M}_c(t) = \frac{i}{4} \text{tr} [G_c(t, t) \boldsymbol{\sigma}] + \frac{\mathbf{B}}{2J} , \quad (5.6)$$

where the classical Green's function G_c has to be determined from its inverse which is defined by $G_c^{-1} = G^{-1} \Big|_{q=0}$. Equation (5.6) determines the magnetization M_c in terms of the exchange constant J and the amount of electron spins $\frac{i}{4} \text{tr} [G_c(t, t) \boldsymbol{\sigma}]$ on the dot. Note, however, that the classical Green's function depends on the magnetization M_c . Thus, equation (5.6) is a self-consistency equation for the magnetization. To be more precise, the classical Green's function depends on the past values of the magnetization. In other words, it is a functional of the magnetization $G_c[\mathbf{M}_c]$. Thus, equation (5.6), is not just any self-consistency equation: it determines the magnetization at one time in terms of its values in the past; in short, it is the quasiclassical equation of motion for the magnetization.

Unfortunately, the dynamics of the magnetization makes it hard to determine the classical Green's function. While this problem was solved for slow magnetization dynamics by [Basko and Vavilov, 2009], we are particularly interested in fast precessions of the magnetization. Slow and fast is in comparison to the life-time of electrons in the dot. For arbitrary precession speed, it is convenient to change to the rotating frame of the dynamical magnetization [Ludwig et al., 2017, Ludwig et al., 2019b, Ludwig et al., 2019a].

5.3 Transition to the magnetization's rotating frame of reference

The time dependence of the magnetization \mathbf{M} combined with the time-nonlocality of the self-energy Σ renders the full action (5.5) quite nontrivial. A strategy that works in many cases, is the expansion of the mean-field around a stationary (or slow) value. However, this strategy would fail here, due to fast precessions of the magnetization. Following [Shnirman et al., 2015], we deal with the difficulties arising from a fast precessing by changing into the magnetization's rotating frame of reference. The dynamics of the magnetization length is also not necessarily slow. To deal with the length dynamics, we perform a spin-dependent $U(1)$ -gauge-transformation, which is motivated by the Ambegaokar-Eckern-Schön-approach [Ambegaokar et al., 1982, Eckern et al., 1984].

The ferromagnetic dot is assumed to be deep in the Stoner regime with a large length of magnetization. The magnetization length $|\mathbf{M}| = M = M_0 + \delta M$ is split into a constant part M_0 and a part δM which is purely dynamical on the Keldysh contour. The dynamical part δM is assumed to be small $\delta M \ll M_0$, such that the magnetization length fluctuates around a large value. In this situation, a description with polar coordinates becomes reasonable. That is, the magnetization is written as $\mathbf{M} = M\mathbf{m}$, where $\mathbf{m} = (\sin \theta \cos \phi, \sin \theta \sin \phi, \cos \theta)$ is the direction of the magnetization. This allows us to easily treat the angular dynamics of \mathbf{m} separately from the dynamical length M .

5.3.1 Angular dynamics

The angular dynamics can be conveniently described in the magnetization's rotating frame of reference. Following [Shnirman et al., 2015], we change to this rotating frame by performing a rotation in spin-space R , such that the magnetization is rotated onto the z -axis at all times

$$R^\dagger \mathbf{m} \sigma R = \sigma_z . \quad (5.7)$$

Formally, we go back to the action (5.4), perform an $SU(2)$ -gauge-transformation for the fermionic fields $\Psi \rightarrow R\Psi$ and $\bar{\Psi} \rightarrow R^\dagger \bar{\Psi}$, and integrate out the fermions again. After re-exponentiating the resulting determinant, follows

$$\mathcal{S} = -i \text{tr} \ln \underbrace{[R^\dagger (i\partial_t - h_d - \Sigma) R]}_{\bar{G}^{-1}} + \mathcal{S}_{\text{HS}} , \quad (5.8)$$

where \bar{G}^{-1} defines the rotating-frame Green's function \bar{G} . More explicitly, the inverse rotating-frame Green's function is given by

$$\bar{G}^{-1} = i\partial_t - \underbrace{\left(\varepsilon_\alpha - M \frac{\sigma_z}{2} + Q \right)}_{\bar{h}_d} - R^\dagger \Sigma R , \quad (5.9)$$

where \bar{h}_d is the effective single-particle Hamiltonian in the rotating frame and $R^\dagger \Sigma R$ is the rotating-frame self-energy. The time dependence of the direction \mathbf{m} transfers to the rotations

R^\dagger, R , which has two important consequences: first, due to this time dependence a new term $Q = -iR^\dagger \dot{R}$ is generated by the time-derivative $i\partial_t$; second, the self-energy is rotated $\Sigma \rightarrow R^\dagger \Sigma R$ even though the self-energy Σ is trivial in spin-space.

The rotations R^\dagger, R affects the self-energy due to its nonlocality in time. To be more precise, the retarded and advanced parts $\Sigma^{R/A}(t-t') = \mp i(\Gamma_l + \Gamma_r)\delta(t-t')$ are trivial in spin-space and local in time-space; therefore, they are not affected by the rotations $R^\dagger \Sigma^{R/A} R = \Sigma^{R/A}$. In strong contrast, the Keldysh part $\Sigma^K(t-t') = -2i[\Gamma_l F_l(t-t') + \Gamma_r F_r(t-t')]$ is nonlocal in time because of the leads' distribution functions $F_{l/r}$. Since only the distribution functions are nonlocal in time, only the distribution functions get rotated $R^\dagger \Sigma^K R = -2i[\Gamma_l \bar{F}_l(t, t') + \Gamma_r \bar{F}_r(t, t')]$, where $\bar{F}_{l/r}(t, t') = R^\dagger(t) F_{l/r}(t-t') R(t')$ are the rotating-frame distribution functions.

The newly generated term Q is also known as Berry-connection [Shnirman et al., 2015]. It is most conveniently discussed for an explicit representation of the rotations R . Following ref. [Shnirman et al., 2015], we choose the Euler-angle representation

$$R = e^{-i\frac{\theta}{2}\sigma_z} e^{-i\frac{\phi}{2}\sigma_y} e^{i\frac{\phi-\chi}{2}\sigma_z}, \quad (5.10)$$

where θ, ϕ characterize the direction of the magnetization, and χ represents a gauge-freedom which will be employed later for simplification. The representation is motivated by the boundary condition on the Keldysh contour $R_+(-T_K) = R_-(-T_K)$, which is now satisfied for $\theta_+(-T_K) = \theta_-(-T_K)$, $\phi_+(-T_K) - \phi_-(-T_K) = 2\pi n$, and $\chi_+(-T_K) - \chi_-(-T_K) = 4\pi m$ with $n, m \in \mathbb{N}$. In this representation, $Q = Q_{\parallel} + Q_{\perp}$ with the spin-diagonal part $Q_{\parallel} = [\dot{\phi}(1 - \cos\theta) - \dot{\chi}] \frac{\sigma_z}{2}$ and the spin-off-diagonal part $Q_{\perp} = e^{i\chi\sigma_z} [\dot{\phi} \sin\theta \frac{\sigma_x}{2} - \dot{\theta} \frac{\sigma_y}{2}] e^{i\phi\sigma_z}$. As Q_{\parallel} is spin-diagonal it gives an additional splitting in energy between spin-up and spin-down electrons, that is, Q_{\parallel} is related to the Berry-phase [Shnirman et al., 2015]. In contrast Q_{\perp} is spin-off-diagonal and, therefore, it is related to the (Landau-Zener) transitions between states with spin-up and spin-down [Shnirman et al., 2015]. The gauge freedom χ can be used to simplify the rotating-frame hamiltonian \bar{h}_d . However, from the current point of view, it is not obvious which choice might be best; thus, we defer it to a later stage.

5.3.2 Length dynamics

Due to the generation of the new term Q , we partially failed to eliminate the angular dynamics from the effective single-particle Hamiltonian. What we did achieve, though, is that the magnetization always points along the z -direction. That is, the dynamical length M occurs with σ_z only. This allows us to treat the dynamical length analog to the electrical potential in chapter 4. In turn, we perform a spin-dependent $U(1)$ -gauge-transformation,

$$U = e^{i\eta \frac{\sigma_z}{2}}. \quad (5.11)$$

In principle, η can be an arbitrary differentiable function. In practice, we want to use η to eliminate the dynamical part of the length δM from the rotating-frame Hamiltonian. The $U(1)$ -

gauge-transformation leads to

$$\mathcal{S} = -i \text{tr} \ln \left[\underbrace{U^* \tilde{G}^{-1} U}_{\tilde{G}^{-1}} \right] + \mathcal{S}_{\text{HS}}, \quad (5.12)$$

where \tilde{G}^{-1} defines the fully rotated Green's function \tilde{G} . More explicitly,

$$\tilde{G}^{-1} = i\partial_t - \underbrace{\left(\varepsilon_\alpha - (M - \dot{\eta}) \frac{\sigma_z}{2} + \tilde{Q} \right)}_{\tilde{h}_d} - \underbrace{D^\dagger \Sigma D}_{\tilde{\Sigma}}, \quad (5.13)$$

where $iU^* \dot{U} = \dot{\eta}$ was used. Furthermore, we introduced the full rotations $D = RU, D^\dagger = U^* R^\dagger$ together with the fully rotated single-particle Hamiltonian \tilde{h}_d and the fully rotated self-energy $\tilde{\Sigma}$. In the following, we drop the adverb "fully" for brevity. Also the Berry-connection is rotated $\tilde{Q} = U^* Q U = Q_{\parallel} + \tilde{Q}_{\perp}$ but the spin-diagonal Berry-phase contribution Q_{\parallel} is not affected.

To eliminate δM from the rotating-frame Hamiltonian \tilde{h}_d , we would like to fix the gauge to $\dot{\eta} = \delta M$. Unfortunately, this violates the boundary condition $\eta_-(-T_K) - \eta_+(-T_K) = 4\pi k$ with $k \in \mathbb{N}$, since $\eta_-(-T_K) - \eta_+(-T_K) = \oint_K dt \delta M = \int_{-T_K}^{T_K} dt \delta M_q = \delta M_q(\omega=0) =: 2T_K \delta M_0^q$. Even though this violation is acceptable in principle [Burmistrov et al., 2019], it is technically much easier to choose a gauge which satisfies this boundary condition. As a compromise we choose,

$$\dot{\eta}_{\pm} = \delta M_{\pm} \mp \frac{\delta M_0^q}{2}, \quad (5.14)$$

which eliminates all of δM apart from its quantum zero mode δM_0^q and simultaneously satisfies the desired boundary condition with $k = 0$. For the action follows

$$\mathcal{S} = -i \text{tr} \ln \left[\underbrace{i\partial_t - \varepsilon_\alpha + M_0 \frac{\sigma_z}{2} + \frac{\delta M_0^q}{2} \frac{\sigma_z}{2} - \tilde{Q} - D^\dagger \Sigma D}_{\tilde{G}^{-1}} \right] + \mathcal{S}_{\text{HS}}. \quad (5.15)$$

Up to this point everything is exact. In the following, however, we will leave exact grounds and perform several approximations with the goal of deriving a quasiclassical equation of motion for the magnetization.

5.4 Quasiclassical approximation

In principle, a variation of the action, equation (5.15), with respect to the quantum components directly leads to the (noiseless) quasiclassical equations of motion. However, since the gauge-transformations R and U are exact, the determination of the quasiclassical approximation has not yet been significantly simplified. To make some real progress, sensible approximations have to be made. This is the major advantage of the rotating-frame: It is much easier to perform useful approximations.

We perform approximations on the level of the action to keep the following derivation more organized. In other words, we change the order of variation and approximation. It is important

to be careful when reversing this order. Since the (noiseless) quasiclassical equation of motion is determined by a variation with respect to quantum components, the first order in quantum components is essential. Thus, by expanding in quantum components at first and only afterwards in other small quantities, we make sure not to generate wrong quasiclassical equations of motion. In particular, we must not expand in tunneling before the expansion in quantum components. Otherwise the important information about the dot's distribution function would be lost. As an expansion in tunneling is not possible, in the following we have to deviate from the original AES-idea [Ambegaokar et al., 1982, Eckern et al., 1984] and its $SU(2)$ -extension [Shnirman et al., 2015].

5.4.1 Expansion in quantum components

For the purpose of expanding in quantum components, we introduce purely classical rotations $D_k = D_c|_{q=0}$, where $\dots|_{q=0}$ means to set the quantum components of all coordinates to zero. Then, we split the rotated self-energy $D^\dagger \Sigma D = D_k^\dagger \Sigma D_k + \delta \tilde{\Sigma}$ into the purely classical part $D_k^\dagger \Sigma D_k = [D_c^\dagger \Sigma D_c]|_{q=0}$ and the rest $\delta \tilde{\Sigma}$. For the Berry-connection we proceed analogously $\tilde{Q} = \tilde{Q}_k + \delta \tilde{Q}$ with $\tilde{Q}_k = \tilde{Q}|_{q=0}$. By construction, $\delta \Sigma$ and $\delta \tilde{Q}$ are at least of first order in quantum components, whereas the zeroth order is completely contained in $D_k^\dagger \Sigma D_k$ and Q_k . For the action follows

$$\mathcal{S} = -i \text{tr} \ln \left[\tilde{G}_c^{-1} + \frac{\delta M_0^q}{2} \frac{\sigma_z}{2} - \delta \tilde{\Sigma} - \delta \tilde{Q} \right] + \mathcal{S}_{\text{HS}} , \quad (5.16)$$

where the classical Green's function \tilde{G}_c was introduced by its inverse $\tilde{G}_c^{-1} = \tilde{G}^{-1}|_{q=0}$. More explicitly,

$$\tilde{G}_c^{-1} = i\partial_t - \varepsilon_\alpha + M_0 \frac{\sigma_z}{2} - \tilde{Q}_k - D_k^\dagger \Sigma D_k . \quad (5.17)$$

By construction, the classical Green's function contains no quantum components and, therefore, its anti-Keldysh part vanishes.

The formal expansion of the action in δM_0^q , $\delta \tilde{\Sigma}$ and $\delta \tilde{Q}$ is straightforward and corresponds to the quasiclassical approximation, since all three (δM_0^q , $\delta \tilde{\Sigma}$, $\delta \tilde{Q}$) are at least of first order in quantum components of the coordinates. For the expansion in δM_0^q we obtain the zero-mode action

$$\mathcal{S}_{\text{ZM}} = -\frac{i}{4} \text{tr} [\tilde{G}_c \delta M_0^q \sigma_z] . \quad (5.18)$$

This contribution is important to determine the length of M_0 but, apart from that, it is not relevant for the dynamics. For the expansion in $\delta \Sigma$ we obtain an Ambegaokar-Eckern-Schön-like action [Ambegaokar et al., 1982, Eckern et al., 1984, Shnirman et al., 2015]

$$\mathcal{S}_{\text{AES}} = i \text{tr} [\tilde{G}_c \delta \tilde{\Sigma}] , \quad (5.19)$$

which describes effects related to tunneling of electrons. For the expansion in $\delta \tilde{Q}$, we split $\delta \tilde{Q} = \delta \tilde{Q}_\parallel + \delta \tilde{Q}_\perp$ into a spin-diagonal part $\delta \tilde{Q}_\parallel$ and a spin-off-diagonal part $\delta \tilde{Q}_\perp$, analogous to $\tilde{Q} = Q_\parallel + \tilde{Q}_\perp$. For the expansion in $\delta \tilde{Q}_\parallel$ an action of the Wess-Zumino-Novikov-Witten-type is

obtained [Shnirman et al., 2015],

$$\mathcal{S}_{\text{WZNW}} = i \text{tr} [\tilde{G}_c \delta Q_{\parallel}] , \quad (5.20)$$

which is related to the Berry-phase. For the expansion in $\delta \tilde{Q}_{\perp}$ a contribution related to the Landau-Zener (LZ) transitions is obtained,

$$\mathcal{S}_{\text{LZ}} = i \text{tr} [\tilde{G}_c \delta \tilde{Q}_{\perp}] . \quad (5.21)$$

However, this contribution will be disregarded below in an adiabatic approximation.

In addition to the contributions originating from the $\text{tr} \ln[\dots]$, the HS-action has to be determined. To first order in quantum components, we obtain

$$\begin{aligned} \mathcal{S}_{\text{HS}} = & -\frac{M_0}{2J} \delta M_q(\omega = 0) - \frac{1}{2J} \int dt \dot{\eta}_q [\dot{\eta}_c - \Omega \sin \theta_c \cos(\phi_c - \omega_d t) - B_0 \cos \theta_c] + \\ & + \int dt \frac{M_c}{2J} \{ \theta_q [\Omega \cos \theta_c \cos(\phi_c - \omega_d t) - B_0 \sin \theta_c] - \phi_q \Omega \sin \theta_c \sin(\phi_c - \omega_d t) \} , \quad (5.22) \end{aligned}$$

where constant terms ($\propto M_0^2, B^2$) have been dropped.

The Hubbard-Stratonovich action (5.22) is independent of the classical Green's function, because it describes the action of the "free" magnetization (HS-field). All other contributions are related to the interplay between the magnetization and the underlying electron system and, therefore, depend on the classical Green's function.

5.4.2 Determination of the classical Green's function

The classical Green's function \tilde{G}_c has to be determined from its inverse,

$$\tilde{G}_c^{-1} = i \partial_t - \underbrace{\left(\varepsilon_{\alpha} - M_0 \frac{\sigma_z}{2} + \tilde{Q}_k \right)}_{\tilde{h}_d} - D_k^{\dagger} \Sigma D_k , \quad (5.23)$$

as defined in equation (5.17). This is a hard task due to the time dependence of the rotating-frame self-energy $D_k^{\dagger} \Sigma D_k$ and the Berry-connection \tilde{Q}_k . It is significantly simplified by assuming the magnetization M_0 to define the largest relevant energy scale in the dot. This allows us to disregard the spin-off-diagonal elements of G_c^{-1} , as these will be suppressed by $\frac{1}{M_0}$ in G_c . In turn, it is sufficient to consider the spin-diagonal elements of \tilde{Q}_k and $D_k^{\dagger} \Sigma D_k$.

Adiabatic approximation and choice of gauge

Disregarding the spin-off-diagonal part of the Berry-connection \tilde{Q}_{\perp}^k means to disregard the Landau-Zener transitions between spin-up and spin-down. This corresponds to an adiabatic approximation, where the angular motion is slow compared to the time-scale defined by the (inverse) length of the magnetization [Shnirman et al., 2015]. The spin-diagonal Berry-phase contribution Q_{\parallel}^k remains also for large magnetization. However, we eliminate the Berry-phase

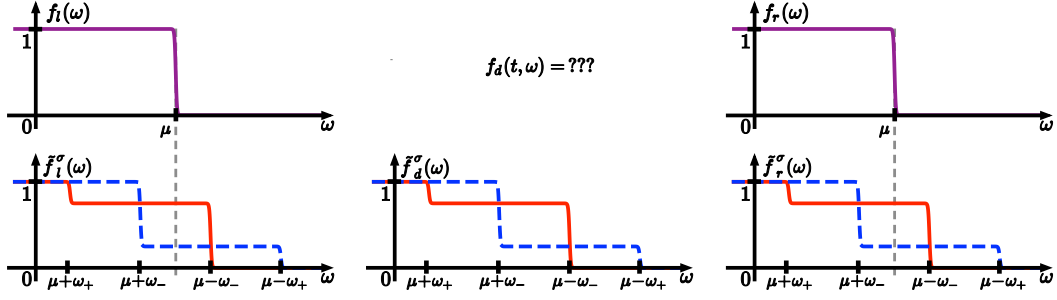


Figure 5.2: This figure illustrates the central problem and the idea for its solution. (**upper line**) In the laboratory frame, the distribution functions of the leads ($f_l(\omega), f_r(\omega)$) are assumed to be equilibrium distribution functions. The distribution function of the ferromagnetic dot ($f_d(t, \omega)$) cannot be directly controlled and, therefore, it is not known a priori. The dynamical magnetization renders the dot's effective single-particle Hamiltonian time-dependent. Consequently, this time dependence appears in a kinetic equation and drives the distribution function away from equilibrium. (**lower line**) Instead of trying to solve a complicated time-dependent kinetic equation, it is much more convenient to change to the magnetization's rotating frame of reference, where the effective single-particle Hamiltonian is approximately time-independent. When changing into a time-dependent frame of reference, this affects the distribution functions have to be carefully rotated as well. In the rotating frame, the distribution functions of the leads become spin-dependent $\tilde{f}_l^\sigma(\omega), \tilde{f}_r^\sigma(\omega)$ and are shown for spin-up (red solid) and spin down (blue dashed). The change into the rotating frame significantly simplifies the determination of the dot's distribution function: the dot's rotating-frame Hamiltonian and the leads' rotating-frame distribution functions are time-independent, such that the dot's distribution function is a simple superposition of those of the leads $\tilde{f}_d^\sigma(\omega) = [\Gamma_l \tilde{f}_l^\sigma(\omega) + \Gamma_r \tilde{f}_r^\sigma(\omega)] / \Gamma_\Sigma$. Due to the absence of bias: $\tilde{f}_d^\sigma(\omega) = \tilde{f}_l^\sigma(\omega) = \tilde{f}_r^\sigma(\omega)$. The figure is derived from a figure in [Ludwig et al., 2019a].

contribution $Q_{\parallel}^k = [\dot{\phi}_c(1 - \cos \theta_c) - \dot{\chi}_c] \frac{\sigma_z}{2}$ by fixing the gauge to $\dot{\chi}_c = \dot{\phi}_c(1 - \cos \theta_c)$. One might be tempted to choose $\dot{\chi} = \dot{\phi}(1 - \cos \theta)$ on the Keldysh contour, as this would eliminate the full Berry-phase contribution Q_{\parallel} ; not just Q_{\parallel}^k . This more general choice, however, would violate the boundary condition $R_+(-T_K) = R_-(-T_K)$, correspondingly, $\chi_+(-T_K) - \chi_-(-T_K) = 4\pi m$ with $m \in \mathbb{N}$. Even though this violation is acceptable in principle, it would be technically very demanding [Burmistrov et al., 2019]. It is much more convenient to choose a gauge that satisfies the boundary condition on the Keldysh contour. Following [Shnirman et al., 2015], we choose

$$\dot{\chi}_c = \dot{\phi}_c(1 - \cos \theta_c), \quad (5.24)$$

$$\chi_q = \phi_q(1 - \cos \theta_c). \quad (5.25)$$

which is as close as one can get to the desired choice $\dot{\chi} = \dot{\phi}(1 - \cos \theta)$ while simultaneously satisfying $\chi_+(-T_K) - \chi_-(-T_K) = 0$. Then we obtain $\delta Q_{\parallel} = \sin \theta_c (\dot{\phi}_c \theta_q - \dot{\theta}_c \phi_q) \frac{\sigma_z}{2}$ to first order in quantum components.

To summarize: the effect of \tilde{Q}_k onto the classical Green's function is eliminated to leading (zeroth) order in $\frac{1}{M_0}$. In turn, the inverse classical Green's function is reduced to,

$$\tilde{G}_c^{-1} \approx i\partial_t - \varepsilon_\alpha + M_0 \frac{\sigma_z}{2} - D_k^\dagger \Sigma D_k. \quad (5.26)$$

Despite the elimination of Q_{\parallel}^k , the Berry-phase remains relevant. By the choice of gauge, it was transferred to the rotating-frame self-energy $D_k^\dagger \Sigma D_k$.

Separation of time-scales in the purely classical rotated self-energy

The basic idea, to deal with the complicated time dependence of the rotating-frame self-energy, is to expand around slow dynamical trajectories. For that purpose, we introduce a slow rotation D_s which arises from the purely classical rotation D_k by keeping only slow coordinates for which we want to employ their slowness; all other coordinates are simply set to zero. We emphasize: for slow coordinates it is optional to include them into D_s . The precise meaning of slow is discussed below. Now, the rotating-frame self-energy is split $D_k^\dagger \Sigma D_k = D_s^\dagger \Sigma D_s + (D_k^\dagger \Sigma D_k - D_s^\dagger \Sigma D_s)$ into a slow contribution $D_s^\dagger \Sigma D_s$ and deviations from it $(D_k^\dagger \Sigma D_k - D_s^\dagger \Sigma D_s)$. Accordingly, the inverse classical Green's function is rewritten as

$$\tilde{G}_c^{-1} = \tilde{G}_s^{-1} - (D_k^\dagger \Sigma D_k - D_s^\dagger \Sigma D_s), \quad (5.27)$$

where we introduced the slow Green's function by its inverse,

$$\tilde{G}_s^{-1} = i\partial_t - \varepsilon_\alpha + \frac{M_0}{2} \sigma_z - D_s^\dagger \Sigma D_s. \quad (5.28)$$

The classical Green's function can now be expanded in $(D_k^\dagger \Sigma D_k - D_s^\dagger \Sigma D_s)$ which describes the deviations from slow trajectories. It follows

$$\tilde{G}_c = \tilde{G}_s + \underbrace{\tilde{G}_s (D_k^\dagger \Sigma D_k - D_s^\dagger \Sigma D_s) \tilde{G}_s}_{\tilde{G}_d} + \dots \quad (5.29)$$

The idea behind this expansion is as follows: when the slow coordinates are slow enough, then the slow Green's function \tilde{G}_s can be approximated by a gradient expansion. The other dynamical coordinates are then taken into account in the dynamical Green's function \tilde{G}_d . "Slow" and "dynamical" are not the opposite of each other, as dynamical can include slow, fast, and intermediate speed.

The meaning of "slow" is defined by our desire to perform a gradient approximation for G_s . While we give a formal discussion in appendix B, it can be easily stated in physical terms. A coordinate is defined as slow, if the typical time-scale of its dynamics $\tau_{coord.}$ is large in comparison to the typical time-scale of tunneling processes $\tau_\Gamma = \frac{1}{\Gamma}$ (with a generic tunneling rate Γ) and the time-scale of thermal noise $\tau_T = \frac{1}{T}$. In other words, a coordinate is called slow, if $\tau_{coord.} \gg \max(\tau_\Gamma, \tau_T)$. That is, it changes slowly compared to adjustments in the distribution function $\tau_{coord.} \gg \tau_\Gamma$ and the thermal noise appears to be white noise on the time-scale of a slow coordinate $\tau_{coord.} \gg \tau_\Gamma$.

Let us now think about the coordinates of the magnetization θ, ϕ, η . The coordinate η is related to the length of magnetization which changes only by tunneling of electrons on or off the dot. Thus, we expect $\tau_\eta \propto \frac{1}{\Gamma}$. Similarly, the angle θ also changes due to tunneling of electrons. However, by simple geometric arguments, the change of θ will be suppressed by the length of the magnetization, correspondingly, the spin S . For its typical time-scale follows $\tau_\theta \propto \frac{S}{\Gamma}$. The situation is more subtle for ϕ . The magnetization can precess around the external magnetic

field with a large frequency $-B$, suggesting $\tau_\phi = \frac{1}{B}$. In addition, ϕ changes due to tunneling of electrons (also geometrically suppressed by S), suggesting $\tau_\phi \propto \frac{S}{\Gamma}$. For large magnetic field, correspondingly, for fast precession ϕ is not a slow coordinate. However, $\dot{\phi}$ is a slow coordinate $\tau_\phi \propto \frac{S}{\Gamma}$, since $-B$ yields only a constant shift in $\dot{\phi}$. In conclusion, for large spin S , the coordinates $\theta, \dot{\phi}$ are slow. However, the dynamics of η is not suppressed by the length of the spin and cannot be assumed as slow.

For the slow rotations we choose $D_s = R_k$. This is possible, as the (relevant spin-diagonal part of the) slowly rotated self-energy $[D_s^\dagger \Sigma D_s]_{\sigma\sigma} = [R_k^\dagger \Sigma R_k]_{\sigma\sigma}$ depends only on θ and $\dot{\phi}$ but is independent of ϕ itself. The retarded and advanced parts are actually trivial

$$[R_k^\dagger \Sigma^{R/A} R_k](\omega) = \mp i\Gamma_\Sigma, \quad (5.30)$$

due to the time-locality and spin-independence of $\Sigma^{R/A}(t-t') = \mp i\Gamma_\Sigma \delta(t-t')$. In contrast, the Keldysh part $\Sigma^K(t-t') = -2i[\Gamma_l F_l(t-t') + \Gamma_r F_r(t-t')]$ is nonlocal in time due to the leads' distribution functions. It follows

$$[R_k^\dagger \Sigma^K R_k]_{\sigma\sigma}(\bar{t}, \omega) = -2i\Gamma_\Sigma \tilde{F}_s^\sigma(\bar{t}, \omega), \quad (5.31)$$

where $\tilde{F}_s^\sigma(\bar{t}, \omega) = [\Gamma_l \tilde{F}_l^\sigma(\bar{t}, \omega) + \Gamma_r \tilde{F}_r^\sigma(\bar{t}, \omega)]/\Gamma_\Sigma$ is the dot's slow spin-dependent rotating-frame distribution function; and $\tilde{F}_{l/r}^\sigma(\bar{t}, \omega) = [R_k^\dagger F_{l/r}(\omega) R_k]_{\sigma\sigma}(\bar{t}, \omega)$ are the spin-diagonal parts of the leads' rotating-frame distribution functions. To determine these distribution functions, we use the slowness of $\theta, \dot{\phi}$ which leads to $\tilde{F}_{l/r}^\sigma(\bar{t}, \omega) = \cos^2 \frac{\theta_c}{2} F_{l/r}(\omega + \sigma \omega_-) + \sin^2 \frac{\theta_c}{2} F_{l/r}(\omega + \bar{\sigma} \omega_+)$ with $\omega_\pm = \dot{\phi}_c(\bar{t})(1 \pm \cos \theta_c(\bar{t}))/2$.

Knowing the slowly rotated self-energy $[R_k^\dagger \Sigma^K R_k]_{\sigma\sigma}(\bar{t}, \omega)$, the slow Green's function can now be determined to zeroth order in a gradient expansion. It follows

$$\tilde{G}_s^{R/A}(\omega) = \frac{1}{\omega - \xi_{\alpha\sigma} \pm i\Gamma_\Sigma}, \quad (5.32)$$

$$\tilde{G}_s^K(\bar{t}, \omega) = \frac{-2i\Gamma_\Sigma}{(\omega - \xi_{\alpha\sigma})^2 + \Gamma_\Sigma} \tilde{F}_s^\sigma(\bar{t}, \omega), \quad (5.33)$$

with the spin-dependent single-particle energy $\xi_{\alpha\sigma} = \varepsilon_\alpha - \frac{M_0}{2}\sigma$ and the slow rotating-frame distribution function

$$\begin{aligned} \tilde{F}_s^\sigma(\bar{t}, \omega) = & \left[\cos^2 \frac{\theta_c}{2} \Gamma_l F_l(\omega + \sigma \omega_-) + \sin^2 \frac{\theta_c}{2} \Gamma_l F_l(\omega + \bar{\sigma} \omega_+) + \right. \\ & \left. + \cos^2 \frac{\theta_c}{2} \Gamma_r F_r(\omega + \sigma \omega_-) + \sin^2 \frac{\theta_c}{2} \Gamma_r F_r(\omega + \bar{\sigma} \omega_+) \right] / \Gamma_\Sigma. \end{aligned} \quad (5.34)$$

Even in absence of external bias, $F_l(\omega) = F_r(\omega)$, the dot's distribution function $\tilde{F}_s^\sigma(\bar{t}, \omega)$ is far from equilibrium due to the dynamics of the magnetization, which enters in $\omega_\pm = \dot{\phi}_c(\bar{t})(1 \pm \cos \theta_c(\bar{t}))/2$.

Besides the slow Green's function \tilde{G}_s , we also need the dynamical Green's function \tilde{G}_d for the determination of the length dynamics. Due to the time-locality of retarded and advanced

parts of the self-energy $\Sigma^{R/A}(t-t') = \mp i\Gamma_\Sigma \delta(t-t')$ follows $D_k^\dagger \Sigma^{R/A} D_k - D_s^\dagger \Sigma^{R/A} D_s = 0$. In turn, the retarded and advanced parts of the dynamical Green's function vanish,

$$\tilde{G}_d^{R/A} = 0. \quad (5.35)$$

In contrast, the Keldysh part of the self-energy is nonlocal in time due to the distribution functions of the leads; therefore, $D_k^\dagger \Sigma^K D_k - D_s^\dagger \Sigma^K D_s \neq 0$. In turn, the Keldysh part of the dynamical correction to the Green's function becomes

$$\tilde{G}_d^K = G_s^R (D_k^\dagger \Sigma^K D_k - R_k^\dagger \Sigma^K R_k) G_s^A, \quad (5.36)$$

to first order in $D_k^\dagger \Sigma^K D_k - D_s^\dagger \Sigma^K D_s$. Higher orders in $D_k^\dagger \Sigma D_k - D_s^\dagger \Sigma D_s$ actually vanish due to combined triviality in spin-space and locality in time-space of $\Sigma^{R/A}$.

5.4.3 Explicit form of quasiclassical action

Now, knowing the classical Green's function, we can determine the various contributions to the action explicitly. For the Zero-mode action follows

$$\mathcal{S}_{\text{ZM}} = \int_{-T_K}^{T_K} dt S(t) \delta M_0^q, \quad (5.37)$$

with the total spin length $S(t) = -\frac{i}{4} \text{tr} [\tilde{G}_c(t, t) \sigma_z]$. For the WZNW-action follows

$$\mathcal{S}_{\text{WZNW}} = -S \int dt \sin \theta_c (\theta_q \dot{\phi}_c - \phi_q \dot{\theta}_c), \quad (5.38)$$

where we have approximated the spin-length by a constant $S(t) \approx S = -\frac{i}{4} \text{tr} [\tilde{G}_s(t, t) \sigma_z]$. Explicitly,

$$S = -\frac{1}{4} \int d\omega \left[\rho_\uparrow(\omega) \tilde{F}_s^\uparrow(t, \omega) - \rho_\downarrow(\omega) \tilde{F}_s^\downarrow(t, \omega) \right], \quad (5.39)$$

which is half the difference between the number of spin-up and spin-down electrons on the dot. Interestingly, S is constant despite the dependence of the distribution function $\tilde{F}_s^\sigma(t, \omega)$ on $\theta_c(t)$ and $\dot{\phi}(t)$. In other words, the precession of the magnetization redistributes spin-up and spin-down electrons in energy space, but it does not change their number. The Landau-Zener action does not contribute to leading (zeroth) order in $1/M_0$,

$$\mathcal{S}_{\text{LZ}} = \mathcal{O}\left(\frac{1}{S}\right) \approx 0, \quad (5.40)$$

since it only contains spin-off diagonal contributions of G_c .

To first order in quantum components the AES-like action becomes,

$$\mathcal{S}_{\text{AES}} = -\int dt \int dt' \sum_{\sigma\sigma'} \text{Im} \left[D_q^{\sigma'\sigma}(t) \alpha_\sigma^R(t, t') (D_c^{\sigma'\sigma}(t'))^* \right], \quad (5.41)$$

where the trace over Keldysh-, time-, and spin-space was taken. The remaining trace over orbital space is included in the definition of the kernel function

$$\alpha_\sigma(t, t') = \text{tr}[\tilde{G}_{c\sigma}^R(t, t')\Sigma^K(t' - t) + \tilde{G}_{c\sigma}^K(t, t')\Sigma^A(t' - t)] . \quad (5.42)$$

For convenience, this kernel function is split into a slow and a dynamical contribution

$$\alpha_\sigma(t, t') = \alpha_{s,\sigma}(t, t') + \alpha_{d,\sigma}(t, t') . \quad (5.43)$$

The slow contribution $\alpha_{s,\sigma}(t, t')$ arises from $\alpha_\sigma(t, t')$ by replacing the classical Green's function with the slow one $\tilde{G}_c \rightarrow \tilde{G}_s$. Analogously, the dynamical contribution $\alpha_{d,\sigma}(t, t')$ arises from $\alpha_\sigma(t, t')$ by replacing the classical Green's function with the dynamical one $\tilde{G}_c \rightarrow \tilde{G}_d$. For the slow kernel follows

$$\begin{aligned} \alpha_{s,\sigma}(\bar{t}, \omega) = & \rho_\sigma \Gamma_l \int d\omega' [\tilde{F}_s^\sigma(\bar{t}, \omega') - F_l(\omega' - \omega)] + \\ & + \rho_\sigma \Gamma_r \int d\omega' [\tilde{F}_s^\sigma(\bar{t}, \omega') - F_r(\omega' - \omega)] , \end{aligned} \quad (5.44)$$

with the spin-dependent density of states defined by $\rho_\sigma(\omega) = \sum \alpha \frac{1}{\pi} \frac{\Gamma_\Sigma}{(\omega - \xi_{\alpha\sigma})^2 + \Gamma_\Sigma^2}$ was assumed to be approximately constant $\rho_\sigma(\omega) \approx \rho_\sigma$ on all scales smaller than M_0 . Interestingly, in the slow kernel (5.44) the dot's distribution function is in the rotating frame, whereas the leads' distribution functions are in the laboratory frame. The integration over the frequency yields explicitly,

$$\alpha_{s,\sigma}(\bar{t}, \omega) = g_\Sigma^\sigma \omega , \quad (5.45)$$

where $g_\Sigma^\sigma = g_l^\sigma + g_r^\sigma$ is the spin-dependent conductance with $g_l^\sigma = 2\rho_\sigma \Gamma_l$ and $g_r^\sigma = 2\rho_\sigma \Gamma_r$. For the dynamical kernel follows

$$\alpha_{d,\sigma}(t, t''') = \int dt' \int dt'' [U_{k\sigma}^\dagger(t') U_{k\sigma}(t'') - 1] \beta_\sigma(t, t', t'', t''') . \quad (5.46)$$

The slow rotations R_k are completely absorbed into the new kernel function $\beta_\sigma(t, t', t'', t''') = G_{s\sigma}^R(t, t') [R_k^\dagger \Sigma^K R_k]_{\sigma\sigma}(t', t'') G_{s\sigma}^A(t'', t''') \Sigma^A(t'' - t)$. In frequency space $t - t' \rightarrow \omega_1$, $t' - t'' \rightarrow \omega_2$, and $t'' - t''' \rightarrow \omega_3$ the new kernel function can be calculated as

$$\beta_\sigma(\omega_1, \omega_2, \omega_3) = i4\Gamma_\Sigma^2 \rho_\sigma \frac{\omega_2}{\omega_1 - \omega_3 + i2\Gamma_\Sigma} + \beta_\sigma(\omega_1, 0, \omega_3) . \quad (5.47)$$

Even though the term $\beta_\sigma(\omega_1, 0, \omega_3)$ formally diverges (with the band-width as natural cut-off), it is independent of ω_2 and, thus, is proportional to $\delta(t' - t'')$ in time-space. Therefore, it drops out of $\alpha_{d,\sigma}(t, t''')$ due to the multiplication with $[U_{k\sigma}^\dagger(t') U_{k\sigma}(t'') - 1]$. For the remaining part follows

$$\alpha_{d,\sigma}(t, t''') = -\sigma \Gamma_\Sigma g_\Sigma^\sigma \delta(t - t''') \int_{-\infty}^t dt' e^{-2\Gamma_\Sigma(t-t')} \dot{\eta}_c(t') , \quad (5.48)$$

where $U_{k\sigma}^*(t') \dot{U}_{k\sigma}(t') = i\dot{\eta}_c(t') \sigma/2$ was used. Since this contribution contains only the dynamical

ical Green's function \tilde{G}_d^K , it is intimately related to adjustments of the distribution function to the dynamics of δM . This part of the action accounts for the information that is stored in the distribution function about the past. The distribution function can store information for the time-scale of electron life-times. This explains why the memory/retardation effect depends on the tunneling rate Γ_Σ .

$$\mathcal{S}_{\text{AES}} = -\tilde{g} \int dt \left\{ \theta_q 4\dot{\theta}_c + \phi_q \sin^2 \theta_c \dot{\phi}_c + \eta_q \left(\dot{\eta}_c - 2\Gamma_\Sigma \int_{-\infty}^t dt' e^{-2\Gamma_\Sigma(t-t')} \dot{\eta}_c(t') \right) \right\}, \quad (5.49)$$

with $\tilde{g} = (g_\Sigma^\uparrow + g_\Sigma^\downarrow)/4$. As we have determined all relevant contributions to the action to first order in quantum components, the derivation of the quasiclassical equation of motion is straightforward now.

5.5 Quasiclassical equation of motion for the magnetization

It is, now, straightforward to derive the quasiclassical equations of motion, because we know all contributions to the action that are of first order in quantum components and not suppressed by the large length of the spin. In addition to the magnetization's dynamics, we should determine M_0 which is the stationary value around which the length fluctuates by δM .

5.5.1 Zero-mode equation

Two contributions to the action contain the quantum zero-mode δM_0^q : the zero-mode action (5.37); and the Hubbard-Stratonovich action (5.22). Taking the variation with respect to the quantum zero-mode leads to the zero-mode equation $\frac{\delta(\mathcal{S}_{\text{ZM}} + \mathcal{S}_{\text{HS}})}{\delta(\delta M_0^q)}|_{q=0} = 0$. Explicitly,

$$\frac{M_0}{2J} = \langle S \rangle, \quad (5.50)$$

with the time-averaged length of the total spin $\langle S \rangle = \frac{1}{2T_K} \int_{-T_K}^{T_K} dt S(t)$. The zero-mode equation can be read in two ways. Seen from one side, it determines the magnetization length M_0 by the exchange constant J and the (time-averaged) length of the spin $\langle S \rangle$. However, the classical Green's function \tilde{G}_c , which governs $S(t)$, depends on M_0 . So, seen from the other side, the zero-mode equation is a self-consistency equation for the length of the magnetization M_0 .

5.5.2 Quasiclassical dynamics of the magnetization

The quasiclassical equation of motion for the magnetization is determined by adding up all remaining parts of the action, $\mathcal{S} = \mathcal{S}_{\text{AES}} + \mathcal{S}_{\text{WZNW}} + \mathcal{S}_{\text{HS}}$, and taking the variation with respect to quantum components θ_q, ϕ_q, η_q . The variation with respect to θ_q and ϕ_q leads to quasiclassical

equations of motion for the angular dynamics $\frac{\delta \mathcal{L}}{\delta \theta_q}|_{q=0} = 0$ and $\frac{\delta \mathcal{L}}{\delta \phi_q}|_{q=0} = 0$. Explicitly²,

$$\sin \theta \dot{\phi} = -\sin \theta B + \cos \theta \cos(\phi - \omega_d t) \Omega - \frac{\tilde{g}}{S} \dot{\theta}, \quad (5.51)$$

$$\sin \theta \dot{\theta} = \frac{\tilde{g}}{S} \sin^2 \theta \dot{\phi} + \sin \theta \sin(\phi - \omega_d t) \Omega, \quad (5.52)$$

where we have dropped the index c for classical components. The variation with respect to η_q leads to the equation of motion for dynamical part of the magnetization length $\frac{\delta \mathcal{L}}{\delta \eta_q}|_{q=0} = 0$. Explicitly,

$$\frac{\delta \dot{M}}{J} = \frac{g_\Sigma^\uparrow + g_\Sigma^\downarrow}{2} \left(\delta M - 2\Gamma_\Sigma \int_{-\infty}^t dt' e^{-2\Gamma_\Sigma(t-t')} \delta M(t') \right), \quad (5.53)$$

where we used $\dot{\eta}_c = \delta M_c$, and dropped the index c for classical components. Interestingly, the angular dynamics θ, ϕ decouple from the length dynamics δM . This decoupling is a consequence of the leads being nonmagnetic.

The equations of motion can be recasted into other useful forms. The angular dynamics can be described in terms of the direction \mathbf{m} , which leads to the Landau-Lifshitz-Gilbert equation,

$$\dot{\mathbf{m}} = \mathbf{m} \times \mathbf{B} - \alpha \mathbf{m} \times \dot{\mathbf{m}}, \quad (5.54)$$

with the Gilbert damping coefficient $\alpha = \tilde{g}/S$. The integro-differential equation for δM can be recasted into a differential equation (for example by using Fourier-transform). It follows,

$$\delta \dot{M} = \left[\frac{g_\Sigma^\uparrow}{2} \left(J - \frac{1}{\rho_\uparrow} \right) + \frac{g_\Sigma^\downarrow}{2} \left(J - \frac{1}{\rho_\downarrow} \right) \right] \delta M, \quad (5.55)$$

where the terms with $\frac{1}{\rho_\sigma}$ originate from the dynamical Green's function \tilde{G}_d^K . These terms are intimately linked to the adjustment of the electron distribution function to the dynamical length δM and are also known as quantum capacity; compare chapter 4.

While the quantum capacity provided only a small correction in case of the Coulomb interaction (chapter 4), it is an essential contribution here. This is most clearly seen for $\rho_\uparrow = \rho_\downarrow = \rho$, which implies $g_\Sigma^\uparrow = g_\Sigma^\downarrow = g_\Sigma$. Then,

$$\delta \dot{M} = g_\Sigma \left(J - \frac{1}{\rho} \right) \delta M. \quad (5.56)$$

Without the quantum capacity ρ , the dynamical part δM would grow away from zero without bounds (all metals with a positive exchange constant $J > 0$ would be Stoner magnets with fully polarized bands). This strange behaviour becomes clear, when we trace back the origin of the quantum capacity; it originates from the adjustment of the distribution function to changes in δM . It is, therefore, related to the kinetic/orbital energy which is stored in the system: that is, if

²Formally, it seems that in the angular equations of motion there should appear a prefactor $\frac{M_0 + \delta M}{2J}/S$ with B_0 and Ω . However, this is an artefact of approximating the spin length S to be constant (5.39). Without this approximation, we should find $\frac{M_0 + \delta M}{2J}/S(t) = 1$.

more electrons are in the dot, then higher levels have to be occupied (Pauli exclusion principle) and, in turn, more kinetic/orbital energy has to be paid. Thus, it is the quantum capacity, which accounts for the changes in kinetic/orbital energy and, therefore, it is an essential contribution for length dynamics of the magnetization.

It is also useful to reconsider the different time-scales involved. The magnetization length δM relaxes on a time-scale of $\tau_{\delta M} = \frac{1}{2\Gamma_{\Sigma}(J\rho-1)}$. Typically, this is of the same order as the life-time of electrons in the dot $\tau_{\Gamma} = \frac{1}{\Gamma_{\Sigma}}$ but can also be much longer (for example close to the Stoner-transition $J\rho \approx 1$). In other words, δM typically varies on similar time-scale as the electronic distribution function. Thus, there can be a strong interplay between the dynamics of δM and the distribution function. And indeed, the quantum capacity, as a result of this interplay, is an essential contribution to the dynamics of δM . For the angular motion, we find $\dot{\theta} \propto \frac{1}{\xi}$ and $\ddot{\phi} \propto \frac{1}{\xi^2}$ which is self-consistent with our intermediate assumption that θ and $\dot{\phi}$ are slow variables for large magnetization/spin. Furthermore, this shows a separation of time-scales between slow angular motion $\theta, \dot{\phi}$ and faster length dynamics δM . This allows us to separate angular motion and length dynamics also in more complicated situations when the dynamics do not decouple exactly. The magnetization will relax very fast to its optimal value $\delta M \rightarrow 0$ and in this sense will adiabatically follow θ and $\dot{\phi}$.

5.5.3 A short comment on fluctuations

The magnetization fluctuates around the quasiclassical trajectory. To determine these fluctuations, we need to take second order in quantum components into account [Schmid, 1982, Eckern et al., 1990]. On the one hand, this means to keep the second order in the AES-like action (5.19). On the other hand, we have to take into account terms of second order in $\delta\Sigma$ and δQ . Fluctuations arising from the second order of the AES-like action have been discussed by [Shnirman et al., 2015] for a single tunnel junction where one lead has a dynamical magnetization. Based on the insight in [Shnirman et al., 2015] but with a different method (Fluctuation relations), fluctuations have been discussed in [Virtanen and Heikkilä, 2017] for a single magnetic tunnel junction where both leads are magnetic (one with fixed magnetization and one with dynamical magnetization). However, for a double tunnel junction considered here, the dynamical magnetization drives the electron system away from equilibrium. The resulting nonequilibrium distribution increases fluctuations of the magnetization. So far, this effect has not been considered in literature; see however [Keßler, 2018] for preliminary results.

5.6 Summary and discussion

This chapter presented a discussion of the magnetization dynamics of a small ferromagnetic quantum dot, which is tunnel-coupled to two normal metal leads and exposed to an external magnetic field. We derived quasiclassical equations of motion for the magnetization length and for the magnetization's angular motion. We found the Landau-Lifshitz-Gilbert equation (5.54) for the angular motion and equation (5.55) for the length dynamics. For the purpose of deriving

the equation of motion, we extended the AES-like method of ref. [Shnirman et al., 2015] to a double tunnel junction. In contrast to the single tunnel junctions considered in ref. [Shnirman et al., 2015, Virtanen and Heikkilä, 2017], in a double tunnel junction it is essential to carefully consider the distribution function of the middle region between the two leads. This was the major new achievement in [Ludwig et al., 2017, Ludwig et al., 2019b].

Interestingly, the distribution function adjusts to the angular dynamics of the magnetization but this adjustment has no back-action onto the angular dynamics. This is a consequence of the leads being nonmagnetic. In strong contrast, the distribution function also adjusts to the dynamical magnetization length and gives rise to the quantum capacity which is essential for the length dynamics. We note that, the length and angular dynamics decouple, which is also due to the leads being nonmagnetic. These facts (no influence of distribution function on the angular motion combined with the decoupling of angular motion from length dynamics) allowed the strongly simplified discussion in chapter 3. For magnetic leads, the angular dynamics starts to interplay with the distribution function and the length dynamics. However, the length dynamics relaxes very fast compared to the time-scales of the angular dynamics and, thus, will adiabatically follow the angular motion. This separation of time-scales allows us to consider the angular dynamics without considering the length dynamics even in more complicated situations with magnetic leads, as discussed in the next chapter. Finally, we note that it is straightforward to include the Coulomb interaction as treated in chapter 4; see [Ludwig et al., 2017, Ludwig et al., 2019b].

Part III

Magnetic double tunnel junction with a dynamical magnetization

Chapter 6

Magnetic double tunnel junction far from equilibrium

Magnetic tunnel junctions are spintronic systems of great interest for technical applications (in particular nonvolatile random access memory) as well as from a conceptual physical perspective (for example tunneling magnetoresistance) [Zhu and Park, 2006, Kawahara et al., 2012, Bhatti et al., 2017]. Most studies assume a spin-dependent electron distribution function which is locally close to equilibrium, that is, the distribution function is described with spin-dependent electrochemical potentials and temperatures; exceptions exist, see for example [Mahfouzi and Nikolić, 2014, Yamamoto et al., 2018] and—for numerical approaches—see [Mahfouzi, 2014]. Here, we focus on the interplay between a dynamical magnetization and a far-from-equilibrium electron distribution. This interplay gives rise to new universal spin-transfer-torque term which turns out to be essential for the magnetization dynamics; see chapter 7.

Explicitly, we consider a magnetic double tunnel junction: a ferromagnetic quantum dot is tunnel-coupled to two leads and exposed to an external magnetic field; see figure 6.1. The left lead is assumed to be magnetic itself, but with a fixed magnetization. The right lead is assumed to be a normal metal. The tunnel coupling between dot and leads is assumed to be spin-conserving and is described by tunneling rates Γ_l^σ and Γ_r for left and right lead respectively. The tunneling to the magnetic left lead depends on spin σ due to the lead's spin-dependent density of states. Both leads are assumed to be in equilibrium locally, but not necessarily with each other. Their distribution functions are given by equilibrium distributions $f_l(\omega) = 1/[e^{(\omega-\mu_l)/T_l} + 1]$ and $f_r(\omega) = 1/[e^{(\omega-\mu_r)/T_r} + 1]$ with electrochemical potentials μ_l, μ_r and temperatures T_l, T_r . The external magnetic field is assumed to have a large constant component B_0 parallel to the fixed magnetization of the left lead. Perpendicular to the fixed component, the magnetic field has a smaller oscillating part of strength Ω which can be used to drive the magnetization with frequency ω_d ; explicitly, $\mathbf{B} = (\Omega \cos \omega_d t, \Omega \sin \omega_d t, B_0)$.

When the dot's free (dynamic) magnetization is not in parallel to the external magnetic field, then the magnetization precesses around the external magnetic field. The dynamic magnetization is affected by Gilbert damping, which tends to relax the magnetization to its energetic minimum (parallel to the external magnetic field). We assume the Gilbert damping to be domi-

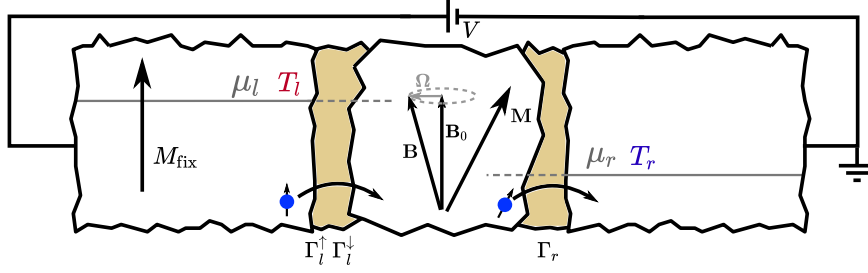


Figure 6.1: This figure schematically shows the system. An itinerant ferromagnetic quantum dot is exposed to an external magnetic field and tunnel-coupled to two leads which are assumed to be in (local) equilibrium. The tunneling is assumed to be spin-conserving with rate Γ_r for tunneling to the nonmagnetic right lead and a spin-dependent rate Γ_l^σ for tunneling to the magnetic left lead. The spin-dependence of the tunneling rate is assumed to arise from a spin-dependent density of states in the left lead. The system can be driven in three distinct ways: via an applied voltage $V = \mu_l - \mu_r$; via different lead temperatures $T_l \neq T_r$; or with an oscillating magnetic field Ω .

nated by the coupling to the leads [Tserkovnyak et al., 2002, Tserkovnyak et al., 2005]; and we disregard internal relaxation mechanisms. The magnetization relaxes towards its energetic minimum, unless some source of driving competes with the damping. The system can be driven in three distinct ways: via voltage bias $\mu_l \neq \mu_r$; via thermal bias $T_l \neq T_r$; via the oscillating external magnetic field with $\Omega \neq 0$ and $\omega_d \neq 0$. Here, we are particularly interested in situations where the magnetization $\mathbf{M} = M(\sin \theta \cos \phi, \sin \theta \sin \phi, \cos \theta)$ is driven into a steady state precession; that is, it precesses at a stationary polar angle θ with a constant frequency $\dot{\phi}$. Such a steady state precession can be sustained by a balance between driving and Gilbert damping. In a steady state precession, the dynamical magnetization renders the dot's effective single-particle Hamiltonian time-dependent. This time dependence drives the electron system away from equilibrium. In turn, a nonequilibrium distribution function develops in the dot, even when neither voltage nor thermal bias is applied.

Our goal is to analyze the interdependency of magnetization dynamics and electron distribution. For that purpose, we derive a quasiclassical equation of motion for the magnetization, where the interplay between dynamical magnetization and far-from-equilibrium distribution is taken into account self-consistently. We obtain equation (6.40), also known as Landau-Lifshitz-Gilbert-Slonczewski equation [Slonczewski, 1996]. As important side results, we determine the average charge current (6.43) and its noise (6.44). But our main result is the hybrid spin-transfer-torque current (6.37). It is a contribution to the Slonczewski spin-transfer-torque (STT) current, which emerges from the interplay between magnetization and distribution. As we will show below, the hybrid STT-current is universal: it depends only on the dynamics of the magnetization, but it is independent of the source of driving.

This chapter is based on [Ludwig et al., 2017, Ludwig et al., 2019b, Ludwig et al., 2019a], but methodically mostly follows [Ludwig et al., 2019b]. However, in contrast to those works, all three ways of driving (voltage, thermal, FMR) are considered in parallel. This allows us to demonstrate the universality of the hybrid STT current, which is governed by the dynamics of the magnetization but does not depend of the way of driving.

6.1 Description of the system

We consider an itinerant ferromagnetic quantum dot. It is exposed to an external magnetic field and tunnel-coupled to two leads; see figure 6.1. One lead is an itinerant ferromagnet itself, while the other lead is a normal metal. The magnetization of the ferromagnetic lead is assumed to be fixed in direction (choose as z -axis) and constant in length. The external magnetic field is assumed to have a large constant part B_0 parallel to the fixed magnetization of the lead but we allow for a smaller part Ω oscillating in the x - y -plane with frequency ω_d ; that is, $\mathbf{B} = (\Omega \cos \omega_d t, \Omega \sin \omega_d t, B_0)$. The time-dependent part of the magnetic field can be used to drive the magnetization as, for example, in ferromagnetic resonance (FMR) experiments. Alternative ways of driving are with voltage $\mu_l \neq \mu_r$ or thermal bias $T_l \neq T_r$ via the Slonczewski STT current.

6.1.1 Hamiltonian, tunneling rates, and distribution functions

Motivated by the universal Hamiltonian for metallic quantum dots [Kurland et al., 2000], we model the quantum dot by

$$H_d = \sum_{\alpha\sigma} \varepsilon_\alpha c_{\alpha\sigma}^\dagger c_{\alpha\sigma} - J\mathbf{S}^2 - \mathbf{B}\mathbf{S}, \quad (6.1)$$

where $c_{\alpha\sigma}^\dagger, c_{\alpha\sigma}$ are creation and annihilation operators for electrons in single-particle state α with spin σ and corresponding single-particle energy ε_α . The total spin operator is given by $\mathbf{S} = \sum_{\alpha\sigma\sigma'} c_{\alpha\sigma}^\dagger \frac{\boldsymbol{\sigma}_{\sigma\sigma'}}{2} c_{\alpha\sigma'}$. For positive exchange constant J , the exchange energy $-J\mathbf{S}^2$ tends to align spins of electrons in the dot. The coupling to the external magnetic field is described by the Zeeman-energy of the total spin $-\mathbf{B}\mathbf{S}$.

The coupling to the leads is included via two effects. First effect: Electrons can tunnel from the leads to the dot and vice versa, thereby, rendering the single-particle states in the dot unstable (finite life-time). We assume spin-conserved tunneling with (spin-dependent) tunneling rates $\Gamma_l^\uparrow, \Gamma_l^\downarrow$ for tunneling to the magnetic left lead and tunneling rate Γ_r for tunneling to the nonmagnetic right lead. The spin-dependence of the tunneling rate Γ_l^σ arises due to a spin-dependent density of states in the magnetic left lead. Second effect: The leads provide heat and particle baths for the dot. As the distribution functions of the leads can be controlled externally, we can assume them to be fixed to (local) equilibrium: $f_l(\omega) = \frac{1}{e^{(\omega-\mu_l)/T_l} + 1}$ and $f_r(\omega) = \frac{1}{e^{(\omega-\mu_r)/T_r} + 1}$ with electrochemical potentials μ_l, μ_r and temperatures T_l, T_r . In contrast, the dot's distribution function cannot be directly controlled in an experiment. Even though one might be able to prepare an initial electron distribution, due to tunneling of electrons this initial distribution would be forgotten after a short transient time. Afterwards, the dot's distribution function is governed by the distribution functions of the leads and the dynamics of the dot's magnetization.

6.1.2 Derivation of an effective action for the magnetization

The system can be driven out of equilibrium in three distinct ways: by a voltage bias for different electrochemical potentials $\mu_l \neq \mu_r$ in the leads; by a thermal bias for different lead temperatures $T_l \neq T_r$; and by an FMR-type driving for $\Omega \neq 0$; or any combination thereof. Independent of the specific type of driving, the system will be driven away from equilibrium. Keldysh formalism is suitable to describe such an out-of-equilibrium situation and we use its path-integral version [Kamenev and Levchenko, 2009, Kamenev, 2011, Altland and Simons, 2010]. The Keldysh generating function is $\mathcal{Z} = \int D[\bar{\Psi}, \Psi] e^{i\mathcal{S}}$ with the action

$$\mathcal{S} = \oint_K dt [\bar{\Psi}(i\partial_t - \hat{\Sigma})\Psi - H_d(\bar{\Psi}, \Psi)] . \quad (6.2)$$

where $\bar{\Psi}, \Psi$ denote all fermionic fields of the dot. For compact notation, we introduced the self-energy operator $[\hat{\Sigma}\Psi](t) = \oint_K dt' \Sigma(t-t')\Psi(t')$, where the self-energy $\Sigma = \Sigma_l + \Sigma_r$ includes all the necessary information about the coupling to the leads; Σ_l and Σ_r arise from the coupling to left and right lead respectively. It is possible to account for the coupling to the leads by just a self-energy, since we assumed the leads to be noninteracting. Formally, this assumption allows to integrate out the leads, which gives rise to the self-energy; see appendix A. The information about tunneling rates is contained in the retarded and advanced parts $\Sigma_\sigma^{R/A}(\omega) = \mp i(\Gamma_l^\sigma + \Gamma_r)$. The information about the leads' distribution functions is contained in the Keldysh part of the self-energy $\Sigma_\sigma^K(\omega) = -2i[\Gamma_l^\sigma F_l(\omega) + \Gamma_r F_r(\omega)]$ with $F_{l/r}(\omega) = 1 - 2f_{l/r}(\omega)$. Since $F_{l/r}(\omega)$ and $f_{l/r}(\omega)$ are in one to one correspondence, we refer to both as distribution functions.

The exchange interaction in the dot's Hamiltonian renders the action in equation (6.2) non-trivial, as it is quartic in fermionic fields. This interaction can be decoupled by a Hubbard-Stratonovich (HS) transformation

$$e^{iJ \oint_K dt \mathbf{S}^2} = \int D\mathbf{B}_{exc} e^{-i \oint_K dt \left(\frac{\mathbf{B}_{exc}^2}{4J} - \mathbf{B}_{exc} \mathbf{S} \right)} , \quad (6.3)$$

where \mathbf{B}_{exc} is the exchange field. A variation with respect to quantum field \mathbf{B}_{exc}^q would yield the classical component $\mathbf{B}_{exc}^c = 2J\langle \mathbf{S} \rangle$. Thus, the exchange field can be viewed as the "mean-field" that arises from the exchange interaction averaged over all electron-spins. The HS-decoupling leads to $\mathcal{Z} = \int D[\bar{\Psi}, \Psi] \int D\mathbf{M} e^{i\mathcal{S}}$ with the effective action

$$\mathcal{S} = \oint_K dt \bar{\Psi} \left[i\partial_t - \underbrace{\left(\varepsilon_\alpha - \mathbf{M} \frac{\boldsymbol{\sigma}}{2} \right)}_{h_d} - \hat{\Sigma} \right] \Psi - \underbrace{\oint_K dt \frac{(\mathbf{M} - \mathbf{B})^2}{4J}}_{\mathcal{S}_{HS}} , \quad (6.4)$$

where we introduced $\mathbf{M} = \mathbf{B}_{exc} + \mathbf{B}$ to which we refer as the magnetization¹. The Hubbard-Stratonovich action \mathcal{S}_{HS} describes the "free" dynamics of the magnetization (HS-field). The interplay between magnetization and the underlying electron system is contained in the effective

¹Actually, it would be more precise to refer to \mathbf{B}_{exc} as magnetization, but in typical ferromagnets the internal field \mathbf{B}_{exc} is much larger than the external field \mathbf{B} . Thus, $\mathbf{M} \approx \mathbf{B}_{exc}$ and it is justified to refer also to \mathbf{M} as magnetization.

single-particle Hamiltonian h_d . As we want to focus on the magnetization dynamics, it is convenient to integrate out the fermions. After re-exponentiation of the resulting determinant follows

$$\mathcal{S} = -i \text{tr} \ln \left[\underbrace{i\partial_t - h_d - \hat{\Sigma}}_{G^{-1}} \right] + \mathcal{S}_{\text{HS}} , \quad (6.5)$$

where G^{-1} defines the effective single-particle Green's function for electrons in the dot G . To be precise: G is not the full Green's function but instead it is of auxiliary character; to obtain the full Green's function of electrons in the dot, the HS-field should be integrated out.

6.2 Ferromagnetic regime and transition to rotating frame

The dot is assumed to be deep in the ferromagnetic Stoner regime with a large length of magnetization which defines the largest relevant energy scale in the dot. In addition, the relaxation of the magnetization length is assumed to be fast on the typical time-scales of θ and ϕ . Being interested mainly in the angular dynamics, this separation of time-scales allows us to disregard the length dynamics, since the length relaxes to its optimal value M_0 almost immediately. In turn, we assume the length to be constant $|\mathbf{M}| = M_0$; for details see chapter 5. The magnetization can then be rewritten as $\mathbf{M} = M_0 \mathbf{m}$, where only the direction $\mathbf{m} = (\sin \theta \cos \phi, \sin \theta \sin \phi, \cos \theta)$ remains dynamical.

The dynamical direction of the magnetization renders the action (6.5) nontrivial: to describe the single-particle dynamics, the problem of a spin in a time-dependent magnetic field has to be solved. Instead of attempting to solve this hard problem, we change into the frame of reference that dynamically follows the magnetization of the dot. In other words, we perform an $SU(2)$ -gauge transformation, that is, a rotation in the spin-space R . This rotation is performed in a way, such that the magnetization always points along the z -direction,

$$R^\dagger \mathbf{M} \boldsymbol{\sigma} R = M_0 \sigma_z . \quad (6.6)$$

Formally, this is achieved by going back to action (6.4), transforming $\Psi \rightarrow R\Psi$ and $\bar{\Psi} \rightarrow \bar{\Psi}R^\dagger$, and integrating out the fermions again. After this rotation, the action becomes

$$\mathcal{S} = -i \text{tr} \ln \left[\underbrace{R^\dagger (i\partial_t - h_d - \hat{\Sigma}) R}_{\tilde{G}^{-1}} \right] + \mathcal{S}_{\text{HS}} , \quad (6.7)$$

where \tilde{G}^{-1} defines the rotating-frame Green's function \tilde{G} . More explicitly,

$$\tilde{G}^{-1} = i\partial_t - \underbrace{\left(\varepsilon_\alpha - M_0 \frac{\sigma_z}{2} + Q \right)}_{\tilde{h}_d} - R^\dagger \Sigma R . \quad (6.8)$$

The magnetization's time dependence is transferred into the rotation R . While the rotation strongly simplifies the magnetic part of the rotating-frame single-particle hamiltonian \tilde{h}_d , it

comes at a cost: first, the time dependence of the rotation gives rise to a new term $Q = -iR^\dagger \dot{R}$ which is also known as Berry connection [Shnirman et al., 2015]; second, the self-energy gets rotated, since it is nontrivial in spin-space and, in addition, contains distribution functions which are nonlocal in time-space.

For the rotation, we choose a representation with Euler-angles ²,

$$R = e^{-i\frac{\phi}{2}\sigma_z} e^{-i\frac{\theta}{2}\sigma_y} e^{i\frac{\chi}{2}\sigma_z}, \quad (6.9)$$

where θ, ϕ characterize the direction \mathbf{m} and the angle χ represents a gauge-freedom [Shnirman et al., 2015]. It follows $Q = Q_{\parallel} + Q_{\perp}$ with the spin-diagonal part $Q_{\parallel} = [\dot{\phi}(1 - \cos\theta) - \dot{\chi}]\frac{\sigma_z}{2}$ and the spin-off-diagonal part $Q_{\perp} = e^{i\chi\sigma_z}[\dot{\phi}\sin\theta\frac{\sigma_x}{2} - \dot{\theta}\frac{\sigma_y}{2}]e^{i\phi\sigma_z}$. The spin-diagonal part Q_{\parallel} contains information about the Berry-phase which is acquired by electron spins that follow the magnetization adiabatically. The spin-off-diagonal part contains information about (Landau-Zener-)transitions between spin-up and spin-down.

The dynamical rotation of the self-energy is related to two facts: first, the tunneling rate to the magnetic lead depends on the relative orientation of the two magnetizations; second, the distribution function on the dot is not only determined by the leads (self-energy Σ) but also by the dynamics of the magnetization (rotation R). The details are more conveniently discussed in the quasiclassical approximation.

6.3 Quasiclassical approximation

In principle, the derivation of quasiclassical equations of motion is quite simple: they follow from a straightforward variation of the action with respect to quantum components. In practice, however, this procedure often leads to complicated integral- or integro-differential-equations of motion for which an exact solution is usually out of reach. In turn, approximations have to be made to gain insights into the dynamics.

It is convenient to reverse the order of variation and approximation and perform approximations on the level of the action rather than in the equations of motion. In reversing this order, it is important to be careful. As the equation of motion is governed by the first order in quantum components, the technically safest way is to expand in quantum components first and only afterwards in other small quantities. Particularly problematic would be an expansion in tunneling before the expansion in quantum components. In this case, important information about the dot's distribution function would be formally lost. In special cases, the lost information can be regained with great intuition; see for example [Altland and Egger, 2009, Altland and Simons, 2010], see however chapter 4. Here, we take the technically safe way and expand in quantum components first.

²The specific form of this choice is motivated by the boundary condition $R_+(-T_K) = R_-(-T_K)$, which is now satisfied for $\theta_+(-T_K) = \theta_-(-T_K)$, $\phi_+(-T_K) - \phi_-(-T_K) = 2\pi n$, and $\chi_+(-T_K) - \chi_-(-T_K) = 4\pi m$ with $n, m \in \mathbb{N}$; compare [Shnirman et al., 2015].

6.3.1 Expansion in quantum components

To perform a quasiclassical approximation, we expand in quantum components. For that purpose, it is convenient to introduce purely classical rotations $R_k = R|_{q=0}$, where $\dots|_{q=0}$ means to set the quantum components of all coordinates to zero; note $R_k \neq R_c = (R_+ + R_-)/2$. The rotated self-energy is separated $R^\dagger \Sigma R = R_k^\dagger \Sigma R_k + \delta \tilde{\Sigma}$ into a purely classical part $R_k^\dagger \Sigma R_k = [R^\dagger \Sigma R]|_{q=0}$ and the rest $\delta \tilde{\Sigma} = R^\dagger \Sigma R - R_k^\dagger \Sigma R_k$. Analogously, the Berry-connection is split, $Q = Q_k + \delta Q$, into a purely classical part $Q_k = Q|_{q=0}$ and the rest $\delta Q = Q - Q_k$. For the action follows

$$\mathcal{S} = -i \text{tr} \ln [\tilde{G}_c^{-1} - \delta \tilde{\Sigma} - \delta Q] + \mathcal{S}_{\text{HS}} , \quad (6.10)$$

where we introduced the classical Green's function \tilde{G}_c by its inverse,

$$\tilde{G}_c^{-1} = i\partial_t - \varepsilon_\alpha + M_0 \frac{\sigma_z}{2} - Q_k - R_k^\dagger \Sigma R_k . \quad (6.11)$$

By construction, the inverse classical Green's function contains classical coordinates θ_c, ϕ_c and the classical gauge freedom χ_c , but no quantum components. In contrast, $\delta \tilde{\Sigma}$ and δQ are at least of first order in quantum components. In turn, an expansion in quantum components corresponds to the expansion in $\delta \tilde{\Sigma}$ and δQ ; even though one would have to be careful with higher than first orders.

A formal expansion in $\delta \tilde{\Sigma}$ and δQ is straightforward and yields the quasiclassical approximation for the action. For the expansion in $\delta \tilde{\Sigma}$, we obtain an Ambegaokar-Eckern-Schön-like action [Shnirman et al., 2015],

$$\mathcal{S}_{\text{AES}} = i \text{tr} [\tilde{G}_c \delta \tilde{\Sigma}] . \quad (6.12)$$

For the expansion in δQ it is convenient to split $\delta Q = \delta Q_{\parallel} + \delta Q_{\perp}$ into the spin-diagonal part δQ_{\parallel} and the spin-off-diagonal part δQ_{\perp} . The expansion in δQ_{\parallel} leads to an action of the Wess-Zumino-Novikov-Witten-type [Shnirman et al., 2015],

$$\mathcal{S}_{\text{WZNW}} = i \text{tr} [\tilde{G}_c \delta Q_{\parallel}] , \quad (6.13)$$

which is related to the Berry-phase. The expansion in δQ_{\perp} leads to the Landau-Zener-action

$$\mathcal{S}_{\text{LZ}} = i \text{tr} [\tilde{G}_c \delta Q_{\perp}] , \quad (6.14)$$

which is related to Landau-Zener-transitions between spin-up and spin-down states.

Besides the contributions arising from the expansion of the $\text{tr} \ln[\dots]$, we have to take the Hubbard-Stratonovich-action into account. Expressed with angles θ, ϕ follows

$$\mathcal{S}_{\text{HS}} = \frac{M_0}{2J} \oint_K dt [B_0 \cos \theta + \Omega \sin \theta \cos(\phi - \omega dt)] , \quad (6.15)$$

where constant terms ($\propto \mathbf{M}^2, \mathbf{B}^2$) have been dropped. The HS-action is independent of the Green's function, since it describes the "free" dynamics of the magnetization (HS-field). The

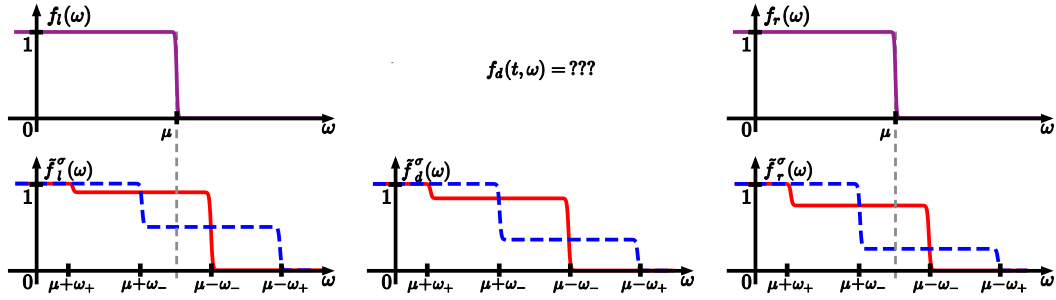


Figure 6.2: (Upper row) Illustration of the main problem: in the laboratory frame the distribution functions of the leads are known, but the dot's distribution function is hard to determine due to the time dependence of the magnetization. (Lower row) Illustration of the basic idea for solution: we change to the magnetization's rotating frame of reference, where the dot's Hamiltonian becomes approximately time-independent and, therefore, the distribution function of the small ferromagnet becomes a superposition of the leads' rotating-frame distribution functions *as they are seen by the dot*. We emphasize that the leads' rotating-frame distribution functions shown in the figure are different, despite them being equal in the laboratory frame of reference. The reason for this is that it is not really the leads' distribution functions which are shown, but the distribution functions as they are seen by the dot. This means, that the tunneling rates are involved; the difference between both leads arises from the spin-dependent tunneling rate of the left lead versus the spin-independent tunneling rate in the other lead.

interplay between magnetization and underlying electron system is essential for the dynamics of the magnetization. This interplay is described by the other three contributions to the action \mathcal{S}_{AES} , $\mathcal{S}_{\text{WZNW}}$, and \mathcal{S}_{LZ} , which crucially depend on the classical Green's function \tilde{G}_c of the electrons. Thus, the classical Green's function has to be determined before we can obtain more explicit forms of these contributions to the action.

6.3.2 Determination of the classical rotating-frame Green's function

The classical rotating-frame Green's function \tilde{G}_c has to be determined from its inverse which was defined in equation (6.11). While it is rather straightforward to deal with the constant part $i\partial_t - \varepsilon_\alpha + M_0\sigma_z/2$, the major difficulties arise from the rotated self-energy $R_k^\dagger \Sigma R_k$ and the Berry-connection Q_k which are both time-dependent. However, the determination of \tilde{G}_c is greatly simplified by the assumption that M_0 defines the largest relevant energy-scale in the dot. In turn, spin-up and spin-down states are always well separated in energy for a given single-particle level α . This allows us to disregard spin-off-diagonal terms of G_c^{-1} upon inversion. In \tilde{G}_c the spin-off-diagonal elements are suppressed by the large value of the magnetization M_0 . Explicitly, this allows us to disregard the spin-off-diagonal part of the rotating-frame self-energy $[R_k^\dagger \Sigma R_k]_{\sigma\bar{\sigma}}$ and the transitions between spin-up and spin-down $Q_{\perp,k}$, which corresponds to an adiabatic approximation (the angular dynamics is slow on the time-scale defined by $1/M_0$). The corresponding spin-diagonal terms $[R_k^\dagger \Sigma R_k]_{\sigma\sigma}$ and $Q_{\parallel,k}$, however, have to be considered carefully.

The spin-diagonal part $Q_{\parallel,k} = [\dot{\phi}_c(1 - \cos \theta_c) - \dot{\chi}_c] \frac{\sigma_z}{2}$ gives rise to an energy splitting between spin-up and spin-down in addition to M_0 . Following reference [Shnirman et al., 2015], we

eliminate $Q_{\parallel,k}$ by a smart choice of gauge,

$$\chi_c = \dot{\phi}_c(1 - \cos \theta_c) , \quad (6.16)$$

$$\chi_q = \phi_q(1 - \cos \theta_c) . \quad (6.17)$$

While the choice of the classical component χ_c seems obvious from the present perspective, the smart part of this gauge lies in the choice of the quantum component χ_q which also eliminates a large part of the full Q_{\parallel} without violating the boundary condition $\chi_+(-T_K) - \chi_-(-T_K) = 4\pi m$. To summarize: $Q_{\perp,k}$ is disregarded in an adiabatic approximation and $Q_{\parallel,k}$ is eliminated by the choice of gauge (6.16). This leaves us with the inverse classical Green's function,

$$G_c^{-1} = i\partial_t - \varepsilon_\alpha + M_0 \frac{\sigma_z}{2} - R_k^\dagger \Sigma R_k . \quad (6.18)$$

Despite the elimination of $Q_{\parallel,k}$, the Berry-phase remains relevant. By the choice of gauge, the Berry-phase is shifted to the rotating-frame self-energy $R_k^\dagger \Sigma R_k$.

The spin-diagonal part of the rotating-frame self-energy $[R_k^\dagger \Sigma R_k]_{\sigma\sigma}$ contains the information about tunneling rates for tunneling to the leads and about distribution functions of the leads as they are "seen" by the dot in the rotating frame. The determination of these rotating-frame tunneling rates and distribution functions, is significantly simplified by assuming θ_c and $\dot{\phi}_c$ to be slow on the scales of inverse tunneling rate (life-time) and inverse lead-temperatures (correlation time of thermal noise). This assumption is motivated by observing that typical changes of θ_c and $\dot{\phi}_c$ are due to tunneling of electrons. However, the change of angles is geometrically suppressed by the length of the total spin length S (corresponding to the magnetization M_0). Consequently, we expect θ_c and $\dot{\phi}_c$ to change roughly at the time-scale of S/Γ , where Γ is a generic tunneling rate. We emphasize that ϕ itself can change much faster, due to the precession around the external magnetic field. Finally, when we have derived the equations of motion, the slowness assumptions have to be checked for self-consistency.

The retarded and advanced parts of the self-energy are given by $[R_k^\dagger \Sigma^{R/A} R_k]_{\sigma\sigma} = \mp i(\Gamma_l^\sigma(\theta_c) + \Gamma_r)$, where the tunneling rate to the left lead, $\Gamma_l^\sigma(\theta_c) = \cos^2 \frac{\theta_c}{2} \Gamma_l^\sigma + \sin^2 \frac{\theta_c}{2} \Gamma_l^{\bar{\sigma}}$, depends on the relative angle θ_c between the fixed magnetization of the left lead and the dynamic magnetization of the dot. The tunneling rate to the nonmagnetic right lead Γ_r remains independent of the orientation of the dot's magnetization. In total, the tunneling rate $\Gamma_\sigma(\theta_c) = \Gamma_l^\sigma(\theta_c) + \Gamma_r$ governs the life-time of electrons on the dot $\tau_\Gamma = 1/\Gamma_\sigma(\theta_c)$. In addition to the tunneling rates, we need to determine the rotating-frame distribution functions of the leads as they are "seen" by the dot. This information is contained in the Keldysh part of the self-energy. Using the slowness of θ_c and $\dot{\phi}_c$, we obtain $[R_k^\dagger \Sigma^K R_k]_{\sigma\sigma} = -2i[\Gamma_l^\sigma(\theta_c) \tilde{F}_l^\sigma(\omega) + \Gamma_r \tilde{F}_r^\sigma(\omega)]$; see also appendix B. Here $\tilde{F}_l^\sigma(\omega) = [\cos^2 \frac{\theta_c}{2} \Gamma_l^\sigma F_l(\omega + \sigma\omega_-) + \sin^2 \frac{\theta_c}{2} \Gamma_l^{\bar{\sigma}} F_l(\omega + \bar{\sigma}\omega_+)]/\Gamma_l^\sigma(\theta_c)$ is the rotating-frame distribution function of the left lead as it is "seen" by the dot; similarly for the right lead $\tilde{F}_r^\sigma(\omega) = [\cos^2 \frac{\theta_c}{2} F_r(\omega + \sigma\omega_-) + \sin^2 \frac{\theta_c}{2} F_r(\omega + \bar{\sigma}\omega_+)]$. The dynamics of the magnetization enters via the Berry-phase shifts $\omega_\pm = \dot{\phi}_c(1 \pm \cos \theta_c)/2$.

Now, knowing the self-energy, we can determine the classical rotating-frame Green's func-

tion. Using the slowness of θ_c and $\dot{\phi}_c$, we obtain

$$\tilde{G}_c^{R/A}(\bar{t}, \omega) = \frac{1}{\omega - \xi_{\alpha\sigma} \pm i\Gamma_\sigma(\theta_c)}, \quad (6.19)$$

$$\tilde{G}_c^K(\bar{t}, \omega) = \frac{-2i\Gamma_\sigma(\theta_c)}{(\omega - \xi_{\alpha\sigma})^2 + \Gamma_\sigma^2(\theta_c)} \tilde{F}_s^\sigma(\bar{t}, \omega), \quad (6.20)$$

to zeroth order in a gradient expansion. The effective single-particle energy is defined as $\xi_{\alpha\sigma} = \varepsilon_\alpha - M_0 \frac{\sigma}{2}$. The dot's rotating-frame distribution function is given by,

$$\begin{aligned} \tilde{F}_s^\sigma(\bar{t}, \omega) = \frac{1}{\Gamma_\sigma(\theta_c)} & \left[\cos^2 \frac{\theta_c}{2} \Gamma_l^\sigma F_l(\omega + \sigma\omega_-) + \sin^2 \frac{\theta_c}{2} \Gamma_l^{\bar{\sigma}} F_l(\omega + \bar{\sigma}\omega_+) + \right. \\ & \left. + \cos^2 \frac{\theta_c}{2} \Gamma_r F_r(\omega + \sigma\omega_-) + \sin^2 \frac{\theta_c}{2} \Gamma_r F_r(\omega + \bar{\sigma}\omega_+) \right], \end{aligned} \quad (6.21)$$

where the index s is short for "slow", to remind us that it is obtained by assuming θ_c and $\dot{\phi}_c$ to be slow. This distribution function is far from equilibrium, as it is a superposition of four different equilibrium distribution functions. Even if neither voltage nor thermal bias is applied, it remains a superposition of two different distribution function provided that the magnetization is precessing at a nontrivial polar angle ($\theta \neq 0, \pi$); see figure 6.2. We emphasize again that the classical Green's function and, thus, also the distribution function is of auxiliary character. Nevertheless, the auxiliary Green's function and the auxiliary distribution function provide exactly the information which we need to determine the quasiclassical action in an explicit form.

6.3.3 Explicit form of the quasiclassical action

We have four contributions to the quasiclassical action: the HS-action (6.15) which describes the "free" dynamics of the HS-field; the AES-like action (6.12) which describes the effect of tunneling of electrons; the WZNW-action (6.13) which is related to the Berry phase; and the LZ-action (6.14) which is related to transitions between spin-up and spin-down states. Knowing the classical Green's function, we are in position to determine these contributions explicitly. We keep only terms of first order in quantum components θ_q, ϕ_q which is sufficient for the quasiclassical equation of motion.

The HS-action (6.15) is straightforward to obtain,

$$\mathcal{S}_{\text{HS}} = \frac{M_0}{2J} \int dt \left\{ \theta_q [\Omega \cos \theta_c \cos(\phi_c - \omega_d t) - B_0 \sin \theta_c] - \phi_q \Omega \sin \theta_c \sin(\phi_c - \omega_d t) \right\}, \quad (6.22)$$

because it is independent of the Green's function.

For the WZNW-action (6.13), which is related to the Berry phase, follows

$$\mathcal{S}_{\text{WZNW}} = - \int dt S(t) \sin \theta_c (\theta_q \dot{\phi}_c - \phi_q \dot{\theta}_c), \quad (6.23)$$

where $S(t)$ is the length of the total spin. Formally, it is defined as $S(t) = -\frac{i}{4} \text{tr} [G_c(t, t) \sigma_z]$. Explicitly, it is given by $S(t) = -\frac{1}{4} \int d\omega [\rho_\uparrow(\omega) F_s^\uparrow(t, \omega) - \rho_\downarrow(\omega) F_s^\downarrow(t, \omega)]$, where $\rho_\sigma(\omega) =$

$\Sigma \alpha \frac{1}{\pi} \frac{\Gamma_{\sigma}(\theta_c)}{(\omega - \xi_{\alpha\sigma})^2 + \Gamma_{\sigma}^2(\theta_c)}$ is the density of states. The total spin-length $S(t)$ is essentially half the difference between the number of spin-up and spin-down electrons on the dot. The length $S(t)$ fluctuates slightly around a constant value $S_0 = \frac{M_0}{2J}$, due to its dependence on θ_c and ϕ_c . However, for a large magnetization deep in the Stoner-regime, these fluctuations are small compared to the size of the spin and we approximate $S(t) \approx S_0$.

The LZ-action (6.14) is related to transitions between spin-up and spin-down states. However, it includes only spin-off-diagonal elements of the classical Green's function. Thus,

$$\mathcal{S}_{\text{LZ}} \approx 0, \quad (6.24)$$

as we have approximated the classical Green's function to be diagonal in spin-space.

The AES-like action (6.12) is related to tunneling of electrons. Due to the Pauli exclusion principle, the tunneling of electrons strongly depends on the distribution functions. Therefore, it is important in the AES-like action to carefully consider the adjustments of the distribution function to the magnetization dynamics. To first order in R_q the AES-like action becomes

$$\mathcal{S}_{\text{AES}} = - \int dt \int dt' \sum_{\sigma\sigma'} \text{Im} \left[R_q^{\sigma'\sigma}(t) \alpha_{\sigma\sigma'}(t, t') (R_c^{\sigma'\sigma}(t'))^* \right], \quad (6.25)$$

where the trace was explicitly taken over Keldysh-, time-, and spin-space. The remaining trace over orbital space is included in the kernel function which is formally defined by $\alpha_{\sigma\sigma'}(t, t') = \text{tr} [\tilde{G}_{c\sigma}^R(t, t') \Sigma_{\sigma'}^K(t' - t) + \tilde{G}_{c\sigma}^K(t, t') \Sigma_{\sigma'}^A(t' - t)]$. More explicitly,

$$\alpha_{\sigma\sigma'}(\bar{t}, \omega) = \int d\omega' \rho_{\sigma}(\omega') \left[\Gamma_l^{\sigma'} [\tilde{F}_s^{\sigma}(\bar{t}, \omega') - F_l(\omega' - \omega)] + \Gamma_r [\tilde{F}_s^{\sigma}(\bar{t}, \omega') - F_r(\omega' - \omega)] \right]. \quad (6.26)$$

where we disregarded the imaginary part, as we expect it to only renormalize the constant part of external magnetic field which is assumed to be already included in B_0 .

We split the kernel function into three parts of clearly distinct physical origin:

$$\alpha_{\sigma\sigma'}(\bar{t}, \omega) = \alpha_{\sigma\sigma'}^d(\omega) + \alpha_{\sigma\sigma'}^b(\bar{t}) + \alpha_{\sigma\sigma'}^h(\bar{t}), \quad (6.27)$$

where the superscripts d, b, h are short for *dissipative*, *bias*, and *hybrid* contributions defined as follows. The dissipative contribution $\alpha_{\sigma\sigma'}^d(\omega)$ contains the frequency dependent parts, which can be easily separated out by defining $\alpha_{\sigma\sigma'}^d(\omega) = \alpha_{\sigma\sigma'}(\bar{t}, \omega) - \alpha_{\sigma\sigma'}(\bar{t}, 0)$. It follows,

$$\alpha_{\sigma\sigma'}^d(\omega) = \int d\omega' \rho_{\sigma}(\omega') \left[\Gamma_l^{\sigma'} [F_l(\omega') - F_l(\omega' - \omega)] + \Gamma_r [F_r(\omega') - F_r(\omega' - \omega)] \right]. \quad (6.28)$$

Interestingly, the dissipative part is independent of the dot's distribution function. In contrast, the remaining part $\alpha_{\sigma\sigma'}(\bar{t}, 0)$ does depend on the dot's distribution function $\tilde{F}_s^{\sigma}(\bar{t}, \omega')$. This distribution function depends not only on the orientation but also on the dynamics of the magne-

tization. To separate orientational from dynamical effects, we introduce a distribution function for a hypothetically fixed (f) magnetization $\tilde{F}_f^\sigma(\bar{t}, \omega') = \tilde{F}_s^\sigma(\bar{t}, \omega')|_{\dot{\theta}, \dot{\phi}=0}$, where $\dots|_{\dot{\theta}, \dot{\phi}=0}$ means to set $\dot{\theta}$ and $\dot{\phi}$ to zero. In other words, we consider a situation where the dot's magnetization is artificially fixed. This leads to $\tilde{F}_f^\sigma(\bar{t}, \omega) = [\Gamma_l^\sigma(\theta_c)F_l(\omega) + \Gamma_r F_r(\omega)]/\Gamma_\sigma(\theta_c)$. Accordingly, we define the bias contribution $\alpha_{\sigma\sigma'}^b(\bar{t}) = \alpha_{\sigma\sigma'}^b(\bar{t}, 0)|_{\dot{\theta}, \dot{\phi}=0}$ which depends on the applied bias and the orientation of the magnetization but, by construction, is independent of the magnetization dynamics. More explicitly,

$$\alpha_{\sigma\sigma'}^b(\bar{t}) = \int d\omega' \rho_\sigma(\omega') \left[\Gamma_l^{\sigma'} [\tilde{F}_f^\sigma(\bar{t}, \omega') - F_l(\omega')] + \Gamma_r [\tilde{F}_f^\sigma(\bar{t}, \omega') - F_r(\omega')] \right]. \quad (6.29)$$

Even though it is not obvious, this contribution vanishes when no bias (voltage or temperature difference) is applied; thus, the name "bias" contribution. The only part that remains to be determined is the contribution arising from the dynamics of the magnetization. It is called "hybrid" contribution and is formally defined by $\alpha_{\sigma\sigma'}^h(\bar{t}) = \alpha_{\sigma\sigma'}^h(\bar{t}, \omega) - \alpha_{\sigma\sigma'}^d(\omega) - \alpha_{\sigma\sigma'}^b(\bar{t})$. More explicitly,

$$\alpha_{\sigma\sigma'}^h(\bar{t}) = \int d\omega' \rho_\sigma(\omega') \left[\Gamma_l^{\sigma'} [\tilde{F}_s^\sigma(\bar{t}, \omega') - \tilde{F}_f^\sigma(\bar{t}, \omega')] + \Gamma_r [\tilde{F}_s^\sigma(\bar{t}, \omega') - \tilde{F}_f^\sigma(\bar{t}, \omega')] \right]. \quad (6.30)$$

This hybrid contribution vanishes for a static magnetization in the dot, since then $\tilde{F}_s^\sigma(\bar{t}, \omega') = \tilde{F}_f^\sigma(\bar{t}, \omega')$ by construction of $\tilde{F}_f^\sigma(\bar{t}, \omega')$. The name "hybrid" will become clear below. It is straightforward to add up dissipative (6.28), bias (6.29), and hybrid (6.30) contributions to check $\alpha_{\sigma\sigma'}^d(\omega) + \alpha_{\sigma\sigma'}^b(\bar{t}) + \alpha_{\sigma\sigma'}^h(\bar{t}) = \alpha_{\sigma\sigma'}^h(\bar{t}, \omega)$, which should hold by construction. Performing the frequency integrations in all three contributions yields

$$\alpha_{\sigma\sigma'}^d(\omega) = g_{\sigma\sigma'} \omega, \quad (6.31)$$

$$\alpha_{\sigma\sigma'}^b(\bar{t}) = I_V^{\sigma\sigma'}(\theta_c) + I_T^{\sigma\sigma'}(\theta_c), \quad (6.32)$$

$$\alpha_{\sigma\sigma'}^h(\bar{t}) = I_h^{\sigma\sigma'}(\theta_c, \dot{\phi}_c), \quad (6.33)$$

where we defined the conductance $g_{\sigma\sigma'} = 2\rho_\sigma(\Gamma_l^{\sigma'} + \Gamma_r)$ and introduced three different current contributions: the voltage bias contribution $I_V^{\sigma\sigma'}(\theta_c) = \frac{2\Gamma_r\Gamma_\Delta}{\Gamma_\sigma(\theta_c)}(\sigma' - \sigma \cos \theta_c)\rho_\sigma V$; the thermal bias contribution $I_T^{\sigma\sigma'}(\theta_c) = \frac{2\Gamma_r\Gamma_\Delta}{\Gamma_\sigma(\theta_c)}(\sigma' - \sigma \cos \theta_c)\rho'_\sigma b_T$ with the thermal bias parameter $b_T = \frac{\pi^2}{6}(T_l^2 - T_r^2)$ and $\Gamma_\Delta = (\Gamma_l^\uparrow - \Gamma_l^\downarrow)/2$; and the hybrid contribution $I_h^{\sigma\sigma'}(\theta_c, \dot{\phi}_c) = g_{\sigma\sigma'} \frac{\Gamma_\Delta \sin^2 \theta_c}{2\Gamma_\sigma(\theta_c)} \dot{\phi}_c$. We assumed the density of states in the dot $\rho_\sigma(\omega)$ to be approximately linear around the right lead's electrochemical potential μ_r ; we use the right lead, since it is the grounded one. That is, we assume $\rho_\sigma(\mu_r + \omega) \approx \rho_\sigma + \rho'_\sigma \omega$ with $\rho_\sigma = \rho_\sigma(\mu_r)$ and $\rho'_\sigma = \partial_\omega \rho_\sigma(\omega)|_{\omega=\mu_r}$. Furthermore, we assume $\rho'_\sigma \approx \mathcal{O}(\frac{1}{M_0})$, as the density of states will typically change on the scale of M_0 . We have disregarded the terms with ρ'_σ for the voltage bias current, the hybrid current, and the dissipative current, since these will be of order $\mathcal{O}(\frac{V}{M_0}, \frac{\omega}{M_0}, \frac{\omega_\pm}{M_0})$. Only for the thermal bias current,

we keep terms with ρ'_σ . While these are also suppressed by $\frac{1}{M_0}$, the thermal effects would vanish for a constant density of states. In other words, to observe effects related to thermally induced transport the temperature difference has to be quite large.

Now, the retarded AES-like action (6.25) can be determined explicitly. To first order in quantum components follows

$$\mathcal{S}_{\text{AES}} = - \int dt \{ \theta_q \tilde{g}(\theta) \dot{\theta} + \phi_q \sin^2 \theta [\tilde{g}(\theta) \dot{\phi} - I_s(\theta, \dot{\phi})] \}, \quad (6.34)$$

where we dropped the index c for classical, that is $\theta = \theta_c, \dot{\phi} = \dot{\phi}_c$. The dissipative contribution is governed by the conductance combination $\tilde{g}(\theta) = \frac{g_{\uparrow\uparrow} + g_{\downarrow\downarrow}}{4} \sin^2 \frac{\theta}{2} + \frac{g_{\uparrow\downarrow} + g_{\downarrow\uparrow}}{4} \cos^2 \frac{\theta}{2}$. The spin-transfer-torque (STT) current is given by

$$I_s(\theta, \dot{\phi}) = I_b^s(\theta) + I_h^s(\theta, \dot{\phi}), \quad (6.35)$$

where, formally, the bias STT-current is defined as $I_b^s(\theta) = \frac{1}{4}[I_b^{\uparrow\uparrow}(\theta) - I_b^{\downarrow\downarrow}(\theta) + I_b^{\downarrow\uparrow}(\theta) - I_b^{\uparrow\downarrow}(\theta)]$ and, analogously, the hybrid STT-current is defined as $I_h^s(\theta, \dot{\phi}) = \frac{1}{4}[I_h^{\uparrow\uparrow}(\theta, \dot{\phi}) - I_h^{\downarrow\downarrow}(\theta, \dot{\phi}) + I_h^{\downarrow\uparrow}(\theta, \dot{\phi}) - I_h^{\uparrow\downarrow}(\theta, \dot{\phi})]$. Explicitly,

$$I_b^s(\theta) = \frac{2\Gamma_\Delta \Gamma_r}{\Gamma_\uparrow(\theta) \Gamma_\downarrow(\theta)} [\tilde{g}(\theta) V + \tilde{g}'(\theta) b_T], \quad (6.36)$$

$$I_h^s(\theta) = \frac{\Gamma_\Delta^2 \sin^2 \theta}{\Gamma_\uparrow(\theta) \Gamma_\downarrow(\theta)} \tilde{g}(\theta) \dot{\phi}, \quad (6.37)$$

where $\tilde{g}'(\theta) = \frac{g'_{\uparrow\uparrow} + g'_{\downarrow\downarrow}}{4} \sin^2 \frac{\theta}{2} + \frac{g'_{\uparrow\downarrow} + g'_{\downarrow\uparrow}}{4} \cos^2 \frac{\theta}{2}$ with $g'_{\sigma\sigma'} = 2\rho'_\sigma(\Gamma_l^{\sigma'} + \Gamma_r)$. The spin-transfer-torque arises when a spin-polarized current flows into the magnetic dot. In turn, the bias and hybrid contributions to the STT-current are governed by $\Gamma_\Delta = (\Gamma_l^\uparrow - \Gamma_l^\downarrow)/2$, because it determines the spin-imbalance of electrons tunneling into the dot from the magnetic left lead. The bias contribution to the spin-transfer-torque current is $\propto \Gamma_r$, which reflects the fact it is related to transport *through* the quantum dot (via an external bias). In strong contrast, the hybrid STT-current also remains for $\Gamma_r = 0$, that is, if only a magnetic lead is attached to the dot and no bias can be applied. Actually, the hybrid STT-current not only remains without external bias, it is independent of the way of driving. In this sense, the hybrid STT-current is quite universal, as it only depends on the dynamics of the magnetization but not on the cause of this dynamics.

6.4 Landau-Lifshitz-Gilbert-Slonczewski equation

The determination of the quasiclassical equation of motion is straightforward now, as all relevant contributions to the action are known explicitly to first order in quantum components; see equations (6.22), (6.23), and (6.34). After adding up these contributions, $\mathcal{S} = \mathcal{S}_{\text{HS}} + \mathcal{S}_{\text{WZNW}} + \mathcal{S}_{\text{AES}}$, we vary with respect to θ_q and ϕ_q which leads to the quasiclassical equations of motion

$\frac{\delta \mathcal{L}}{\delta \theta_q} \Big|_{q=0} = 0$ and $\frac{\delta \mathcal{L}}{\delta \phi_q} \Big|_{q=0} = 0$. Explicitly, we find

$$\sin \theta \dot{\phi} = -\sin \theta B_0 + \cos \theta \cos(\phi - \omega_d t) \Omega - \frac{\tilde{g}(\theta)}{S} \dot{\theta}, \quad (6.38)$$

$$\sin \theta \dot{\theta} = \frac{\sin^2 \theta}{S} [\tilde{g}(\theta) \dot{\phi} - I_s(\theta, \dot{\phi})] + \sin \theta \sin(\phi - \omega_d t) \Omega. \quad (6.39)$$

These equations of motion describe the angular dynamics of the dot's magnetization. From equation (6.39), the name "hybrid" STT-current can be understood: even though the hybrid STT-current arises formally as a contribution to the spin-transfer-torque, it is proportional to $\dot{\phi}$ and, therefore, rather acts as a renormalization of the damping. To be precise, it acts as anti-Landau-Lifshitz-damping.

It is possible to recast the two equations of motion for angles θ, ϕ into a single vectorial equation of motion for the magnetization's direction \mathbf{m} . As a result, we obtain the Landau-Lifshitz-Gilbert-Slonczewski equation

$$\dot{\mathbf{m}} = \mathbf{m} \times \mathbf{B} - \alpha(\theta) \mathbf{m} \times \dot{\mathbf{m}} + \frac{1}{S} \mathbf{m} \times (\mathbf{I}_s(\theta, \dot{\phi}) \times \mathbf{m}), \quad (6.40)$$

with the Gilbert damping coefficient $\alpha(\theta) = \frac{\tilde{g}(\theta)}{S}$ and a spin-transfer-torque current $\mathbf{I}_s(\theta, \dot{\phi})$ of Slonczewski-type [Slonczewski, 1996]. This spin-transfer-torque current is parallel to the fixed magnetization of the left lead $\mathbf{I}_s(\theta, \dot{\phi}) \parallel \mathbf{M}_{\text{fix}}$ and its magnitude is given by $I_s(\theta, \dot{\phi}) = I_b^s(\theta) + I_h^s(\theta, \dot{\phi})$. The dynamics described by this equation of motion is extensively discussed in chapter 7.

6.5 Charge current and its noise

Besides the dynamics of the magnetization, we are also interested in the charge current which is transported through the system. Compared to a direct measurement of magnetization's angular motion, the charge current is relatively easy to measure in many cases. However, charge current and magnetization dynamics are closely related due to the spin-transfer-torque current and its inverse effect (pumping current). Therefore, the charge current and its noise offer a way for indirect measurement of the magnetization dynamics. We shortly sketch the formal derivation of charge current and its noise, before we give the results which also can be motivated by simple physical reasoning.

6.5.1 Formal derivation via counting fields

The charge current and its noise can be formally derived with the help of counting fields; see appendix A. To determine the charge transport through the left junction, we introduce a counting field λ into the corresponding self-energy $\Sigma_l \rightarrow \Sigma_l(\lambda) = e^{-i\lambda} \Sigma_l e^{i\lambda}$ appearing in the action (6.2). In turn, the counting field appears in the Keldysh partition function $\mathcal{Z} \rightarrow \mathcal{Z}(\lambda)$ and the Green's function G_λ , which is defined by its inverse $G_\lambda^{-1} = i\partial_t - \varepsilon_\alpha + \mathbf{M} \frac{\boldsymbol{\sigma}}{2} - \Sigma(\lambda)$. The counting fields

has only a quantum component which is chosen to be constant in time. Then, $\mathcal{Z}(0) = 1$ and the Keldysh partition function is a moment-generating function for the charge transported into the left lead; that is, $\langle Q_l \rangle = i\partial_{\lambda_q} \mathcal{Z}(\lambda)|_{\lambda=0}$ and $\langle Q_l^2 \rangle = (i\partial_{\lambda_q})^2 \mathcal{Z}(\lambda)|_{\lambda=0}$ and analog for higher moments. The zero-frequency current is then determined via the relation $\langle Q_l \rangle = \int dt I_l$. Similarly, the zero-frequency noise is determined via the cumulant $\langle\langle Q_l^2 \rangle\rangle = \int dt S_l$.

In principle, the transported charge and its noise can be determined by straightforwardly taking the derivative with respect to λ_q . It leads to $\langle Q_l \rangle = -i \int D\mathbf{m} \text{tr}[G_0 \Sigma'_l] e^{i\mathcal{S}}$ where $\Sigma'_l = \partial_{\lambda_q} \Sigma_l(\lambda)|_{\lambda=0}$. Analogously, the noise is given by $\langle\langle Q_l^2 \rangle\rangle = \int D\mathbf{m} \{ \text{tr}[G_0 \Sigma''_l] + \text{tr}[G'_0 \Sigma'_l] \} e^{i\mathcal{S}}$ where $\Sigma''_l = \partial_{\lambda_q}^2 \Sigma_l(\lambda)|_{\lambda=0}$ and $G'_0 = \partial_{\lambda_q} G_\lambda|_{\lambda=0} = G_0 \Sigma'_l G_0$. In practice, however, we don't know the laboratory-frame Green's function G_0 . Therefore, it is much more convenient to change to the rotating frame, before one takes the derivative with respect to the counting field. The rotating-frame Green's function \tilde{G}_λ is defined by its inverse $\tilde{G}_\lambda^{-1} = i\partial_t - \varepsilon_\alpha + M_0 \frac{\sigma_z}{2} - Q - R^\dagger \Sigma(\lambda) R$. Taking the derivative with respect to the counting field, now, leads to the transported charge $\langle Q_l \rangle = -i \int D\mathbf{m} \text{tr}[\tilde{G}_0 \tilde{\Sigma}'_l] e^{i\mathcal{S}}$ where Green's function \tilde{G}_0 and self-energy $\tilde{\Sigma}'_l = R^\dagger \partial_{\lambda_q} \Sigma_l(\lambda)|_{\lambda=0} R$ are both in the rotating frame. Analogously, the noise is found to be $\langle\langle Q_l^2 \rangle\rangle = \int D\mathbf{m} \{ \text{tr}[\tilde{G}_0 \tilde{\Sigma}''_l] + \text{tr}[\tilde{G}'_0 \tilde{\Sigma}'_l] \} e^{i\mathcal{S}}$ where $\tilde{\Sigma}''_l = R^\dagger \partial_{\lambda_q}^2 \Sigma_l(\lambda)|_{\lambda=0} R$ and $\tilde{G}'_0 = \partial_{\lambda_q} \tilde{G}_\lambda|_{\lambda=0} = \tilde{G}_0 \tilde{\Sigma}'_l \tilde{G}_0$.

The main contributions to the transported charge $\langle Q_l \rangle = -i \int D\mathbf{m} \text{tr}[\tilde{G}_0 \tilde{\Sigma}'_l] e^{i\mathcal{S}}$ and its noise $\langle\langle Q_l^2 \rangle\rangle = \int D\mathbf{m} \{ \text{tr}[\tilde{G}_0 \tilde{\Sigma}''_l] + \text{tr}[\tilde{G}'_0 \tilde{\Sigma}'_l] \} e^{i\mathcal{S}}$ can be determined by a saddle-point approximation. Because pre-exponential factors do not influence a saddle-point approximation much, the main contributions are determined by the saddle-points of the action \mathcal{S} . For large magnetization (spin), we assume the quasiclassical saddle-points to be dominating. In other words, the major contributions to the transported charge and its noise are determined by the quasiclassical dynamics of the magnetization, which is described by the Landau-Lifshitz-Gilbert-Slonczewski equation (6.40). While fluctuations around quasiclassical trajectories can become important for very long measurement times [Virtanen and Heikkilä, 2017], here we focus on the contributions arising from the quasiclassical trajectories themselves. Formally, this restricts our analysis to very-low- instead of zero-frequency for the current and its noise. However, we neglect this difference between very-low- and zero-frequency in the following, which is possible when the spin (magnetization) is large enough.

6.5.2 Results for steady state precessions

When we wait long enough, the driven magnetization goes into a steady state precession which is determined by a balance between damping and driving. The magnetization, then, precesses at a constant polar angle $\theta = \theta_0$ with a constant frequency $\dot{\phi} = \dot{\phi}_0$, where θ_0 and $\dot{\phi}_0$ are determined by the Landau-Lifshitz-Gilbert-Slonczewski equation (6.40). For these steady state precessions, the charge current and its noise can be correctly guessed by simple physical reasoning.

The amount of charges transported into the left lead Q_l is an observable. In turn, the charge current I_l and its noise S_l are also observables. As observables, I_l and S_l are independent of the frame of reference. Thus, we can determine the average charge current by use of Landauer's formula [Landauer, 1957], where we replace the laboratory-frame distribution functions by the

rotating-frame distribution functions. As a result, we obtain

$$I_l^0 = \frac{1}{2} \sum_{\sigma} \int d\omega g_l^{\sigma}(\omega) [\tilde{F}_l^{\sigma}(\omega) - \tilde{F}_s^{\sigma}(\omega)], \quad (6.41)$$

where $g_l^{\sigma}(\omega) = 2\rho_{\sigma}(\omega)\Gamma_l^{\sigma}(\theta_0)$ is the spin-resolved conductance of the left junction. Further, $\tilde{F}_s^{\sigma}(\omega)$ is the dot's rotating-frame distribution function and $\tilde{F}_l^{\sigma}(\omega)$ is the left lead's rotating-frame distribution function as it is seen by the dot; see figure 6.2. The superscript 0 in I_l^0 is to remind us that this result is restricted to steady state precession with θ_0 and $\dot{\phi}_0$. For the right tunnel junction, the charge current and its noise can be obtained in complete analogy. Formally, we would introduce the counting field with $\Sigma_r \rightarrow \Sigma_r(\lambda) = e^{-i\lambda}\Sigma_r e^{i\lambda}$. Explicitly, for the current we can use the formulas of the left junction and replace the junction's conductance $g_l^{\sigma}(\omega) \rightarrow g_r^{\sigma}(\omega)$ and the lead's distribution function $\tilde{F}_l^{\sigma}(\omega) \rightarrow \tilde{F}_r^{\sigma}(\omega)$. This leads to

$$I_r^0 = \frac{1}{2} \sum_{\sigma} \int d\omega g_r^{\sigma}(\omega) [\tilde{F}_r^{\sigma}(\omega) - \tilde{F}_s^{\sigma}(\omega)], \quad (6.42)$$

with the spin-resolved conductance of the right junction $g_r^{\sigma}(\omega) = 2\rho_{\sigma}(\omega)\Gamma_r$. Since the quantum dot cannot store charges for an infinite time, the zero-frequency charge current has to be the same in both junctions $I_l^0 = -I_r^0$. This can be confirmed explicitly, by inserting the dot's distribution function (6.21) into equations (6.41) and (6.42). Accordingly, we can define the zero-frequency charge current $I = -I_r^0 = I_l^0$ which is independent of the junction. An explicit calculation yields

$$I = \sum_{\sigma} g_t^{\sigma} \left[V - \frac{\Gamma_{\Delta}}{2\Gamma_l^{\sigma}(\theta_0)} \sin^2 \theta_0 \dot{\phi}_0 \right] - \sum_{\sigma} g'_{t,\sigma} b_T, \quad (6.43)$$

where $g_t^{\sigma} = 2\rho_{\sigma} \frac{\Gamma_l^{\sigma}(\theta_0)\Gamma_r}{\Gamma_{\sigma}(\theta_0)}$ is the spin-resolved total conductance and we defined analogously $g'_{t,\sigma} = 2\rho'_{\sigma} \frac{\Gamma_l^{\sigma}(\theta_0)\Gamma_r}{\Gamma_{\sigma}(\theta_0)}$. Note that we only kept thermal contributions with ρ'_{σ} . The other contributions $\propto V, \dot{\phi}_0$ are suppressed by the large length of the magnetization M . While this is also true for the thermal part, we allow the temperatures to be large enough, such that the thermal bias parameter $b_T = \frac{\pi^2}{6}(T_l^2 - T_r^2)$ is of similar size as the magnetization; note that the temperature is still smaller than M (typical temperatures $T \sim \sqrt{M}$).

For the noise corresponding to the charge current through the left junction, S_l^0 , we obtain

$$S_l^0 = \sum_{\sigma} \int d\omega g_t^{\sigma}(\omega) \left\{ [1 - \tilde{F}_s^{\sigma}(\omega)\tilde{F}_l^{\sigma}(\omega)] + \frac{\Gamma_r}{\Gamma_{\sigma}(\theta_0)} \tilde{F}_s^{\sigma}(\omega) [\tilde{F}_l^{\sigma}(\omega) - \tilde{F}_s^{\sigma}(\omega)] \right\}, \quad (6.44)$$

where $g_t^{\sigma}(\omega) = 2\rho_{\sigma}(\omega) \frac{\Gamma_l^{\sigma}(\theta_0)\Gamma_r}{\Gamma_{\sigma}(\theta_0)}$ is the spin-resolved total conductance of the magnetic double tunnel junction. To obtain the analog result for the right junction, we can either proceed formally via the counting field or we exchange the tunneling rates $\Gamma_l^{\sigma}(\theta_0) \leftrightarrow \Gamma_r$, and replace the lead's distribution function $\tilde{F}_l^{\sigma}(\omega) \rightarrow \tilde{F}_r^{\sigma}(\omega)$. It follows,

$$S_r^0 = \sum_{\sigma} \int d\omega g_t^{\sigma}(\omega) \left\{ [1 - \tilde{F}_s^{\sigma}(\omega)\tilde{F}_r^{\sigma}(\omega)] + \frac{\Gamma_r}{\Gamma_l^{\sigma}(\theta_0)} \tilde{F}_s^{\sigma}(\omega) [\tilde{F}_r^{\sigma}(\omega) - \tilde{F}_s^{\sigma}(\omega)] \right\}. \quad (6.45)$$

Similar to the current, charge conservation demands $S_l^0 = S_r^0$, as the dot cannot store charges for an infinitely long time (zero-frequency). Again, this can be checked explicitly by inserting the dot's distribution function (6.21) into equations (6.44) and (6.45). This allows to define $S = S_l^0 = S_r^0$, which is the noise of charge current independent of the junction.

6.6 Summary and discussion

In this chapter, we derived the equation of motion for a dynamical magnetization of an itinerant magnet which is tunnel-coupled to a magnetic lead and a normal metal lead. A particular focus was put on the interplay between the angular motion of a magnetization and the electron distribution function. A magnetization in steady state precession drives the electron system into a nonequilibrium state. In turn, a nonequilibrium electron distribution develops in the middle region; see figure 6.2. This nonequilibrium distribution has a back-action onto the magnetization dynamics via the Slonczewski spin-transfer-torque (STT) current. More explicitly, we found that a hybrid STT-current originates from the nonequilibrium features in the distribution function that are induced by the precessing magnetization. This "hybrid" contribution, while formally an STT current, acts like a renormalization of damping. Interestingly, the hybrid current is universal in the sense that it depends on the dynamics of the magnetization but not on the way of driving.

Finally, we discussed the derivation of the zero-frequency charge current which is transported through the magnetic double tunnel junction, when the magnetization is driven into a steady state precession. This is particularly interesting for spintronics, where a central topic is the manipulation of magnetization dynamics with charge currents and vice versa. In the next chapter we use the formal results obtained here and discuss the magnetic double tunnel junction from a rather spintronic perspective.

Chapter 7

Driven magnetic double tunnel junction

As derived in the previous chapter, the magnetization's angular dynamics in a magnetic double tunnel junction, figure 7.1, is described by the Landau-Lifshitz-Gilbert-Slonczewski (LLGS) equation¹

$$\dot{\mathbf{m}} = \mathbf{m} \times \mathbf{B} - \alpha(\theta) \mathbf{m} \times \dot{\mathbf{m}} + \mathbf{m} \times (\mathbf{I}_s(\theta, \dot{\phi}) \times \mathbf{m})/S, \quad (7.1)$$

where $\mathbf{m} = \mathbf{M}/M = (\sin \theta \cos \phi, \sin \theta \sin \phi, \cos \theta)$ is the direction of the magnetization. The first term, $\mathbf{m} \times \mathbf{B}$, describes the precession of the magnetization around the external magnetic field $\mathbf{B} = (\Omega \cos \omega_d t, \Omega \sin \omega_d t, B_0)$. The second term, $-\alpha(\theta) \mathbf{m} \times \dot{\mathbf{m}}$, describes the damping of the magnetization and is also known as Gilbert damping. The third term, $\frac{1}{S} \mathbf{m} \times (\mathbf{I}_s(\theta, \dot{\phi}) \times \mathbf{m})$, describes the influence of spin-polarized currents onto the magnetization dynamics and is also known as Slonczewski spin-transfer-torque (STT) [Slonczewski, 1996].

We can relate the Gilbert damping coefficient $\alpha(\theta)$ and the Slonczewski STT-current $\mathbf{I}_s(\theta, \dot{\phi})$ to the parameters of our model, figure 7.1, as we have derived the LLGS-equation (7.1) for this model in chapter 6. The Gilbert damping is assumed to be governed by the coupling to the leads, which allows for dissipation of energy and angular momentum [Tserkovnyak et al., 2002, Tserkovnyak et al., 2005]. Its damping coefficient is $\alpha(\theta) = \tilde{g}(\theta)/S$, where $S = M/(2J)$ is the spin-length and $\tilde{g}(\theta) = \frac{g_{\uparrow\uparrow} + g_{\downarrow\downarrow}}{4} \sin^2 \frac{\theta}{2} + \frac{g_{\uparrow\downarrow} + g_{\downarrow\uparrow}}{4} \cos^2 \frac{\theta}{2}$ is the spin-relaxation conductance with $g_{\sigma\sigma'} = 2\rho_\sigma(\Gamma_l^{\sigma'} + \Gamma_r)$. The STT-current $\mathbf{I}_s(\theta, \dot{\phi})$ is parallel to the fixed magnetization \mathbf{M}_{fix} . It contains two contributions $\mathbf{I}_s(\theta, \dot{\phi}) = I_b^s(\theta) + I_h^s(\theta, \dot{\phi})$, which are the bias contribution $I_b^s(\theta)$ and the hybrid contribution $I_h^s(\theta, \dot{\phi})$. As the name implies, the bias STT-current $I_b^s(\theta)$ arises when a bias is applied; that is, either a voltage $V = \mu_l - \mu_r$ or a thermal bias $b_T = \frac{\pi^2}{6}(T_l^2 - T_r^2)$. Explicitly, $I_b^s(\theta) = \frac{2\Gamma_\Delta \Gamma_r}{\Gamma_\uparrow(\theta)\Gamma_\downarrow(\theta)} [\tilde{g}(\theta)V + \tilde{g}'(\theta)b_T]$, with $\Gamma_\Delta = (\Gamma_l^\uparrow - \Gamma_l^\downarrow)/2$ and $\Gamma_\sigma(\theta) = \cos^2 \frac{\theta}{2} \Gamma_l^\uparrow + \sin^2 \frac{\theta}{2} \Gamma_l^\downarrow + \Gamma_r$. And $\tilde{g}'(\theta)$ is defined analogously to $\tilde{g}(\theta)$ but with

¹We assumed θ and $\dot{\phi}$ to be slow on the scale of the life-time of electrons in the dot $1/\Gamma_\sigma(\theta)$. The angle ϕ itself may change much faster. Ultimately, the slowness assumption for $\theta, \dot{\phi}$ should be checked for self-consistency. When the magnetization is close enough to a stable steady state precession (constant θ_0 and $\dot{\phi}_0$), then we expect the (relaxation) dynamics to be slow. However, for a more detailed discussion, we should include fluctuations analog to [Shnirman et al., 2015].

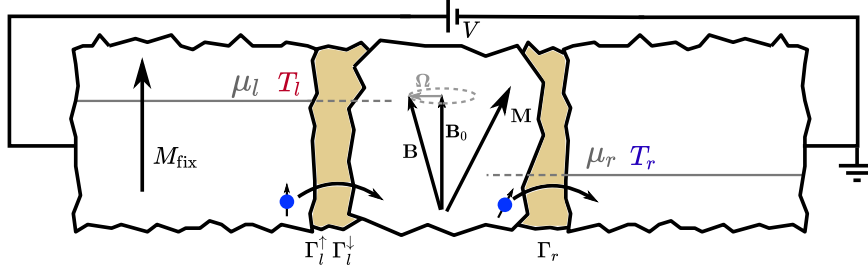


Figure 7.1: This is a schematic view of the magnetic double tunnel junction under general driving conditions. An itinerant ferromagnetic quantum dot is exposed to an external magnetic field $\mathbf{B} = (\Omega \cos \omega_d t, \Omega \sin \omega_d t, B_0)$ and tunnel-coupled to two leads which are assumed to be in (local) equilibrium. One lead is an itinerant ferromagnet with a fixed magnetization \mathbf{M}_{fix} , while the other lead is a normal metal. The states in the dot are described by a spin-dependent density of states, which is weakly energy dependent $\rho_\sigma(\mu_r + \omega) \approx \rho_\sigma + \rho'_\sigma \omega$, where $\rho_\sigma = \rho_\sigma(\mu_r)$ and $\rho'_\sigma = \partial_\omega \rho_\sigma(\omega)|_{\omega=\mu_r} = \mathcal{O}(1/S)$. The coupling to the leads is described by the tunneling rates $\Gamma_l^\sigma, \Gamma_r$, where the tunneling rate to the left lead is spin-dependent due to the fixed magnetization. The system can be driven in three distinct ways: via an applied voltage $V = \mu_l - \mu_r$; via different temperatures in the leads $T_l \neq T_r$; or with an oscillating magnetic field Ω .

the replacement $g_{\sigma\sigma'} \rightarrow g'_{\sigma\sigma'} = 2\rho'_\sigma(\Gamma_l^{\sigma'} + \Gamma_r)$. We emphasize that, due to the hybrid STT-current $I_h^s(\theta)$, the Slonczewski term remains relevant even in absence of external bias ($V = 0$ and $T_l = T_r$).

The hybrid STT-current $I_h^s(\theta)$ is new in this thesis, correspondingly, in [Ludwig et al., 2017, Ludwig et al., 2019b]. It is a universal contribution to the LLGS equation in the following sense: the hybrid STT-current is governed by the magnetization dynamics but it is independent of the source of driving. It arises from the adjustment of the electron distribution to the dynamics of the magnetization and, thus, it describes an effective "self-interaction" of the magnetization dynamics. Explicitly, the hybrid STT-current is given by $I_h^s(\theta) = \frac{\Gamma_\uparrow^2 \sin^2 \theta}{\Gamma_\uparrow(\theta)\Gamma_\downarrow(\theta)} \tilde{g}(\theta) \dot{\phi}$. To understand the origin of the name "hybrid", we write the LLGS-equation (7.1) in coordinate form,

$$\sin \theta \dot{\phi} = -\sin \theta B_0 + \cos \theta \cos(\phi - \omega_d t) \Omega - \frac{\tilde{g}(\theta)}{S} \dot{\theta}, \quad (7.2)$$

$$\sin \theta \dot{\theta} = \frac{\sin^2 \theta}{S} [\tilde{g}(\theta) \dot{\phi} - I_s(\theta, \dot{\phi})] + \sin \theta \sin(\phi - \omega_d t) \Omega. \quad (7.3)$$

In this form, the Gilbert damping appears as $\tilde{g}(\theta) \dot{\theta}$ and $\tilde{g}(\theta) \dot{\phi}$ in equations (7.2) and (7.3) respectively. The hybrid STT-current $I_h^s(\theta, \dot{\phi})$ formally arises as a part of the STT-current $I_s(\theta, \dot{\phi})$. However, it is proportional to $\tilde{g}(\theta) \dot{\phi}$ and, thus, acts as a renormalization of damping rather than a usual STT-current. More precisely, the hybrid STT-current acts like anti-Landau-Lifshitz-damping. So, it is an STT-current but it acts as (anti-)damping. Therefore, we call it "hybrid".

Besides the magnetization dynamics, we are interested in the flow of charge current. In particular, because it is relatively easy to measure, at least when compared to a direct measurement of the magnetization dynamics. As derived in chapter 6, the zero-frequency charge current is given by

$$I = \sum_\sigma g_r^\sigma(\theta_0) \left[V - \frac{\Gamma_\Delta}{2\Gamma_l^\sigma(\theta_0)} \sin^2 \theta_0 \dot{\phi}_0 \right] - \sum_\sigma g'_{r,\sigma}(\theta_0) b_T, \quad (7.4)$$

where the magnetization was assumed to be in a steady state precession with a constant polar angle $\theta = \theta_0$ and a constant precession frequency $\dot{\phi} = \dot{\phi}_0$. The spin-resolved total conductance is given by $g_t^\sigma(\theta_0) = 2\rho_\sigma\Gamma_l^\sigma(\theta_0)\Gamma_r/\Gamma_\sigma(\theta_0)$ and the correction due to the slight energy dependence of the dot's density of states is given by $g'_{t,\sigma}(\theta_0) = 2\rho'_\sigma\Gamma_l^\sigma(\theta_0)\Gamma_r/\Gamma_\sigma(\theta_0)$. The charge current contains three contributions of different physical origin: the current arising due to the voltage bias $\propto V$; the thermoelectric current arising due to the thermal bias $\propto b_T$; and the hybrid charge-current $\propto \dot{\phi}_0$ which is generated by the precessing magnetization. The hybrid charge-current can be viewed as a strong nonequilibrium version of the pumping current discussed in [Tserkovnyak et al., 2008].

In the following, we specialize these general results to three specific cases: purely FMR-type driving; purely voltage bias; and purely thermal bias. Thereby, we reproduce the results of [Ludwig et al., 2017, Ludwig et al., 2019b, Ludwig et al., 2019a]. Furthermore, this allows us to clearly demonstrate that the hybrid STT-current and the closely related hybrid charge-current are very relevant in magnetic double tunnel junctions. In more general terms: the dynamical interplay between magnetization and electron distribution is relevant in spintronic systems.

7.1 Purely FMR-driving: emergence of additional steady state precessions

In this section, we consider the magnetic double tunnel junction to be driven by ferromagnetic resonance only; see figure 7.2. Explicitly, we assume the driving part of the external magnetic field to have a finite strength $\Omega \neq 0$ and to oscillate at a finite frequency $\omega_d \neq 0$. But no external bias is applied. That is, the electrochemical potentials and the temperatures are assumed to be equal in both leads ($\mu_l = \mu_r =: \mu$ and $T_l = T_r =: T$). Then, the coordinate form of the LLGS-equation is reduced to,

$$\dot{\phi} - \frac{\alpha(\theta)}{\sin \theta} \dot{\theta} = (B_0 + \omega_d) - \Omega \cot \theta \cos \varphi, \quad (7.5)$$

$$\dot{\theta} + \hat{\alpha}(\theta) \sin \theta \dot{\varphi} = \hat{\alpha}(\theta) \sin \theta \omega_d - \Omega \sin \varphi, \quad (7.6)$$

where we introduced $\varphi = \omega_d t - \phi$ to eliminate the explicit time dependence of the driving field. The angle φ describes how much the magnetization lags behind the driving field. The hybrid STT-current was absorbed into the definition of a renormalized damping coefficient $\hat{\alpha}(\theta) = \frac{\Gamma_\Sigma^2 - \Gamma_\Lambda^2}{\Gamma_\Sigma^2 - \Gamma_\Lambda^2 \cos^2 \theta} \alpha(\theta)$. Although equations (7.5) and (7.6) are first order differential equations, due to the nonlinearity it is not straightforward to solve them analytically. For our purposes, however, a full solution is not necessary.

We are mainly interested in the magnetization's long time-behaviour. In particular, we want to know which stable steady state precessions are supported by the FMR-type driving. As there is no explicit time dependence in the equations of motion, we expect the angles θ and φ to relax to stationary values θ_0, φ_0 . These are determined by $\dot{\theta}, \dot{\varphi} = 0$; explicitly,

$$B_0 + \omega_d = \Omega \cot \theta_0 \cos \varphi_0, \quad (7.7)$$

$$\hat{\alpha}(\theta_0) \omega_d \sin \theta_0 = \Omega \sin \varphi_0. \quad (7.8)$$

The stationary solution's stability can be inferred from the dynamics in their vicinity. For that purpose, one substitutes $\varphi = \varphi_0 + \delta\varphi, \theta = \theta_0 + \delta\theta$ into the equations of motion (7.5) and (7.6) and expands in the deviations $\delta\varphi, \delta\theta$. A stationary solution is stable, if small deviations relax to zero. When stable solutions θ_0, φ_0 exist, the magnetization's long-time behaviour is easy to infer. After the decay of transient effects, the magnetization precesses around z -axis at a constant angle θ_0 . The magnetization lags behind the driving field by a constant angle φ_0 . In turn, it precesses at same frequency as the driving field $\dot{\phi}_0 = \omega_d$. That is, the magnetization is in a steady state precession with polar angle θ_0 and frequency $\dot{\phi}_0 = \omega_d$. The angles θ_0, φ_0 are determined by the balance between Gilbert damping, hybrid STT-current, and FMR-type driving.

7.1.1 Classification into three regimes of different driving strength

To get at least some analytical insight which can be used as guideline, we consider driving at resonance frequency $\omega_d = -B_0$. This will allow us to identify three different regimes of driving

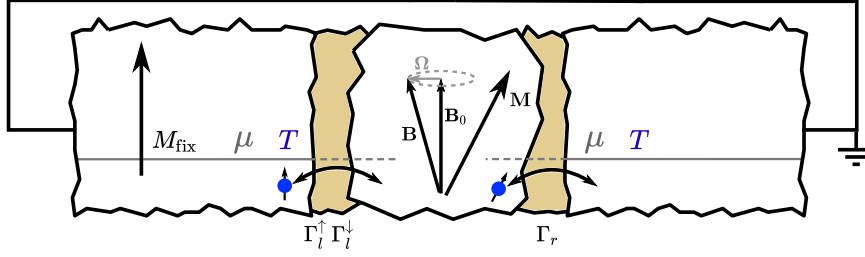


Figure 7.2: Schematic view of the system with FMR-type driving ($\Omega \neq 0$ and $\omega_d \neq 0$) but without external bias ($V = 0$ but $T_l = T_r$). The Gilbert damping tends to align the magnetization towards the external magnetic field. However, the FMR-type driving competes with Gilbert damping and drives the magnetization into a steady state precession.

strength: weak, strong, and indefinite.

At resonance, equations (7.7) and (7.8) simplify to

$$0 = \cot \theta_0 \cos \varphi_0 , \quad (7.9)$$

$$\hat{\alpha}(\theta_0) B_0 \sin \theta_0 = \Omega \sin \varphi_0 , \quad (7.10)$$

From the second equation combined with $\sin \theta_0 \geq 0$ and $\hat{\alpha}(\theta_0) \geq 0$ follows that the magnetization lags *behind* the driving field $\varphi_0 \geq 0$. In turn, we infer from the first equation that either $\theta_0 = \pi/2$ or $\varphi_0 = \pi/2$. Thus, two types of stationary solutions exist: either

$$\varphi_0 = \frac{\pi}{2} \quad \text{and} \quad \hat{\alpha}(\theta_0) B_0 \sin \theta_0 = \Omega ; \quad (7.11)$$

or

$$\theta_0 = \frac{\pi}{2} \quad \text{and} \quad \Omega \sin \varphi_0 = \hat{\alpha}(\pi/2) B_0 . \quad (7.12)$$

Solutions of type (7.11) can only exist when driving is weak enough ($\Omega \leq \max_{\theta_0} \hat{\alpha}(\theta_0) B_0 \sin \theta_0$). Solutions of type (7.12) can only exist when driving is strong enough ($\Omega \geq \hat{\alpha}(\pi/2) B_0$). This suggests to define two values of critical driving strength: the lower critical driving strength $\Omega_l = \hat{\alpha}(\pi/2) B_0$; and the upper critical driving strength $\Omega_u = \max_{\theta_0} \hat{\alpha}(\theta_0) B_0 \sin \theta_0$. By definition $\Omega_l \leq \Omega_u$. Consequently, three different regimes of driving-strength can exist:

- Weak driving $\Omega < \Omega_l$: For weak driving, only the solution of type (7.11) exist. The damping is strong enough to keep the magnetization close to the north pole or, at least, away from the equator.
- Strong driving $\Omega > \Omega_u$: For strong driving, only solutions of the type (7.12) exist. The magnetization always reaches the equator when it is driven at the resonance frequency.
- Indefinite driving strength $\Omega_l < \Omega < \Omega_u$: In the regime of indefinite driving strength, solutions of both types (7.11) and (7.12) exist simultaneously. This is possible due to the specific θ_0 -dependence of the renormalized damping coefficient $\hat{\alpha}(\theta_0)$. Driving appears to be weak in vicinity of the poles while it appears to be strong in vicinity of the equator.

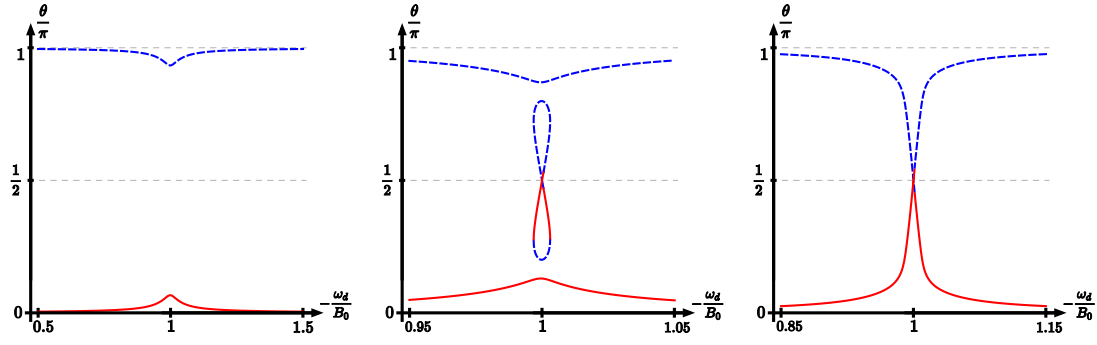


Figure 7.3: The stationary solutions for θ_0 are shown in dependence on the driving frequency $\frac{\omega_d}{B_0}$ for $\alpha_0 = \frac{\rho_F \Gamma_Y}{2S} = 0.04$, $\frac{\Gamma_\Delta}{\Gamma_Y} = -0.9$, $\rho_\Delta = 0$. From left to right: weak driving $\Omega/(\alpha_0 B_0) = 0.175$; indefinite driving strength $\Omega/(\alpha_0 B_0) = 0.2375$; and strong driving $\Omega/(\alpha_0 B_0) = 0.3$. The stability is indicated by colour (red solid = stable; blue dashed = unstable). **(left)** When driving is weak, it cannot really compete with Gilbert damping. In turn, the stable stationary solution always stays close to the north pole ($\theta = 0$). **(right)** When driving is strong, it can easily compete with Gilbert damping. At resonance, the magnetization is driven to the equator and it can even go to the southern hemisphere (above $\theta = \pi/2$). **(middle)** For indefinite driving strength, driving appears to be weak in vicinity of the poles but strong in vicinity of the equator. In turn, it combines the features of weak and strong driving and, interestingly, allows for two stable steady state precessions.

For all three regimes, figure 7.3 shows stationary solutions of θ_0 with their stability. The emergence of the additional stable solution in the indefinite driving regime can be traced back to the hybrid STT-current. The hybrid STT-current is a consequence of the nonequilibrium distribution that is induced by the magnetization's steady state precession. Thus, the additional steady state precessions in vicinity of the equator are (partially) self-sustained: the precessing magnetization drives the electron distribution into a nonequilibrium state; the nonequilibrium distribution gives rise to the hybrid STT-current which is necessary to sustain the steady state precession. This clearly demonstrates the importance of the interplay between magnetization dynamics and electron distribution.

7.1.2 Charge current and its noise

A magnet with precessing magnetization acts as a spin-fountain and pumps a spin-current into adjacent leads [Tserkovnyak et al., 2002, Brataas et al., 2002, Tserkovnyak et al., 2005]. The magnetic lead acts as a spin-filter, such that the pumped spin-current is accompanied by a charge current [Tserkovnyak et al., 2008]. For steady state precessions the average charge current is given by equation (7.4). In absence of external bias ($V = 0$ and $b_T = 0$), only the hybrid contributions remain and we find

$$I = - \sum_{\sigma} g_t^{\sigma}(\theta_0) \frac{\Gamma_{\Delta} \sin^2 \theta_0 \dot{\phi}_0}{2\Gamma_l^{\sigma}(\theta_0)}, \quad (7.13)$$

where $\Gamma_{\Delta} \sin^2 \theta_0 \dot{\phi}_0 / [2\Gamma_l^{\sigma}(\theta_0)]$ acts as a spin-dependent voltage. However, the noise of charge current is not the standard shot noise corresponding to this voltage. Instead, from equation

(6.44), we find the noise

$$S = \sum_{\sigma} g_i^{\sigma}(\theta_0) \left[2T + \gamma_{\sigma}(\theta_0) \sin^2 \theta_0 \left(\frac{\dot{\phi}_0}{2} \coth \frac{\dot{\phi}_0}{2T} - T \right) \right], \quad (7.14)$$

where $\gamma_{\sigma}(\theta_0) = [\Gamma_{\Sigma}(\Gamma_l^{\sigma}(\theta_0))^2 + \Gamma_r \Gamma_l^{\sigma} \Gamma_l^{\bar{\sigma}} + \Gamma_r^2 (\Gamma_l^{\sigma} + \Gamma_l^{\bar{\sigma}})/2] / [\Gamma_{\sigma}^2(\theta_0) \Gamma_l^{\sigma}(\theta_0)]$. We emphasize that the Fano-factor (noise-to-signal ratio) $\mathcal{F} = S/I$ strongly depends on Γ_{Δ} .

For $\Gamma_{\Delta} \rightarrow 0$ we reproduce the results of chapter 3, or correspondingly [Ludwig et al., 2019a], and the Fano-factor diverges $\mathcal{F} \rightarrow \infty$ even at zero temperature. This result makes clear that the hybrid charge current is different from a "standard" charge current for applied voltage.

7.1.3 Summary: purely FMR-driving

Stable steady state precessions of the dot's magnetization are supported by FMR-type driving. Three different regimes of driving strength exist; see figure 7.3. We found the typical FMR-peak for weak driving. Also for strong driving, the FMR-peak for stationary θ_0 is rather typical; only its stability close to the resonance frequency is a bit surprising. The most interesting behaviour was found for the intermediate regime of indefinite driving strength. In this regime, driving can simultaneously appear to be weak in vicinity of the poles but strong in vicinity of the equator. This allows for the existence of two stable steady state precessions. The steady state precession in vicinity of the equator is particularly interesting. It is self-sustained: the precessing magnetization drives the electron distribution into a nonequilibrium state; the nonequilibrium distribution gives rise to the hybrid STT-current which is necessary to sustain the steady state precession.

7.2 Purely voltage bias: sudden switch of stability

In this section, we consider the magnetic double tunnel junction to be driven only by voltage bias $V = \mu_l - \mu_r \neq 0$; see figure 7.4. That is, neither thermal bias nor FMR-type driving is applied ($T_l = T_r =: T$ and $\Omega = 0$). Then, the LLGS-equation in coordinate form is reduced to,

$$\dot{\phi} = -B_0 - \alpha(\theta)\dot{\theta}/\sin\theta, \quad (7.15)$$

$$\dot{\theta} = \sin\theta [\hat{\alpha}(\theta)\dot{\phi} - I_b^s(\theta)/S], \quad (7.16)$$

where the bias STT-current is given by $I_b^s(\theta) = \frac{2\Gamma_\Delta\Gamma_r}{\Gamma_\uparrow(\theta)\Gamma_\downarrow(\theta)} \tilde{g}(\theta)V$. The hybrid STT-current is absorbed into the renormalized damping coefficient $\hat{\alpha}(\theta) = \frac{\Gamma_\Sigma - \Gamma_\Delta^2}{\Gamma_\Sigma^2 - \Gamma_\Delta^2 \cos^2\theta} \alpha(\theta)$. Since $\alpha(\theta) = \tilde{g}(\theta)/S$, the magnetization precesses around the external magnetic field at the frequency $\dot{\phi} = -B_0 + \mathcal{O}(1/S^2) \approx -B_0$. Beyond that, the dynamics of ϕ will only be diffusive, as there is no drift term.

Knowing the precession frequency $\dot{\phi} = -B_0$, we would now like to understand the dynamics of θ . From equation (7.16) follows,

$$\dot{\theta} = -\sin\theta \hat{\alpha}(\theta) (B_0 + \lambda_0 V), \quad (7.17)$$

where $\lambda_0 = 2\Gamma_\Delta\Gamma_r/(\Gamma_\Sigma^2 - \Gamma_\Delta^2)$. As $\sin\theta \hat{\alpha}(\theta) > 0$ for finite $\theta (\neq 0, \pi)$, the polar angle θ is driven either towards the north pole (for $B_0 + \lambda_0 V > 0$) or towards the south pole (for $B_0 + \lambda_0 V < 0$). These two regimes are separated by the switching voltage $V_{sw} = -\lambda_0 B_0$. Interestingly, no stable steady state precessions exist. Only when the applied voltage V is fine-tuned onto the switching voltage V_{sw} , then steady state precession exist for all polar angles θ . However, these are of marginal stability (neither stable nor unstable). The stationary solutions are shown with their stability in figure 7.5.

In more physical terms, the dynamics can be understood as follows (for concreteness we consider $\Gamma_\Delta < 0$). Without bias ($V = 0$), there is no driving that could compete with damping. In turn, the magnetization relaxes to its energetically most favourable state at the north pole ($\theta = 0$). For voltages below the switching voltage ($V < V_{sw}$), driving via STT-current is too weak to compete with damping. Therefore, the stationary solution at the north-pole remains stable up to the switching voltage. Above the switching voltage ($V > V_{sw}$), in contrast, driving via STT-current overpowers damping. The magnetization is driven towards the south pole ($\theta = \pi$) which, in turn, becomes stable.

Right at the switching voltage ($V = V_{sw}$) we have $\dot{\theta} = 0$. In words, the Gilbert damping is exactly compensated by the combination of hybrid STT-current and bias STT-current. Thus, all polar angles $\theta_0 \in [0, \pi]$ are stationary solutions; but only of marginal stability. Would we include fluctuations, the dynamics of the polar angle would become diffusive. This behaviour extends to the vicinity of the switching voltage, where restoring forces are small. In other words, we observe a critical slowing down at the switching voltage. This hints at a (strongly nonequilibrium dissipative) phase transition, which might be interesting to investigate in future works.

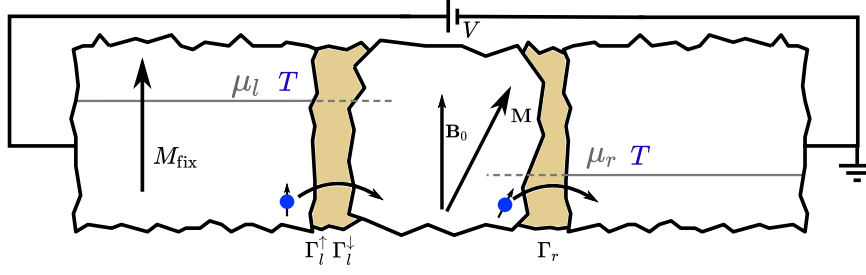


Figure 7.4: Schematic view of the system with purely voltage bias ($V = \mu_l - \mu_r \neq 0$); neither thermal bias nor FMR-type driving is applied ($T_l = T_r =: T$ and $\Omega = 0$). The Gilbert damping tends to align the magnetization towards the external magnetic field $\mathbf{B} = (0, 0, B_0)$. However, the voltage bias can be used to drive a current through the system which leads to an STT-current that can compete with Gilbert damping.

One might expect an intermediate regime, where damping and driving compensate each other at finite polar angles and, thereby, give rise to stable steady state precessions. However, this intermediate regime does not exist in our model. Its nonexistence can be traced back to the hybrid STT-current. In other words, when the magnetization precesses at a finite polar angle, the electron distribution adjusts itself in such a way that the modified STT-current renders the precession unstable.

7.2.1 Charge current and its noise

As there is no precession of the magnetization, we do not expect any surprises for the charge current at stationary solutions. And indeed, the charge current is determined by Ohm's law,

$$I = g_t(\theta_0)V . \quad (7.18)$$

The total conductance $g_t(\theta_0) = g_t^\uparrow(\theta_0) + g_t^\downarrow(\theta_0)$ depends on the orientation of the magnetization. When the voltage V is tuned across the switching voltage V_{sw} , the magnetization switches between the north pole and the south pole. Thus, also a jump in charge current is observed ($g_t(0) \neq g_t(\pi)$) This behaviour is shown in figure 7.5.

Analogously, we expect no surprises for the zero-frequency noise of charge current. Without precessions, we expect standard shot noise (compare chapter 2),

$$S = \sum_{\sigma} g_t^{\sigma}(\theta_0) \left[2T + \frac{[\Gamma_l^{\sigma}(\theta_0)]^2 + \Gamma_r^2}{[\Gamma_l^{\sigma}(\theta_0) + \Gamma_r]^2} \left(V \coth \frac{V}{2T} - 2T \right) \right] , \quad (7.19)$$

where both spin-resolved charge currents contribute independently. However, when the applied voltage is close to the switching voltage, fluctuations could drive the magnetization away from the poles. Thus, in vicinity of the transition, one could very well observe interesting influences of the magnetization dynamics onto the noise of charge current. However, this analysis goes beyond the discussion in this thesis. But it poses an interesting conceptual problem which might be addressed in future.

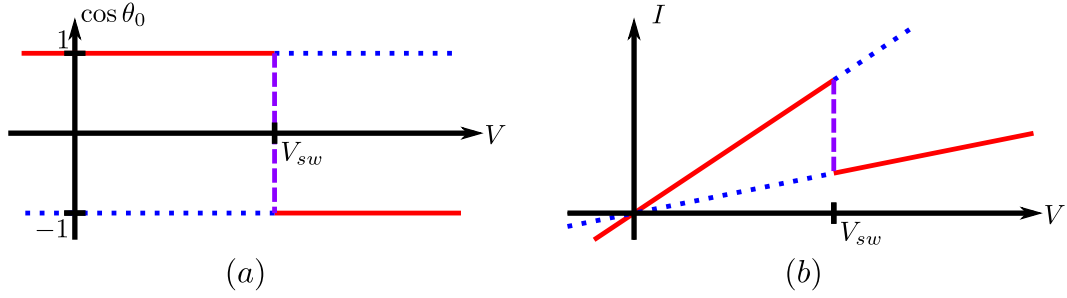


Figure 7.5: (a) The stationary solutions for $\cos \theta_0$ are shown in dependence on the voltage V . When it is increased above the switching voltage V_{sw} , driving overpowers damping and the stable stationary solution (red solid) jumps from the north pole to the south pole. Similarly, the unstable stationary solution (blue dotted) jumps from the south pole to the north pole. Only when the voltage V is fine-tuned onto the switching voltage V_{sw} we find steady state precession for all polar angles $\theta_0 \in [0, \pi]$; however, these are only of marginal stability (purple dashed). (b) The charge current is shown in dependence on the applied voltage. As the magnetization is either at the north pole or at the south pole but not in a steady state precession, we simply find Ohm's law (linear relation). The conductance depends on the orientation of the magnetization and, thus, the current changes to a new value when the voltage is increased above the switching voltage. Reprinted figure with permission from [T. Ludwig, I. S. Burmistrov, Y. Gefen, and A. Shnirman, *Physical Review B* **95**, 075425 (2017)] Copyright (2017) by the American Physical Society. The original work is found under <https://dx.doi.org/10.1103/PhysRevB.95.075425>.

7.2.2 Summary: purely voltage biased situation

Interestingly, no stable steady state precessions exist for purely voltage bias. This nonexistence can be traced back to the hybrid STT-current or, correspondingly, to the dynamical interplay between magnetization and electron distribution.

This is in strong contrast to earlier works in which, justified by a strong internal relaxation, an equilibrium rotating-frame distribution was assumed. Consequently, no hybrid STT-current has been found. In turn, stable steady state precessions have been predicted; see for example [Chudnovskiy et al., 2008, Swiebodzinski et al., 2010, Kamenev, 2011]. For an accurate description of real systems both limiting cases, strong nonequilibrium and strong internal relaxation, might be too extreme. The intermediate regime between these two limiting cases, however, has not yet been explored. It should be addressed in future works.

7.3 Purely thermal bias: hybrid current can enhance the thermoelectric effect

In this section, we consider the magnetic double tunnel junction to be driven by thermal bias only; see figure 7.6. Explicitly, we assume different temperatures in both leads $T_l \neq T_r$. But the bias voltage and the oscillating part of the external magnetic field are assumed to be zero ($\mu_l = \mu_r =: \mu$ and $\Omega = 0$). Then, the coordinate form of the LLGS-equation is reduced to,

$$\dot{\phi} = -B_0 - \frac{\alpha(\theta)}{\sin \theta} \dot{\theta}, \quad (7.20)$$

$$\dot{\theta} = \sin \theta [\hat{\alpha}(\theta) \dot{\phi} - I_b^s(\theta)/S], \quad (7.21)$$

where the bias STT-current $I_b^s(\theta) = \frac{2\Gamma_\Delta \Gamma_r}{\Gamma_\uparrow(\theta)\Gamma_\downarrow(\theta)} \tilde{g}'(\theta) b_T$ is governed by the thermal bias parameter $b_T = \frac{\pi^2}{6} (T_l^2 - T_r^2)$. The hybrid STT-current was absorbed into the renormalized damping coefficient $\hat{\alpha}(\theta) = \frac{\Gamma_\Sigma^2 - \Gamma_\Delta^2}{\Gamma_\Sigma^2 - \Gamma_\Delta^2 \cos^2 \theta} \alpha(\theta)$. Since $\alpha(\theta) = \tilde{g}(\theta)/S$, the magnetization precesses around the external magnetic field at the frequency $\dot{\phi} = -B_0 + \mathcal{O}(1/S^2) \approx -B_0$. Beyond that, the dynamics of ϕ will only be diffusive, as there is no drift term.

The dynamics of θ is governed by the competition between (renormalized) damping $\hat{\alpha}(\theta) \dot{\phi}$ and driving via thermally induced STT-current $I_b^s(\theta)$. Using $\dot{\phi} = -B_0$, we obtain

$$\dot{\theta} = -\sin \theta \hat{\alpha}(\theta) \left[B_0 + \lambda_0 \frac{\tilde{g}'(\theta)}{\tilde{g}(\theta)} b_T \right], \quad (7.22)$$

where $\lambda_0 = 2\Gamma_\Delta \Gamma_r / (\Gamma_\Sigma^2 - \Gamma_\Delta^2)$. Stationary solutions θ_0 always exist at the poles, since $\sin \theta = 0$ for $\theta = 0, \pi$. Additional stationary solutions exist for $\left[B_0 + \lambda_0 \frac{\tilde{g}'(\theta_0)}{\tilde{g}(\theta_0)} b_T \right] = 0$, which is straightforward to solve for $\cos \theta_0$. It follows,

$$\cos \theta_0 = \frac{\Gamma_\Sigma \rho_\Sigma B_0 + \lambda_0 \rho'_\Sigma b_T}{\Gamma_\Delta \rho_\Delta B_0 + \lambda_0 \rho'_\Delta b_T}, \quad (7.23)$$

where $\rho_{\Sigma/\Delta} = \rho_\uparrow \pm \rho_\downarrow$ and $\rho'_{\Sigma/\Delta} = \rho'_\uparrow \pm \rho'_\downarrow$. Equation (7.23) describes additional stationary solutions only if the right hand side is in the interval $(-1, 1)$. Stationary solutions with $\theta_0 \neq 0, \pi$ describe steady state precessions of the magnetization. In particular, we are interested in stable steady state precessions, where small deviations $\delta\theta$ from θ_0 relax back to zero.

For simplicity, we consider a symmetric density of states ($\rho_\uparrow = \rho_\downarrow$ and $\rho'_\uparrow = -\rho'_\downarrow$). Then, $\rho_\Delta = 0$ and $\rho'_\Sigma = 0$. Equation (7.23) is reduced to

$$\cos \theta_0 = \frac{\Gamma_\Sigma \rho_\Sigma B_0}{\lambda_0 \Gamma_\Delta \rho'_\Delta b_T}, \quad (7.24)$$

which can only be solved for $|b_T| > \left| \frac{\Gamma_\Sigma \rho_\Sigma B_0}{\lambda_0 \Gamma_\Delta \rho'_\Delta} \right|$. So, we identify a critical strength of thermal bias $b_T^0 = \left| \frac{\Gamma_\Sigma \rho_\Sigma B_0}{\lambda_0 \Gamma_\Delta \rho'_\Delta} \right|$ and, with it, three regimes of driving: a regime of weak driving $|b_T| < b_T^0$ and two regimes of strong driving $|b_T| > b_T^0$; see figure 7.6.

The weak driving regime is somewhat boring: damping always overpowers driving such

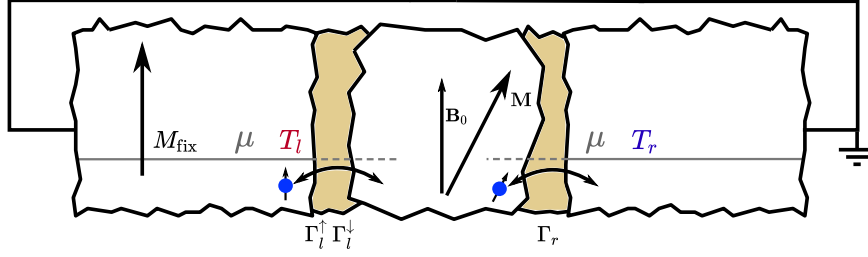


Figure 7.6: Schematic view of the system with purely thermal bias ($T_l \neq T_r$); but neither voltage bias nor FMR-type driving is applied ($\mu_l = \mu_r =: \mu$ and $\Omega = 0$). The Gilbert damping tends to align the magnetization towards the external magnetic field $\mathbf{B} = (0, 0, B_0)$. However, under a thermal bias a current through flows through the system which leads to an STT-current that can compete with Gilbert damping.

that the only stationary solutions are at the poles (stable at the north pole; unstable at the south pole). In the two strong driving regimes, the driving can compete with the damping. In turn, the dynamics becomes more interesting: these two regimes deserve a separate discussion. For concreteness, we assume $\rho'_\Delta < 0$ in the following.

For strong *positive* thermal bias $b_T > b_T^0$, we find a regime of double-stability. The thermally induced STT-current drives the magnetization towards the poles. On the northern hemisphere, damping and driving cooperate and push the magnetization towards the north pole which remains stable. On the southern hemisphere, the situation is more subtle. However, close to the pole driving overpowers damping and the south pole becomes locally stable. So, both poles are stable simultaneously. This regime of double-stability is possible, since the direction of the thermally induced STT-current depends on the orientation of the magnetization. The same is true for the charge current. In other words, the direction of the thermoelectric current depends on the orientation of the magnetization; see figure 7.7.

In the regime of strong *negative* thermal bias, $b_T < -b_T^0$, stable steady state precessions arise from the competition between (renormalized) damping and thermally induced STT-current. Most interesting is the effect of the precessing magnetization onto the charge current,

$$I = - \sum_{\sigma} g_i^{\sigma}(\theta_0) \frac{\Gamma_{\Delta} \sin^2 \theta_0 \dot{\phi}_0}{2\Gamma_l^{\sigma}(\theta_0)} - \sum_{\sigma} g'_{i,\sigma}(\theta_0) b_T . \quad (7.25)$$

It has two contributions: a thermal contribution $\propto b_T$ which corresponds to the standard thermoelectric effect; and a hybrid contribution $\propto \dot{\phi}_0$ which is induced by the precession of the magnetization. For $\Gamma_{\Delta} > 0$, both have the same sign; see figure 7.7. Thus, we conclude: the hybrid charge-current can enhance the thermoelectric effect.

7.3.1 Summary: purely thermal bias

For thermal bias, two different types of strong driving regimes can emerge: a regime of double-stability, where both poles are stable; and a regime of stable steady state precessions. Both of these strong driving regimes are interesting. In the regime of double stability we expect the

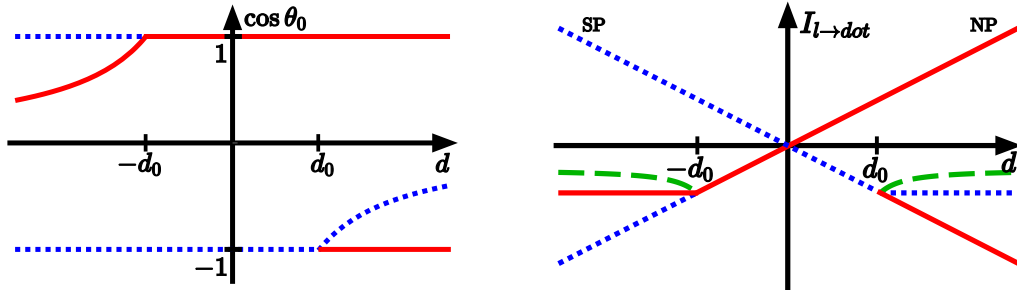


Figure 7.7: [Notation in figure: $d = b_T$, $d_0 = b_T^0$, and $I_{l \rightarrow dot} = I$] **(left)** The stationary solutions for θ_0 are shown with their stability (red solid = stable; blue dotted = unstable). For weak driving $|b_T| < b_T^0$, damping is always stronger than driving and, thus, only the north pole is stable. For strong positive driving $b_T > b_T^0$, the thermal bias drives the magnetization towards the poles, such that both poles become stable. For strong negative driving $b_T < -b_T^0$, the thermal bias drives the magnetization towards the equator, such that stable steady state precessions emerge from the angle-dependent competition between damping and driving. Reprinted figure with permission from [T. Ludwig, I. S. Burmistrov, Y. Gefen, and A. Shnirman, *Physical Review B* **99**, 045429 (2019)] Copywrite (2019) by the American Physical Society. The original work is found under <https://dx.doi.org/10.1103/PhysRevB.99.045429>. **(right)** The charge current is shown for stable (red solid) and unstable (blue dotted) steady state precessions. For comparison, we also show a hypothetical situation (green dashed), where the magnetization is fixed ($\dot{\phi}_0 = 0$) at the same polar angle θ_0 which we would obtain for the steady state precession at bias b_T . Practically, this means to disregard the hybrid charge-current in the hypothetical situation. Interestingly, in the regime of double-stability $b_T > b_T^0$, the direction of the charge current depends on the orientation of the magnetization. Even more interesting is the regime of stable steady state precessions $b_T < -b_T^0$. The actual flow of charge-current with a precessing magnetization is larger than in the hypothetical situation with a fixed magnetization, despite the same polar angle θ_0 . In other words, the hybrid charge-current enhances the thermoelectric effect. Reprinted figure with permission from [T. Ludwig, I. S. Burmistrov, Y. Gefen, and A. Shnirman, *Physical Review B* **99**, 045429 (2019)] Copywrite (2019) by the American Physical Society. The original work is found under <https://dx.doi.org/10.1103/PhysRevB.99.045429>.

charge current to alternate its direction depending on the orientation of the magnetization. Most interesting, from the perspective of this thesis, is the regime of steady state precessions. In this regime, the thermoelectric current is enhanced by the hybrid charge-current. From a more general perspective, the magnetic double tunnel junction can be viewed as a thermally driven adiabatic pump, where the thermoelectric current and the hybrid charge-current flow in the same direction. Besides being of conceptual interest, this might become important in technical applications; in particular, for the conversion of waste heat into useful electrical energy.

7.4 Summary and discussion

The magnetization dynamics in a magnetic double tunnel junction, figure 7.1, is described by the Landau-Lifshitz-Gilbert-Slonczewski equation (7.1). Interestingly, the Slonczewski spin-transfer-torque (STT) term remains even in absence of external bias. This is due to the hybrid STT-current which emerges out of the interplay between the magnetization dynamics and the electron distribution.

We explicitly demonstrated the relevance of the hybrid STT-current and the related hybrid charge current in three situations: for FMR-type driving, for voltage bias, and for thermal bias. For FMR-type driving, a new type of self-sustained steady state precessions emerges due to the hybrid STT-current. For voltage bias, in contrast, the hybrid STT-current leads to an extinction of stable steady state precessions. Finally, for thermal bias, the hybrid charge-current can enhance the thermoelectric effect.

In conclusion: the hybrid STT-current and the closely related hybrid charge-current can lead to strong qualitative effects. In other words, the interplay between magnetization dynamics and electron distribution must be taken into account for magnetic double tunnel junctions.

Chapter 8

Summary and conclusion

A dynamical mean-field drives the electron distribution away from equilibrium (chapter 3). Vice versa, the electron distribution governs the flow of charge- and spin-currents (chapter 2) and, thereby, it can affect the mean-field dynamics. Thus, an interplay between mean-fields and electron distributions emerges. In order to understand this interplay we studied double tunnel junctions, where the electrons in the middle region interact either via Coulomb-repulsion (chapter 4) or via exchange interaction (chapters 5 and 6).

The Coulomb-repulsion gives rise to the electrical potential as its corresponding mean-field. The interplay between electrical potential and electron distribution induces a correction to the RC -relaxation law (chapter 4). The correction is also known as quantum capacity and it is closely related to the Pauli exclusion principle. Coulomb-repulsion and Pauli exclusion principle cooperate, as both act repulsively. Therefore, the quantum capacity yields only a quantitative correction to the dynamics of the electrical potential.

The exchange interaction gives rise to a magnetization as its corresponding mean-field. The interplay between magnetization and electron distribution induces three particularly interesting effects. *The first effect.* A precessing magnetization drives the electron distribution into a strong nonequilibrium state and, thereby, it generates noise of charge current. This noise is governed by the geometric Berry-phase associated with the precession of the magnetization. It remains finite and carries information about the magnetization dynamics, even when the charge current vanishes on average (chapter 3). *The second effect.* Analogously to the electrical potential, a quantum capacity arises for the dynamics of the magnetization length. However, in strong contrast to Coulomb-repulsion, the exchange interaction is attractive. Thus, it competes with Pauli exclusion principle. As a result, the quantum capacity turns out to be essential for the magnetization's length dynamics. Without quantum capacity, the magnetization would grow without bounds even for the tiniest positive exchange constant (chapter 5). *The third effect.* Via its precession, the magnetization drives the electron distribution into a nonequilibrium state and, thereby, changes the flow of charge- and spin-currents. An altered spin-current has a back-action onto the magnetization's angular dynamics. This gives rise to a spin-transfer-torque (STT) current, which we call hybrid STT-current. It depends on the dynamics of the magnetization but not on the source of driving. In this sense, it is a universal contribution to the Landau-Lifshitz-

Gilbert-Slonczewski equation (chapter 6).

The hybrid current can cause drastic effects in magnetic double tunnel junctions (chapter 7). *For FMR-type driving*, the hybrid STT-current can give rise to a new type of self-sustained steady state precessions. Self-sustained means the following: the precessing magnetization generates a nonequilibrium electron distribution that induces the hybrid STT-current which is necessary to sustain the steady state precession. *For driving via voltage bias*, the hybrid STT-current leads to an extinction of stable steady state precessions. When the magnetization precesses at any specific polar angle, the electron distribution adjust in such a way that it renders the precession unstable. *For driving via thermal bias*, the hybrid STT-current is quantitatively important for the stable steady state precessions. In this context, the hybrid charge-current is more interesting. Analog to the hybrid STT-current, the hybrid charge-current emerges from the precession of the magnetization. Interestingly, the hybrid charge current can flow into the same direction as the thermoelectric current which drives the magnetization. Thus, the hybrid charge-current can enhance the thermoelectric effect.

Conclusion

We have clearly demonstrated that the dynamical interplay between mean-fields and electron distributions can lead to drastic effects in magnetic double tunnel junctions. Is this interplay also important in other spintronic systems? Probably yes! Our results justify a deeper investigation.

Acknowledgements

First of all, I want to thank my supervisor, *Alexander Shnirman*. In particular, I thank you very much for teaching me how to do research and also for teaching me to see the physics behind the formalism. It has been a great pleasure to work for you and with you.

In addition, I want to thank *Igor S. Burmistrov* and *Yuval Gefen* who are coauthors for all my papers so far. Many thanks to you for hosting me for three months at Landau Institute and Weizmann Institute, respectively. Also I thank you very much for the great collaboration; I learned a lot from you in all our discussions.

Also, I want to thank all *my friends, colleagues, and former colleagues from TKM*. Because of you, the working atmosphere at TKM is absolutely great. I enjoyed working with you very much; thank you so much! Beyond this, I want to thank some of you in particular. At first, *Jörg Schmalian*, thank you very much for (kor-)refereeing my thesis; I hope you enjoyed to read it. Very special thanks go to *Elio König-Tarasevich* and *Michael Schütt*: both of you took an essential role in my education as a condensed matter physicist; thank you very much for sharing so many of your deep insights. Also many thanks to *Matthias Hecker*, *Egor Kiselev*, and *Markus Klug* for the many great discussions we had and for proof-reading parts of my thesis and the valuable feedback you gave; thank you very much! During my time at TKM I also enjoyed participating in a book-seminar about condensed matter, in these seminars I learned a lot. So, many thanks also go to the other members of our book-seminar group: *Matthias Bard*, *Mareike Hoyer*, *Julia Link*, and *Philipp Weiß*; thank you very much. Learning Keldysh formalism is not an easy quest; many subtle but relevant points have to be considered. Thus, I appreciate very much the many discussions I had with *Pia Gagel* and *Pablo Schad*; thank you very much for sharing your insights into nonequilibrium physics in general and into Keldysh formalism in particular. Finally, I want to give special thanks to *Matthias Keßler*. I learned a lot from our collaboration during your Master-thesis; many thanks to you. Also I want to thank *Bhilahari Jeevanesan*: we had many interesting discussions about broad questions of physics, mathematical and technical details, and also many funny discussions about physical and mathematical riddles; thank you very much!

Very special thanks go to *Marcus Elstner* and *Mathias Gutmann*. It always was a great pleasure to attend your seminars about philosophy of physics. I learned a lot about science and research in general and about physics in particular. Without your great seminars, I might not have managed to find my way into condensed matter physics. Thank you very much for sharing your deep insights with me. In this context, I also want to thank all of the long-term members of

the discussion group about philosophy of physics: *Robin Lorenz*, *Jens Salomon*, *Bettina Stöhr*, *Jan-Hendrik Treude*, *Daniel Wenz*, and *Peter Wichers*. It was a great time we had together, discussing so many topics in relation to physics, philosophy, mathematics, research, and science in general; thank you so much. In the same context, I want to thank *Johannes Kleiner* for our long and deep discussions about philosophy and physics; thank you very much.

During my course of study, I had always enjoyed to work together with many of my fellow students. In particular, I want to thank *Martin Schumann*. In the first semesters we worked together very closely, which helped me to get through the Bachelor courses; thank you very much. Also many thanks go to *Paul Schnäbele*, *Anna Stopka*, *Stefan Beyl*, and *Anna Weigel* for the great time we had together while preparing for the final exams of our Bachelor degree. I learned a lot and I had a lot of fun during this time; thank you very much. In addition, I want to thank *Daniela Mockler* for the nice and insightful time during our preparation for a mathematics exam in a late semester; many thanks to you.

I thank the DFG for financially supporting my work under the Research Grant No. SH 81/3-1. I thank the Russian Foundation for Basic Research for supporting my work at Landau Institute for theoretical physics under the Grant No. 19-32-50005. I thank the Karlsruhe House of Young Scientists (KHYS) of KIT for financially supporting my stay at the Weizmann Institute of Science (WIS) in Israel under the Research Travel Grant. I also thank the Feinberg Graduate school of WIS for organizational support of my stay at WIS.

Last, but most of all, I thank *all my family*; in particular, my brother *Maximilian* and my parents *Karin* and *Michael*: thank you so much for your unlimited support throughout all my life. And *Maria*: thank you very much for your infinite patience with me, while I was writing this thesis.

Part IV

Appendices

Appendix A

Proper treatments of leads and introduction of counting fields

In this appendix, we discuss how the leads can be treated properly. In addition, we discuss the introduction of counting fields for the charge current. We closely follow [Ludwig et al., 2017, Ludwig et al., 2019b] and [Ludwig et al., 2019a].

The two main results: leads can be included via a self-energy; and counting fields appear in the self-energy.

A.1 Proper treatment of the leads

We consider a quantum dot which is tunnel-coupled to two normal metal leads. For simplicity, we disregard spin in the derivation. The Hamiltonian of the full systems is given by,

$$H = H_d + H_l + H_r . \quad (\text{A.1})$$

The Hamiltonian of the dot is assumed to be of the form $H_{\text{dot}} = H_0 + H_{\text{int.}}$, where $H_0 = \sum_{\alpha} \epsilon_{\alpha} c_{\alpha}^{\dagger} c_{\alpha}$ accounts for the single-particle states α with energies ϵ_{α} and (two-particle) interactions are included in $H_{\text{int.}}$. The left lead is described by

$$H_l = \sum_{n=1}^{N_l} \int \frac{dk}{2\pi} (\epsilon_{nk} + V) c_{nk}^{\dagger} c_{nk} + \sum_{n=1}^{N_l} \sum_{\alpha} \int \frac{dk}{2\pi} \left(t_{l,\alpha n} c_{\alpha}^{\dagger} c_{nk} + t_{l,\alpha n}^* c_{nk}^{\dagger} c_{\alpha} \right) , \quad (\text{A.2})$$

which includes the tunnel coupling to the dot. The states in the left lead are described by momentum k and transport channel index n . The corresponding single-particle energy $\epsilon_{nk} + V$ is shifted with the applied voltage V . The tunneling matrix $t_{l,\alpha n}$ is assumed to depend only on the channel, but not on the momentum. As the dot's single-particle Hamiltonian H_0 is chosen to be diagonal, most of the randomness arising from disorder is transferred to the tunneling matrix $t_{\alpha n}$. The right lead is described analogously; that is, $H_r = \sum_{n'=1}^{N_r} \int \frac{dk}{2\pi} \epsilon_{n'k} c_{n'k}^{\dagger} c_{n'k} + \sum_{n'=1}^{N_r} \sum_{\alpha} \int \frac{dk}{2\pi} \left(t_{r,\alpha n'} c_{\alpha}^{\dagger} c_{n'k} + t_{r,\alpha n'}^* c_{n'k}^{\dagger} c_{\alpha} \right)$. In contrast to the left lead, the right lead is assumed to be grounded. Thus, there is no voltage shift in the single-particle states.

In addition to the Hamiltonian, we need to specify the distribution functions of the leads. We assume equilibrium distributions in both leads. That is, $f_l(\omega) = 1/[e^{(\omega-\mu_l)/T_l} + 1]$ and $f_r(\omega) = 1/[e^{(\omega-\mu_r)/T_r} + 1]$. The chemical potentials of both leads are assumed to be equal but the electrochemical potentials differ by the applied voltage: $\mu_l = \mu + V$ and $\mu_r = \mu$. While we could specify an initial distribution function of the dot, it is not necessary. After a short transient time, the dot's distribution function will be governed by the coupling to the leads and their distribution functions.

A.1.1 The effective action

We use the Keldysh formalism in its path-integral version [Kamenev and Levchenko, 2009, Altland and Simons, 2010, Kamenev, 2011]. The Keldysh generating function is given by $\mathcal{Z} = \int D[\bar{\Psi}, \Psi] e^{i\mathcal{S}}$ with the action

$$\mathcal{S} = \oint_K dt [\bar{\Psi} i\partial_t \Psi - H(\bar{\Psi}, \Psi)] . \quad (\text{A.3})$$

The integral is over the Keldysh contour and, here, $\bar{\Psi}, \Psi$ denote all fermionic fields of the dot and the leads. As the leads are noninteracting, we can integrate them out. It follows,

$$\mathcal{S} = \oint_K dt [\bar{\Psi}_d i\partial_t \Psi_d - H_{\text{dot}}(\bar{\Psi}_d, \Psi_d)] - \oint_K dt \oint_K dt' \bar{\Psi}_d(t) \Sigma(t-t') \Psi_d(t') , \quad (\text{A.4})$$

where $\bar{\Psi}_d, \Psi_d$ denote only the fermionic fields of the dot. A self-energy term, $\Sigma(t-t') = \Sigma_l(t-t') + \Sigma_r(t-t')$, arises from the coupling to the leads. From the coupling to the left lead we obtain $\Sigma_l(t-t') = t_l G_l t_l^\dagger$, where the Green's function is defined by its inverse $G_l^{-1} = i\partial_t - (\varepsilon_{nk} + V)$. Analogously, $\Sigma_r(t-t') = t_r G_r t_r^\dagger$ with $G_r^{-1} = i\partial_t - \varepsilon_{nk}$. To write the action (A.4) more compact, we introduce a self-energy operator $[\hat{\Sigma}\Psi_d](t) = \oint_K dt' \Sigma(t-t') \Psi_d(t')$. Then,

$$\mathcal{S} = \oint_K dt [\bar{\Psi}_d (i\partial_t - \hat{\Sigma}) \Psi_d - H_{\text{dot}}(\bar{\Psi}_d, \Psi_d)] . \quad (\text{A.5})$$

This result justifies to include the coupling to the leads only via a self-energy operator.

To determine the self-energies $\Sigma_l(t-t') = t_l G_l(t-t') t_l^\dagger$ and $\Sigma_r(t-t') = t_r G_r(t-t') t_r^\dagger$, we have to find the leads' Green's functions at first. To retain the information about the leads' distribution functions, we have to be careful with the regularization. This regularization problem is typical for the path integral version of the Keldysh technique and has a standard solution when the distribution function is fixed in time [Kamenev and Levchenko, 2009, Altland and Simons, 2010, Kamenev, 2011]. It follows,

$$G_l^{R/A}(\omega) = \frac{1}{\omega - \varepsilon_{nk} - V \pm i\delta} \quad (\text{A.6})$$

$$G_l^K(\omega) = -2\pi i \delta(\omega - \varepsilon_{nk} - V) F_l(\omega) , \quad (\text{A.7})$$

where $\pm i\delta$ is an infinitesimal shift for proper regularization and $F_l(\omega) = 1 - 2f_l(\omega)$ is the left

lead's distribution function¹. Analogously for the right lead, $G_r^{R/A}(\omega) = \frac{1}{\omega - \varepsilon_{n'k} \pm i\delta}$ and $G_r^K(\omega) = -2\pi i \delta(\omega - \varepsilon_{n'k}) F_r(\omega)$ with $F_r(\omega) = 1 - 2f_r(\omega)$.

For the self-energy follows

$$\Sigma_{l,\alpha\beta}^{R/A}(\omega) = \sum_{n=1}^{N_l} \int \frac{dk}{2\pi} \frac{t_{l,\alpha n} t_{l,\beta n}^*}{\omega - \varepsilon_{nk} - V \pm i\delta} \quad (\text{A.8})$$

$$\Sigma_{l,\alpha\beta}^K(\omega) = -2\pi i \sum_{n=1}^{N_l} \int \frac{dk}{2\pi} t_{l,\alpha n} t_{l,\beta n}^* \delta(\omega - \varepsilon_{nk} - V) F_l(\omega). \quad (\text{A.9})$$

Disregarding the principal value contribution (real part) to the retarded/advanced self-energy, we obtain,

$$\Sigma_{l,\alpha\beta}^{R/A}(\omega) = \mp i \Gamma_{l,\alpha\beta}(\omega), \quad (\text{A.10})$$

$$\Sigma_{l,\alpha\beta}^K(\omega) = -2i \Gamma_{l,\alpha\beta}(\omega) F_l(\omega), \quad (\text{A.11})$$

with the tunneling rate $\Gamma_{\alpha\beta}(\omega) = \pi \sum_{n=1}^{N_l} \rho_n(\omega) t_{l,\alpha n} t_{l,\beta n}^*$ which is determined by the density of states of channel n in the left lead $\rho_n(\omega) = \int \frac{dk}{2\pi} \delta(\omega - \varepsilon_{nk} - V)$. In both leads, we assume a large number of channels that are weakly and randomly coupled to the states in the dot. In addition, we assume the leads' densities of states to be approximately constant around their respective electrochemical potential. Then, we can approximate the tunneling rates as diagonal in orbital-space, independent of the orbital index α , and independent of energy ω —that is, $\Gamma_{l,\alpha\beta}(\omega) \approx \Gamma_l$ and $\Gamma_{r,\alpha\beta}(\omega) \approx \Gamma_r$; for details we refer to [Ludwig et al., 2017].

A.1.2 Extension to a magnetic lead

When the left lead is magnetic with a fixed magnetization M_{fix} , then its Green's function is modified. The magnetization changes the energy of single-particle states in dependence on the spin $G_l^{-1} = i\partial_t - (\varepsilon_{nk} + V - M_{\text{fix}}\sigma_z/2)$. Then, $G_{l,\sigma}^{R/A}(\omega) = \frac{1}{\omega - \varepsilon_{nk} - V + M_{\text{fix}}\sigma/2 \pm i\delta}$ and $G_{l,\sigma}^K(\omega) = -2\pi i \delta(\omega - \varepsilon_{nk} - V + M_{\text{fix}}\sigma/2) F_l(\omega)$. In turn, the self-energy $\Sigma_{l,\alpha\beta\sigma}^{R/A}(\omega) = \mp i \Gamma_{l,\alpha\beta}^\sigma(\omega)$ and $\Sigma_{l,\alpha\beta\sigma}^K(\omega) = -2i \Gamma_{l,\alpha\beta}^\sigma(\omega) F_l(\omega)$ becomes spin-dependent as well. However, the equilibrium distribution function $F_l(\omega)$ remains independent of the spin. The spin-dependence arises solely from the tunneling rate $\Gamma_{\alpha\beta}^\sigma(\omega) = \pi \sum_{n=1}^{N_l} \rho_n^\sigma(\omega) t_{l,\alpha n} t_{l,\beta n}^*$ which depends on spin through the transport-channel-resolved density of states $\rho_n^\sigma(\omega) = \int \frac{dk}{2\pi} \delta(\omega - \varepsilon_{nk} - V + M_{\text{fix}}\sigma/2)$. Again, for many channels that are weakly and randomly coupled to the states in the dot, we can approximate $\Gamma_{l,\alpha\beta}^\sigma(\omega) \approx \Gamma_l^\sigma$ which is the spin-dependent tunneling rate [Ludwig et al., 2017].

A.2 Introduction of counting fields

Let us now discuss how we can use the method of counting fields to derive the charge current and its noise. Still, we closely follow the presentation of [Ludwig et al., 2019a]; for the original

¹We refer to both, $F_l(\omega)$ and $f_l(\omega)$, as distribution functions. This is possible as they are in one-to-one correspondence.

idea, see [Virtanen and Heikkilä, 2017].

Formally, we introduce the counting field before the leads are integrated out. That is, we should introduce counting fields with the action A.3. To determine the charge which flows through the left tunnel junction into the left lead, we add to the action

$$\mathcal{S}_c = - \oint_K dt \dot{\lambda}(t) N_l(\bar{\Psi}_l, \Psi_l), \quad (\text{A.12})$$

where $N_l(\bar{\Psi}_l, \Psi_l) = \sum_n \int dk \bar{\Psi}_{l,nk} \Psi_{l,nk}$ is the number of electrons in the left lead. That is, in the Keldysh partition function $\mathcal{Z} = \int D[\bar{\Psi}, \Psi] e^{i\mathcal{S}}$ we replace $\mathcal{S} \rightarrow \mathcal{S} + \mathcal{S}_c$. Thereby, the Keldysh partition function depends on the counting field. The new counting-field-action \mathcal{S}_c is eliminated by a gauge-transformation: $\Psi_{l,nk} \rightarrow e^{-i\lambda(t)} \Psi_{l,nk}$ and $\bar{\Psi}_{l,nk} \rightarrow \bar{\Psi}_{l,nk} e^{-i\lambda(t)}$. Effectively, this modifies the tunneling matrices $t_l \rightarrow e^{-i\lambda(t)} t_l$ and $t_l^\dagger \rightarrow t_l^\dagger e^{i\lambda(t)}$. We can, now, integrate out the leads again. The counting field appears in the self-energy associated with the left lead,

$$\Sigma_l(t-t') \rightarrow e^{-i\lambda(t)} \Sigma_l(t-t') e^{+i\lambda(t')}. \quad (\text{A.13})$$

The counting field is assumed to have only a quantum component $\lambda_\pm(t) = \pm\lambda_q(t)/2$ and, for simplicity, it is assumed to be constant in time $\lambda_q(t) = \lambda$. The simplifying constant-in-time assumption restricts the derivation to zero-frequency current and noise.

So, after all these manipulations the Keldysh partition function is given by

$$\mathcal{Z}(\lambda) = \int D[\bar{\Psi}_d, \Psi_d] e^{i\mathcal{S}(\lambda)}. \quad (\text{A.14})$$

It depends on the counting field via the action,

$$\mathcal{S}(\lambda) = \oint_K dt [\bar{\Psi}_d (i\partial_t - \hat{\Sigma}_\lambda) \Psi_d - H_d(\bar{\Psi}_d, \Psi_d)], \quad (\text{A.15})$$

with the self-energy operator defined by $[\hat{\Sigma}_\lambda \Psi_d](t) = \oint dt' \Sigma_\lambda(t-t') \Psi_d(t')$, where $\Sigma_\lambda = \Sigma_l(\lambda) + \Sigma_r$ with $\Sigma_l(\lambda) = e^{-i\lambda(t)} \Sigma_l(t-t') e^{+i\lambda(t')}$. Now, the main point is that the counting field was introduced in equation (A.12) such that the average charge that is transported into the left lead is given by

$$\langle Q_l \rangle = i\partial_\lambda \mathcal{Z}(\lambda) \Big|_{\lambda=0}. \quad (\text{A.16})$$

The second moment is given by

$$\langle Q_l^2 \rangle = (i\partial_\lambda)^2 \mathcal{Z}(\lambda) \Big|_{\lambda=0}. \quad (\text{A.17})$$

Higher moments are obtained analogously. The charge current and its noise can, then, be obtained via $\langle Q_l \rangle = \int dt I_l$ and $\langle\langle Q_l \rangle\rangle = \langle Q_l^2 \rangle - \langle Q_l \rangle^2 = \int dt S_l$.

The formulas for current flowing into the right lead can be obtained in complete analogy; only the counting field should be introduced with $N_r(\bar{\Psi}_r, \Psi_r)$ instead of $N_l(\bar{\Psi}_l, \Psi_l)$.

A.2.1 Noninteracting case

As the simplest case, we consider the electrons in the dot to be noninteracting $H_d = \sum_{\alpha} \varepsilon_{\alpha} c_{\alpha}^{\dagger} c_{\alpha}$. Then, the dot's fermionic fields can be integrated out as well. It follows,

$$\mathcal{Z}(\lambda) = e^{i\mathcal{S}(\lambda)} \quad (\text{A.18})$$

with the action

$$\mathcal{S}(\lambda) = -i \operatorname{tr} \ln \left[\underbrace{i\partial_t - \varepsilon_{\alpha} - \Sigma_{\lambda}}_{G_{\lambda}^{-1}} \right]. \quad (\text{A.19})$$

Using equation (A.16), a straightforward differentiation yields $\langle Q_l \rangle = -i \operatorname{tr} [G_0 \Sigma'_l]$, where $\Sigma'_l = \partial_{\lambda} \Sigma_l(\lambda)|_{\lambda=0}$ and $G_0^{-1} = i\partial_t - \varepsilon_{\alpha} - \Sigma$. Using $\Sigma^{R/A}(\omega) = \mp i(\Gamma_l + \Gamma_r) = \mp i\Gamma_{\Sigma}$ and $\Sigma^K(\omega) = -2i\Gamma_{\Sigma} F_d(\omega)$ with $F_d(\omega) = [\Gamma_l F_l(\omega) + \Gamma_r F_r(\omega)]/\Gamma_{\Sigma}$, we obtain $G_0^{R/A}(\omega) = 1/(\omega - \varepsilon_{\alpha} \pm i\Gamma_{\Sigma})$ for the retarded/advanced Green's function and $G_0^K(\omega) = -2i\Gamma_{\Sigma} F_d(\omega)/[(\omega - \varepsilon_{\alpha})^2 + \Gamma_{\Sigma}^2]$ for the Keldysh Green's function. In turn, the transported charge is found to be given by

$$\langle Q_l \rangle = \int dt \int d\omega \rho \Gamma_l [F_l(\omega) - F_d(\omega)], \quad (\text{A.20})$$

where the density of states $\rho(\omega) = \sum_{\alpha} \frac{1}{\pi} \frac{\Gamma_{\Sigma}}{(\omega - \varepsilon_{\alpha})^2 + \Gamma_{\Sigma}^2}$ was assumed to be approximately constant $\rho(\omega) \approx \rho$. Now, we can easily read off the average charge current at zero-frequency $I_l = \int d\omega \rho \Gamma_l [F_l(\omega) - F_d(\omega)]$. For the right lead follows analogously $I_r = \int d\omega \rho \Gamma_r [F_r(\omega) - F_d(\omega)]$. Charge conservation requires $I_l = -I_r$, which is indeed satisfied for $F_d(\omega) = [\Gamma_l F_l(\omega) + \Gamma_r F_r(\omega)]/\Gamma_{\Sigma}$.

Using equation (A.17) and taking the derivative twice leads to $\langle Q_l^2 \rangle = \langle Q_l \rangle^2 + N_l^{(1)} + N_l^{(2)}$, where $N_l^{(1)} = \operatorname{tr}[G_0 \Sigma_l'']$ and $N_l^{(2)} = \operatorname{tr}[G_0' \Sigma_l']$ with $\Sigma_l'' = \partial_{\lambda}^2 \Sigma_l(\lambda)|_{\lambda=0}$ and $G_0' = \partial_{\lambda} G_{\lambda}|_{\lambda=0} = G_0 \Sigma_l' G_0$. Note that $N_l^{(2)}$ includes G_0' which accounts for changes of the Green's function with the counting field. This term accounts for the change of the dot's distribution function with the tunneling of each electron. For the second cumulant we obtain $\langle\langle Q_l^2 \rangle\rangle = \langle Q_l^2 \rangle - \langle Q_l \rangle^2 = N_l^{(1)} + N_l^{(2)}$ with

$$N_l^{(1)} = \int dt \int d\omega \rho(\omega) \Gamma_l [1 - F_d(\omega) F_l(\omega)], \quad (\text{A.21})$$

$$N_l^{(2)} = \int dt \int d\omega \frac{\Gamma_l^2}{\Gamma_{\Sigma}} \left[2\bar{\rho}(\omega) F_d(\omega) F_l(\omega) - \bar{\rho}(\omega) F_d(\omega) F_d(\omega) - \rho(\omega) - 2F_l^2(\omega)(\bar{\rho}(\omega) - \rho(\omega)) \right], \quad (\text{A.22})$$

where we have defined two differently broadened densities of states $\rho(\omega) = \sum_{\alpha} \frac{1}{\pi} \frac{\Gamma_{\Sigma}}{(\omega - \varepsilon_{\alpha})^2 + \Gamma_{\Sigma}^2}$ and $\bar{\rho}(\omega) = \sum_{\alpha} \frac{1}{\pi} \frac{2\Gamma_{\Sigma}^3}{[(\omega - \varepsilon_{\alpha})^2 + \Gamma_{\Sigma}^2]^2}$. Assuming the difference in broadenings to be irrelevant, we can approximate $\bar{\rho}(\omega) \approx \rho(\omega)$. Then, we obtain

$$\langle\langle Q_l^2 \rangle\rangle = \int dt \int d\omega \frac{\rho \Gamma_l \Gamma_r}{\Gamma_{\Sigma}} \left\{ [1 - F_d(\omega) F_l(\omega)] + \frac{\Gamma_l}{\Gamma_r} F_d(\omega) [F_l(\omega) - F_d(\omega)] \right\}, \quad (\text{A.23})$$

where we assumed the density of states to be approximately constant $\rho(\omega) \approx \rho$. Now, via the relation $\langle\langle Q_l^2 \rangle\rangle = \int dt S_l$, the charge current noise S_l is easy to obtain.

The result for the right junction can be derived, again, in complete analogy. We would obtain the analog form but with the replacement $F_l(\omega) \rightarrow F_r(\omega)$ and with exchanged broadenings $\Gamma_l \leftrightarrow \Gamma_r$. At zero-frequency, charge conservation demands $\langle\langle Q_l^2 \rangle\rangle = \langle\langle Q_r^2 \rangle\rangle$ or, correspondingly, $S_l = S_r$. And indeed, this is satisfied for the nonequilibrium distribution $F_d(\omega) = [\Gamma_l F_l(\omega) + \Gamma_r F_r(\omega)]/\Gamma_\Sigma$.

Appendix B

Wigner transformation and gradient expansion

In this quite formal appendix, we describe the Wigner transformation and the gradient expansion, which is used several times throughout the main text. We closely follow the derivation in [Ludwig et al., 2019b]. The main results are the zeroth-order terms of the gradient expansion, equations (B.6) and (B.7). As important side results, we derive the formally exact gradient expansions, equations (B.12) and (B.16), which provide a formal criterion for the validity of the zeroth-order approximation.

B.1 The Wigner transformation

The Wigner transformation is a specific Fourier transformation. For a two-time function $f(t, t')$, the Wigner transform is defined as the Fourier transformation in the time-difference $(t - t') \rightarrow \omega$, while the time-sum $\frac{t+t'}{2}$ is left untouched. To express this formally, we define the function \tilde{f} from f with re-organized time-arguments,

$$\tilde{f}(\bar{t}, \tilde{t}) = \tilde{f}\left(\frac{t+t'}{2}, t-t'\right) = f(t, t'), \quad (\text{B.1})$$

where $\bar{t} = \frac{t+t'}{2}$ is the "center of mass"-time and $\tilde{t} = t - t'$ is the "relative"-time. The Wigner transformation of $f(t, t')$ is now defined by

$$\tilde{f}(\bar{t}, \omega) = \int d\tilde{t} e^{i\omega\tilde{t}} \tilde{f}(\bar{t}, \tilde{t}). \quad (\text{B.2})$$

It is particularly useful, when $\tilde{f}(\bar{t}, \tilde{t})$ varies fast with \tilde{t} but only slowly with \bar{t} . Such a separation of time-scales can be employed in a gradient expansion, as discussed in the next section.

B.2 The Gradient expansion

In this section of the appendix, we describe the gradient expansion for the convolution of two functions,

$$f(t, t'') = \int dt' g(t, t') h(t', t'') , \quad (\text{B.3})$$

and also for three functions,

$$f(t, t''') = \int dt' \int dt'' g(t, t') h(t', t'') k(t'', t''') . \quad (\text{B.4})$$

The gradient expansion for the convolution of two functions can be easily found in literature, for example in references [Altland and Simons, 2010, Kamenev, 2011]. We present it in a way which is easily generalizable to the convolution of three functions.

Before setting out for a formal derivation, it is useful to understand, what we expect as a result in zeroth-order. For that purpose, we switch to the "center of mass"-times and the "relative"-times. That is, in equation (B.3) we rewrite $\tilde{f}(\frac{t+t''}{2}, t-t'') = f(t, t'')$, $\tilde{g}(\frac{t+t'}{2}, t-t') = g(t, t')$, and $\tilde{h}(\frac{t'+t''}{2}, t'-t'') = h(t', t'')$ to obtain

$$\tilde{f}\left(\frac{t+t''}{2}, t-t''\right) = \int dt' \tilde{g}\left(\frac{t+t'}{2}, t-t'\right) \tilde{h}\left(\frac{t'+t''}{2}, t'-t''\right) . \quad (\text{B.5})$$

We assume, for a moment, that both functions, \tilde{g} and \tilde{h} , are independent of their "center of mass"-time arguments $\tilde{g}(\frac{t+t'}{2}, t-t') = \tilde{g}(t-t')$ and $\tilde{h}(\frac{t'+t''}{2}, t'-t'') = \tilde{h}(t'-t'')$. Then, $\tilde{f}(\frac{t+t''}{2}, t-t'') = \tilde{f}(t-t'')$ and it becomes straightforward to rewrite the convolution by the standard Fourier-transformation $f(t-t'') = \int dt' \tilde{g}(t-t') \tilde{h}(t'-t'') \rightarrow \tilde{f}(\omega) = \tilde{g}(\omega) \tilde{h}(\omega)$. If the functions are not independent of their center-of-mass time but change "very slowly" with it, then we expect the functions to adiabatically follow changes in the center-of-mass time. In turn, for the zeroth order in the gradient expansion we expect

$$\tilde{f}_0(\bar{t}, \omega) = \tilde{g}(\bar{t}, \omega) \tilde{h}(\bar{t}, \omega) , \quad (\text{B.6})$$

where we have added an index 0 to indicate that it is the zeroth order of the gradient expansion. Analogously, for the convolution of three functions, equation (B.4), we expect

$$\tilde{f}_0(\bar{t}, \omega) = \tilde{g}(\bar{t}, \omega) \tilde{h}(\bar{t}, \omega) \tilde{k}(\bar{t}, \omega) . \quad (\text{B.7})$$

Although these zeroth order results can be easily guessed, it is still worthwhile to provide a formal derivation. In particular, this allows us to provide a criterion for "very slow" changes with the center-of-mass time.

B.2.1 Formal gradient expansion for the convolution of two functions

We start from equation (B.3) and define $\bar{t} = \frac{t+t''}{2}$ and $\tilde{t} = t - t''$. Using the Wigner transformations we obtain,

$$\tilde{f}(\bar{t}, \omega) = \int d\tilde{t} \int dt' \int \frac{d\omega'}{2\pi} \int \frac{d\omega''}{2\pi} e^{i[\omega\bar{t} - \omega'(\bar{t} + \frac{\tilde{t}}{2} - t') - \omega''(t' - \bar{t} + \frac{\tilde{t}}{2})]} \tilde{g}\left(\frac{\bar{t} + \frac{\tilde{t}}{2} + t'}{2}, \omega'\right) \tilde{h}\left(\frac{t' + \bar{t} - \frac{\tilde{t}}{2}}{2}, \omega''\right). \quad (\text{B.8})$$

We use the desired zero order result, equation (B.6), to guide us through redefinitions of time- and frequency-integrals: we want to reach $\tilde{f}(\bar{t}, \omega) = \int \int \int \dots \tilde{g}(\bar{t} + \dots, \omega + \dots) \tilde{h}(\bar{t} + \dots, \omega + \dots)$. For the frequency integrals it is straightforward; we change variables to $\omega_1 = \omega' - \omega$ and $\omega_2 = \omega'' - \omega$. For the integral over t' we shift $t' \rightarrow t' + \bar{t}$. It follows,

$$\tilde{f}(\bar{t}, \omega) = \int d\tilde{t} \int dt' \int \frac{d\omega_1}{2\pi} \int \frac{d\omega_2}{2\pi} e^{-i[\omega_1(\frac{\tilde{t}}{2} - t') - \omega_2(t' + \frac{\tilde{t}}{2})]} \tilde{g}\left(\bar{t} + \frac{\tilde{t} + t'}{2}, \omega + \omega_1\right) \tilde{h}\left(\bar{t} + \frac{t' - \frac{\tilde{t}}{2}}{2}, \omega + \omega_2\right), \quad (\text{B.9})$$

which is already in a form close to the desired zeroth order result. For convenience, we bring the exponentials into a nicer form by substituting $t_1 = \frac{\tilde{t}}{2} - t'$ and $t_2 = t' + \frac{\tilde{t}}{2}$,

$$\tilde{f}(\bar{t}, \omega) = \int dt_1 \int dt_2 \int \frac{d\omega_1}{2\pi} \int \frac{d\omega_2}{2\pi} e^{-i(\omega_1 t_1 + \omega_2 t_2)} \tilde{g}\left(\bar{t} + \frac{t_2}{2}, \omega + \omega_1\right) \tilde{h}\left(\bar{t} - \frac{t_1}{2}, \omega + \omega_2\right). \quad (\text{B.10})$$

To obtain the formal gradient expansion, we expand \tilde{g} in ω_1 and \tilde{h} in ω_2 . The resulting series is integrated over ω_1, ω_2 which leads to derivatives of δ -functions that can be handled by partial integration. Finally, we obtain,

$$\tilde{f}(\bar{t}, \omega) = \sum_{m,n=0}^{\infty} \frac{(-1)^m}{n!m!} \left(\frac{i}{2}\right)^{m+n} [\partial_{\bar{t}}^m \partial_{\omega}^n \tilde{g}(\bar{t}, \omega)] [\partial_{\bar{t}}^n \partial_{\omega}^m \tilde{h}(\bar{t}, \omega)]. \quad (\text{B.11})$$

It can be recasted into a more compact form:

$$\tilde{f}(\bar{t}, \omega) = \exp\left[-\frac{i}{2}(\partial_{\bar{t}}^{\bar{h}} \partial_{\omega}^g + \partial_{\bar{t}}^g \partial_{\omega}^{\bar{h}})\right] \tilde{g}(\bar{t}, \omega) \tilde{h}(\bar{t}, \omega). \quad (\text{B.12})$$

The subscripts indicate, as usual, the variable with respect to which to differentiate. The superscripts indicate the function, on which the derivative acts. For a bar $\bar{}$ in a superscript one has to include a factor of (-1) . For example, the first order term is given by $\tilde{f}_1(\bar{t}, \omega) = -\frac{i}{2}(\partial_{\bar{t}}^{\bar{h}} \partial_{\omega}^g + \partial_{\bar{t}}^g \partial_{\omega}^{\bar{h}}) \tilde{g}(\bar{t}, \omega) \tilde{h}(\bar{t}, \omega) = -\frac{i}{2} \{ [\partial_{\omega} \tilde{g}(\bar{t}, \omega)] [-\partial_{\bar{t}} \tilde{h}(\bar{t}, \omega)] + [\partial_{\bar{t}} \tilde{g}(\bar{t}, \omega)] [\partial_{\omega} \tilde{h}(\bar{t}, \omega)] \}$. We emphasize that equation (B.12) is still exact. The zeroth order result, equation (B.6), is straightforwardly obtained by keeping only the zeroth order term in the exponential series and disregarding all higher orders. The main point of this formal derivation is to obtain a precise criterion for "very slow": the first and higher order terms have to be small compared to the zeroth order.

B.2.2 Formal gradient expansion for the convolution of three function

The derivation for the convolution of three functions, equation (B.4), is completely parallel to that for two functions. We define $\bar{t} = \frac{t+t''}{2}$ and $\tilde{t} = t - t''$ and perform the Wigner transform. It follows,

$$\begin{aligned} \tilde{f}(\bar{t}, \omega) &= \int d\tilde{t} \int dt' \int dt'' \int \frac{d\omega'}{2\pi} \int \frac{d\omega''}{2\pi} \int \frac{d\omega'''}{2\pi} e^{i[\omega\bar{t} - \omega'(\bar{t} + \frac{\tilde{t}}{2} - t') - \omega''(t' - t'') - \omega'''(t'' - \bar{t} + \frac{\tilde{t}}{2})]} \times \\ &\times \tilde{g}\left(\frac{\bar{t} + \frac{\tilde{t}}{2} + t'}{2}, \omega'\right) \tilde{h}\left(\frac{t' + t''}{2}, \omega''\right) \tilde{k}\left(\frac{t'' + \bar{t} - \frac{\tilde{t}}{2}}{2}, \omega'''\right). \end{aligned} \quad (\text{B.13})$$

Again a form close to the desired zeroth order result is obtained by a substitution in frequencies $\omega_1 = \omega' - \omega$, $\omega_2 = \omega'' - \omega$, and $\omega_3 = \omega''' - \omega$ together with a shift in time-integrals $t' \rightarrow t' + \bar{t}$ and $t'' \rightarrow t'' + \bar{t}$. It follows,

$$\begin{aligned} \tilde{f}(\bar{t}, \omega) &= \int dt_1 \int dt_2 \int dt_3 \int \frac{d\omega_1}{2\pi} \int \frac{d\omega_2}{2\pi} \int \frac{d\omega_3}{2\pi} e^{-i(\omega_1 t_1 + \omega_2 t_2 + \omega_3 t_3)} \times \\ &\times \tilde{g}\left(\bar{t} + \frac{t_2 + t_3}{2}, \omega + \omega_1\right) \tilde{h}\left(\bar{t} + \frac{t_3 - t_1}{2}, \omega + \omega_2\right) \tilde{k}\left(\bar{t} - \frac{t_1 + t_2}{2}, \omega + \omega_3\right), \end{aligned} \quad (\text{B.14})$$

where $t_1 = \frac{\tilde{t}}{2} - t'$, and $t_2 = t' - t''$, and $t_3 = t'' + \frac{\tilde{t}}{2}$. Expanding in $\omega_1, \omega_2, \omega_3$, succeeded by term-wise integration over $\omega_1, \omega_2, \omega_3$ and, finally, partial integration of t_1, t_2, t_3 , leads to,

$$\begin{aligned} \tilde{f}(\bar{t}, \omega) &= \sum_{n,m,k=0}^{\infty} \frac{1}{n!m!k!} \left(\frac{-i}{2}\right)^{n+m+k} \sum_{n'=0}^n \sum_{m'=0}^m \sum_{k'=0}^k \binom{n}{n'} \binom{m}{m'} \binom{k}{k'} (-1)^{n+m-m'} \times \\ &\times \left[\partial_{\bar{t}}^{m'+(k-k')} \partial_{\omega}^n \tilde{g}(\bar{t}, \omega) \right] \left[\partial_{\bar{t}}^{k'+(n-n')} \partial_{\omega}^m \tilde{h}(\bar{t}, \omega) \right] \left[\partial_{\bar{t}}^{n'+(m-m')} \partial_{\omega}^k \tilde{k}(\bar{t}, \omega) \right]. \end{aligned} \quad (\text{B.15})$$

This very inconveniently looking result can be recasted into the more pleasant form,

$$\tilde{f}(\bar{t}, \omega) = \exp \left[-\frac{i}{2} \left(\partial_{\bar{t}}^{\bar{h}\bar{k}} \partial_{\omega}^g + \partial_{\bar{t}}^{g\bar{k}} \partial_{\omega}^h + \partial_{\bar{t}}^{g\bar{h}} \partial_{\omega}^k \right) \right] \tilde{g}(\bar{t}, \omega) \tilde{h}(\bar{t}, \omega) \tilde{k}(\bar{t}, \omega), \quad (\text{B.16})$$

where superscripts again denote on which functions a derivative acts with the $\bar{}$ indicating, again, to include a factor of (-1) . For example, $\partial_{\bar{t}}^{g\bar{k}}(\tilde{g}\tilde{k}) = (\partial_{\bar{t}}\tilde{g})\tilde{k} + \tilde{g}(-\partial_{\bar{t}}\tilde{k})$ and $\partial_{\bar{t}}^{\bar{h}\bar{k}}(\tilde{h}\tilde{k}) = (-\partial_{\bar{t}}\tilde{h})\tilde{k} + \tilde{h}(-\partial_{\bar{t}}\tilde{k})$. The desired zeroth order result, equation (B.7), is obtained by keeping only the zeroth order in the exponential. The notion of "very slow" is defined by the negligibility of higher order terms compared to the zeroth order.

Bibliography

- [Aliev and Cascales, 2018] Aliev, F. and Cascales, J. P. (2018). *Noise in spintronics: from understanding to manipulation*. CRC Press.
- [Altland and Egger, 2009] Altland, A. and Egger, R. (2009). Nonequilibrium dephasing in coulomb blockaded quantum dots. *Phys. Rev. Lett.*, 102:026805.
- [Altland and Simons, 2010] Altland, A. and Simons, B. D. (2010). *Condensed matter field theory (second edition)*. Cambridge University Press.
- [Ambegaokar et al., 1982] Ambegaokar, V., Eckern, U., and Schön, G. (1982). Quantum dynamics of tunneling between superconductors. *Phys. Rev. Lett.*, 48:1745–1748.
- [Anderson, 1972] Anderson, P. W. (1972). More is different. *Science*, 177(4047):393–396.
- [Arakawa et al., 2015] Arakawa, T., Shiogai, J., Ciorga, M., Utz, M., Schuh, D., Kohda, M., Nitta, J., Bougeard, D., Weiss, D., Ono, T., et al. (2015). Shot noise induced by nonequilibrium spin accumulation. *Physical review letters*, 114(1):016601.
- [Basko and Vavilov, 2009] Basko, D. M. and Vavilov, M. G. (2009). Stochastic dynamics of magnetization in a ferromagnetic nanoparticle out of equilibrium. *Phys. Rev. B*, 79:064418.
- [Berger, 1996] Berger, L. (1996). Emission of spin waves by a magnetic multilayer traversed by a current. *Physical Review B*, 54(13):9353.
- [Berkov and Miltat, 2008] Berkov, D. V. and Miltat, J. (2008). Spin-torque driven magnetization dynamics: Micromagnetic modeling. *Journal of Magnetism and Magnetic Materials*, 320(7):1238–1259.
- [Bhatti et al., 2017] Bhatti, S., Sbiaa, R., Hirohata, A., Ohno, H., Fukami, S., and Piramanayagam, S. (2017). Spintronics based random access memory: a review. *Materials Today*, 20(9):530–548.
- [Blanter and Büttiker, 2000] Blanter, Y. M. and Büttiker, M. (2000). Shot noise in mesoscopic conductors. *Physics reports*, 336(1-2):1–166.
- [Brataas et al., 2002] Brataas, A., Tserkovnyak, Y., Bauer, G. E. W., and Halperin, B. I. (2002). Spin battery operated by ferromagnetic resonance. *Phys. Rev. B*, 66:060404.

- [Bruus and Flensberg, 2004] Bruus, H. and Flensberg, K. (2004). *Many-body quantum theory in condensed matter physics: an introduction*. Oxford university press.
- [Burmistrov et al., 2019] Burmistrov, I., Gefen, Y., Shapiro, D., and Shnirman, A. (2019). Mesoscopic stoner instability in open quantum dots: suppression of coleman-weinberg mechanism by electron tunneling. *arXiv preprint arXiv:1910.11581*.
- [Büttiker et al., 1993] Büttiker, M., Thomas, H., and Prêtre, A. (1993). Mesoscopic capacitors. *Physics Letters A*, 180(4-5):364–369.
- [Cascales et al., 2015] Cascales, J. P., Herranz, D., Ebels, U., Katine, J. A., and Aliev, F. G. (2015). Detection of spin torque magnetization dynamics through low frequency noise. *Applied Physics Letters*, 107(5):052401.
- [Chudnovskiy et al., 2008] Chudnovskiy, A., Swiebodzinski, J., and Kamenev, A. (2008). Spin-torque shot noise in magnetic tunnel junctions. *Physical review letters*, 101(6):066601.
- [Eckern et al., 1990] Eckern, U., Lehr, W., Menzel-Dorwarth, A., Pelzer, F., and Schmid, A. (1990). The quasiclassical langevin equation and its application to the decay of a metastable state and to quantum fluctuations. *Journal of Statistical Physics*, 59(3-4):885–934.
- [Eckern et al., 1984] Eckern, U., Schön, G., and Ambegaokar, V. (1984). Quantum dynamics of a superconducting tunnel junction. *Phys. Rev. B*, 30:6419–6431.
- [Fano, 1947] Fano, U. (1947). Ionization yield of radiations. ii. the fluctuations of the number of ions. *Physical Review*, 72(1):26.
- [Foros et al., 2009] Foros, J., Brataas, A., Bauer, G. E., and Tserkovnyak, Y. (2009). Noise and dissipation in magnetoelectronic nanostructures. *Physical Review B*, 79(21):214407.
- [Ingold and Nazarov, 1992] Ingold, G.-L. and Nazarov, Y. V. (1992). Charge tunneling rates in ultrasmall junctions. In *Single charge tunneling*, pages 21–107. Springer.
- [Johnson, 1928] Johnson, J. B. (1928). Thermal agitation of electricity in conductors. *Physical review*, 32(1):97.
- [Kamenev, 2011] Kamenev, A. (2011). *Field theory of non-equilibrium systems*. Cambridge University Press.
- [Kamenev and Levchenko, 2009] Kamenev, A. and Levchenko, A. (2009). Keldysh technique and non-linear σ -model: basic principles and applications. *Advances in Physics*.
- [Kamra and Belzig, 2016a] Kamra, A. and Belzig, W. (2016a). Magnon-mediated spin current noise in ferromagnet— nonmagnetic conductor hybrids. *Physical Review B*, 94(1):014419.
- [Kamra and Belzig, 2016b] Kamra, A. and Belzig, W. (2016b). Super-poissonian shot noise of squeezed-magnon mediated spin transport. *Physical review letters*, 116(14):146601.

- [Kawahara et al., 2012] Kawahara, T., Ito, K., Takemura, R., and Ohno, H. (2012). Spin-transfer torque ram technology: Review and prospect. *Microelectronics Reliability*, 52(4):613–627.
- [Keßler, 2018] Keßler, M. (2018). Master thesis at the Institute for Theoretical Condensed Matter physics at the Karlsruhe Institute of Technology; Title: *Spin-Torque and Persistent Precession in Anisotropic Ferromagnets*; Supervisor: Alexander Shnirman.
- [Kurland et al., 2000] Kurland, I. L., Aleiner, I. L., and Altshuler, B. L. (2000). Mesoscopic magnetization fluctuations for metallic grains close to the stoner instability. *Phys. Rev. B*, 62:14886–14897.
- [Landauer, 1957] Landauer, R. (1957). Spatial variation of currents and fields due to localized scatterers in metallic conduction. *IBM Journal of Research and Development*, 1(3):223–231.
- [Landauer, 1998] Landauer, R. (1998). Condensed-matter physics: The noise is the signal. *Nature*, 392(6677):658.
- [Ludwig et al., 2017] Ludwig, T., Burmistrov, I. S., Gefen, Y., and Shnirman, A. (2017). Strong nonequilibrium effects in spin-torque systems. *Phys. Rev. B*, 95:075425.
- [Ludwig et al., 2019a] Ludwig, T., Burmistrov, I. S., Gefen, Y., and Shnirman, A. (2019a). Current noise geometrically generated by a driven magnet. *arXiv preprint arXiv:1906.02730*.
- [Ludwig et al., 2019b] Ludwig, T., Burmistrov, I. S., Gefen, Y., and Shnirman, A. (2019b). Thermally driven spin transfer torque system far from equilibrium: Enhancement of thermoelectric current via pumping current. *Phys. Rev. B*, 99:045429.
- [Mahfouzi, 2014] Mahfouzi, F. (2014). *Nonequilibrium green function approach to elastic and inelastic spin-charge transport in topological insulator-based heterostructures and magnetic tunnel junctions*. PhD thesis, University of Delaware.
- [Mahfouzi and Nikolić, 2014] Mahfouzi, F. and Nikolić, B. K. (2014). Signatures of electron-magnon interaction in charge and spin currents through magnetic tunnel junctions: A nonequilibrium many-body perturbation theory approach. *Phys. Rev. B*, 90:045115.
- [Meir and Wingreen, 1992] Meir, Y. and Wingreen, N. S. (1992). Landauer formula for the current through an interacting electron region. *Phys. Rev. Lett.*, 68:2512–2515.
- [Moodera et al., 2007] Moodera, J. S., Santos, T. S., and Nagahama, T. (2007). The phenomena of spin-filter tunnelling. *Journal of Physics: Condensed Matter*, 19(16):165202.
- [Nazarov and Blanter, 2009a] Nazarov, Y. and Blanter, Y. M. (2009a). *Quantum transport: introduction to nanoscience*. Cambridge university press.
- [Nazarov and Blanter, 2009b] Nazarov, Y. and Blanter, Y. M. (2009b). *Quantum transport: introduction to nanoscience (section 2.4.1)*. Cambridge university press.

- [Negele and Orland, 1998] Negele, J. W. and Orland, H. (1998). Quantum many-particle systems (advanced book classics).
- [Nyquist, 1928] Nyquist, H. (1928). Thermal agitation of electric charge in conductors. *Physical review*, 32(1):110.
- [Schmid, 1982] Schmid, A. (1982). On a quasiclassical langevin equation. *Journal of Low Temperature Physics*, 49(5-6):609–626.
- [Schottky, 1918] Schottky, W. (1918). Über spontane stromschwankungen in verschiedenen elektrizitätsleitern. *Annalen der physik*, 362(23):541–567.
- [Shnirman et al., 2015] Shnirman, A., Gefen, Y., Saha, A., Burmistrov, I. S., Kiselev, M. N., and Altland, A. (2015). Geometric quantum noise of spin. *Phys. Rev. Lett.*, 114:176806.
- [Slonczewski, 1996] Slonczewski, J. C. (1996). Current-driven excitation of magnetic multilayers. *Journal of Magnetism and Magnetic Materials*, 159(1-2):L1–L7.
- [Swiebodzinski et al., 2010] Swiebodzinski, J., Chudnovskiy, A., Dunn, T., and Kamenev, A. (2010). Spin torque dynamics with noise in magnetic nanosystems. *Phys. Rev. B*, 82:144404.
- [Titov and Gutman, 2016] Titov, M. and Gutman, D. B. (2016). Korshunov instantons out of equilibrium. *Phys. Rev. B*, 93:155428.
- [Tserkovnyak et al., 2002] Tserkovnyak, Y., Brataas, A., and Bauer, G. E. W. (2002). Enhanced gilbert damping in thin ferromagnetic films. *Phys. Rev. Lett.*, 88:117601.
- [Tserkovnyak et al., 2005] Tserkovnyak, Y., Brataas, A., Bauer, G. E. W., and Halperin, B. I. (2005). Nonlocal magnetization dynamics in ferromagnetic heterostructures. *Rev. Mod. Phys.*, 77:1375–1421.
- [Tserkovnyak et al., 2008] Tserkovnyak, Y., Moriyama, T., and Xiao, J. Q. (2008). Tunnel-barrier-enhanced dc voltage signals induced by magnetization dynamics in magnetic tunnel junctions. *Phys. Rev. B*, 78:020401.
- [Van Kampen, 2007] Van Kampen, N. G. (2007). *Stochastic processes in physics and chemistry*, volume 3. Elsevier.
- [Virtanen and Heikkilä, 2017] Virtanen, P. and Heikkilä, T. T. (2017). Spin pumping and torque statistics in the quantum noise limit. *Phys. Rev. Lett.*, 118:237701.
- [Yamamoto et al., 2018] Yamamoto, K., Gomonay, O., Sinova, J., and Schwiete, G. (2018). Spin transfer torques and spin-dependent transport in a metallic f/af/n tunneling junction. *Phys. Rev. B*, 98:014406.
- [Zhu and Park, 2006] Zhu, J.-G. J. and Park, C. (2006). Magnetic tunnel junctions. *Materials today*, 9(11):36–45.